Numerical Analysis of Anisotropic Wetting on Chemical Stripe-Patterned Surfaces

A Dissertation

by

Shajid Rahman (Student ID: 1018102108)

Under the Supervision of

Dr. Md. Ashiqur Rahman

MASTER OF SCIENCE IN MECHANICAL ENGINEERING

Department of Mechanical Engineering

BANGLADESH UNIVERSITY OF ENGINEERING AND TECHNOLOGY

December 2022

RECOMMENDATION OF THE BOARD OF EXAMINERS

The thesis titled "**Numerical Analysis of Anisotropic Wetting on Chemical Stripe-Patterned Surfaces**" submitted by Shajid Rahman, Student No.: 1018102108, Session: October 2018, has been accepted as satisfactory in partial fulfilment of the requirement for the degree of Master of Science in Mechanical Engineering on December 18, 2022.

BOARD OF EXAMINERS

Dr. Md. Ashiqur Rahman
Professor
Department of Mechanical Engineering
BUET, Dhaka-1000

Chairman
(Supervisor)

Dr. Muhammad Ashiqur Rahman
Professor and Head
Department of Mechanical Engineering
BUET, Dhaka-1000

Member
(Ex- officio)

Dr. Mohammad Nasim Hasan
Professor
Department of Mechanical Engineering
BUET, Dhaka-1000

Member
(Internal)

Dr. Md. Shakhawat Hossain Firoz
Professor
Department of Chemistry
BUET, Dhaka-1000

Member
(External)

CANDIDATE'S DECLARATION

It is hereby declared that this thesis/project or any part of it has not been submitted elsewhere for the award of any degree or diploma.

Shajid Rahman

Shajid Rahman

Dedicated to

Dr. Md. Ashiqur Rahman, the person who changed my life

ACKNOWLEDGEMENTS

I would like to offer my deepest gratitude and respect to my supervisor, Dr. Md. Ashiqur Rahman, Professor, Department of Mechanical Engineering, BUET for his support throughout this journey. His profound knowledge, excellency, experience, guidance in this particular research area have motivated me to go forward more intensely & elucidated my obscure ideas and knowledge. He granted me immense independence over my research as well as monitored and suggested his valuable thinking and academic ideas which made this rigorous and hectic path easier. Interesting and critical discussion sessions with him were something I would always cherish as they have changed my thinking process and perspective as a researcher as well as a human being. I also thank him for providing me laboratory facilities for the simulation part of this work and mental support with his patience, words and caring throughout the whole time.

Following that, I am blessed to acknowledge Anjan Goswami, Assistant Professor, Department of Mechanical Engineering, AUST for his utmost help both in theoretical and simulation part of this research. His concept and intelligent guidance helped me to find and carry on the research work in desirable direction.

Md. Ikram Khan, an energetic and brilliant member of the BUET faculty who is currently an Assistant Professor in the Department of Mechanical Engineering, has constantly pushed me and generously shared his knowledge and expertise, which helped me get to the desired goal for my study.

Professor Kenneth A. Brakke, Department of Mathematics, Susquehanna University, Pennsylvania is the person of admiration for his book “Physics of Microdroplets” which helped me building up appropriate theoretical knowledge in details. Developing “Surface Evolver” as an open-source program is one of his most remarkable achievements for which I offer him my earnest gratitude.

Finally, I would like to thank my family members, friends and well-wishers for the support and love they provided.

TABLE OF CONTENTS

LIST OF TABLES

LIST OF FIGURES

NOMENCLATURE

Notation	Definition
G	Gibbs free energy
E_s	Free Surface energy
F_g	Gravitational force
G_s	Gravitational Energy
γ_{lv}	Liquid-vapor surface tension
γ_{sv}	Solid-vapor surface tension
γ_{sl}	Solid-liquid surface tension
θ	Young or equilibrium contact angle
θ_W	Wenzel contact angle
θ_{CB}	Cassie-Baxter contact angle
r	Surface roughness factor
f_s	Cassie roughness factor or solid fraction area
E_s	Droplet's free surface energy
E	Total droplet energy
E_{norm}	Droplet's normalized surface energy
T	Surface tension per unit length
$\theta_\perp$	Perpendicular contact angle
$\theta_\parallel$	Parallel contact angle
θ_{phobic}	Hydrophobic Contact Angle
θ_{philic}	Hydrophilic Contact Angle
n	Hydrophobic Stripe Width
m	Hydrophilic Stripe Width

ABSTRACT

There is a considerable need and scope for improved prediction and approximation of wetting behavior on chemically patterned surfaces for designing such surfaces with tunable wettability. In this study, anisotropic wetting on chemical stripe-patterned surface with alternating hydrophobic/hydrophilic stripes is investigated. It focuses on the effects of wettability contrast by introducing stripes of wettability of different ranges. The numerical analysis has been performed using the open access software 'Surface Evolver'. Analysis of the shape and movement of the three-phase contact line, and examination of droplet energetics and the stability of liquid droplet with a range of wettability contrast of the chemical stripe-patterned surfaces has been carried out.

To investigate the stability and energetics of droplet, normalized energy for a range of droplet volume has been calculated to seek the most stable state of a droplet. It is found that the lowest value of normalized energy indicates the equilibrium state that we consider to be the most stable. Additionally, the volume of droplet which exhibits the minimum normalized energy increases with the number of chemical stripes. Thus, the system becomes more stable when droplet is of small volume and resides on fewer number of stripes. Moreover, a narrow- hydrophilic stripe is found to be more preferable compared to the hydrophobic stripe for attaining the global energy minima.

Wider hydrophilic stripe causes both parallel and perpendicular contact angles to decrease for a preferred spreading in the parallel direction. Furthermore, droplet residing on more stripes displays a decrease in the degree of anisotropy. Because of a larger energy barrier in the perpendicular direction, droplet prefers to spread toward the parallel grooves/stripes. Liquid droplet is observed to distort, where the droplet distortion is defined as the ratio of the length of the elongated droplet in the major to minor. Distortion increases with an increment in the volume of the droplet and the wider hydrophilic stripe causes a more elongated droplet shape resulting in large distortion. The shape of a droplet evolves from an oval/elliptical to spherical geometry in our study when droplet volume is increased. At the stable state, it becomes spherical and with further increment in the volume, the oval/elliptical shape reappears.

The findings of the present study can provide a reliable guideline for the prediction of wetting behavior on chemical-stripe patterned surfaces to facilitate the design of such surfaces with controlled wettability.

Chapter 01

1.1 Introduction

Understanding the physics of wetting on solid surfaces has attracted a considerable amount of attention to investigate the insights into nature's phenomenon as well as to implement the perception in engineering applications. These occurrences are all around us, and many of them, like the "lotus leaf effect" as a superhydrophobic surface and self-cleaning qualities, have become archetypes for their distinctive behavior. Spherical shaped free droplets behave differently both physically and characteristically while in contact with solid surfaces due to interactions at solid-liquid interface. These interfacial interactions result in determining the amount of the liquid's tendency of spreading over or adhering to a solid surface, known as surface wettability. Wettability, to put it simply, is a measurement of a liquid's ability to wet a surface. It is characterized by the contact angle between liquid droplet and solid surface which is responsible for the deformation of droplet's shape associated with the interfacial surface tension. So, the physics of wetting is very important to comprehend because of its potential to create a cloud of new applications as well as to create tunable surfaces/devices as per our demand for vast range of application such as refrigeration and air-conditioning system [1-2], self-cleaning devices [3], anti-icing surfaces [4], and microfluidics systems [5]. This chapter will depict a deep insight into the fundamentals of wetting: key factors to explain the behavior and interactions of surfaces of multiple phases.

1.1.2 Motivation of the Present Study

Anisotropic wetting characteristic of liquid droplet on chemically patterned alternating (hydrophobic/hydrophilic) wettable stripes is what spurs us on to do more research for this thesis. To be more specific, how physical characteristics of a liquid droplet change due to the chemical non-uniformity of a surface is our area of research interest. The ability to control surfaces'

wettability for desired directional wetness opens up a world of possibilities for engineering applications, particularly in fluidic-based systems.

In complex situations like printing mechanisms [6] and optoelectronic device applications [7], uniform surfaces frequently fall short of some strict requirements for distinctive and desirable properties. However, these exacting requirements can be met by using heterogeneous wettability substrates with an appropriate design and utilization of water-repellent and water-loving characteristics. Different regions on such surfaces have distinct wettability, thus exhibiting excellent capability in precisely regulating the solid–liquid interactions.

There are numerous instances of organisms in nature that have modified their "skin" to achieve particular wetting properties [34,35]. The impressive water management of the desert beetle Stenocara, which uses the heterogeneous wettability strategy to collect and transport water for survival in the Namib Desert, one of the driest locations on Earth, is a prime example. When it's humid in the morning, the hydrophilic bumps on the beetle's hydrophobic back can capture fog and condense it into big water droplets. The hydrophobic area then acts as a route to direct the water droplets into its mouth. In nature, materials like lotus leaves are seen that are extremely hydrophobic can roll water off of their surface. These ideas have greatly inspired the design and utilization of heterogeneous wettability for various applications. Therefore, significant attempts have been made to accurately understand, imitate, and apply these natural designs and tactics in engineering applications.

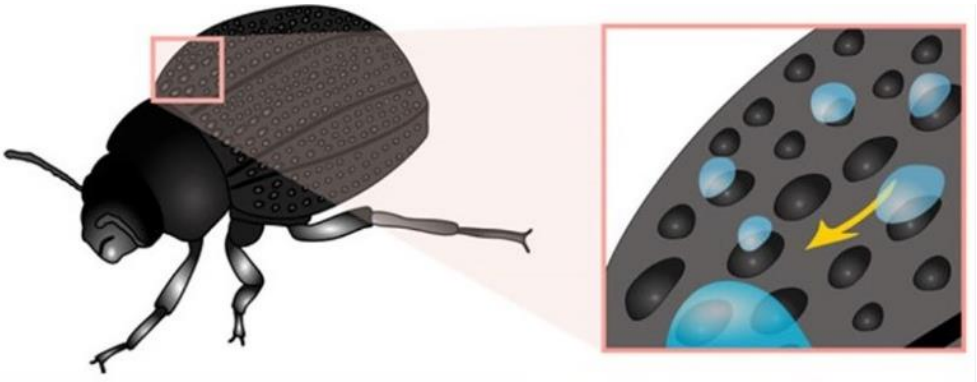

Fig 1.1.2 (a): Fog harvesting *Stenocara Gracilipes* modified skin with hydrophobic bumps and hydrophilic valleys.

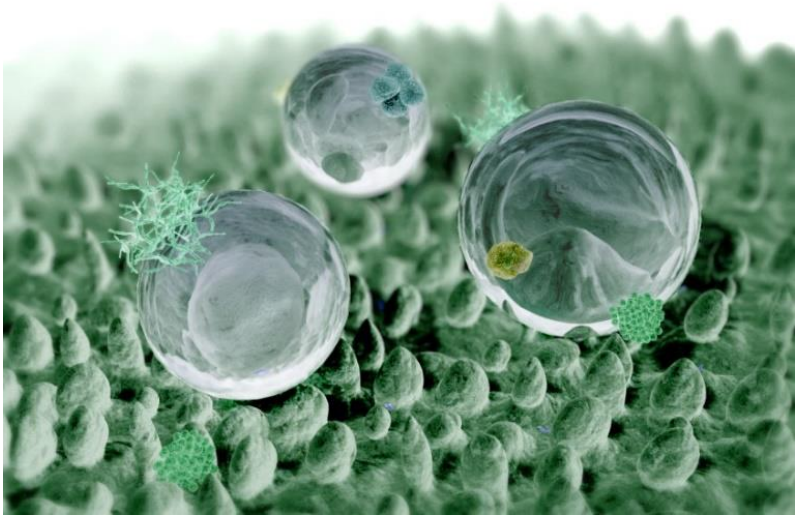

Fig 1.1.2 (b): Lotus leaf surface microstructure

To predict the shape and behavior of liquid droplet on an alternating wettable surface and how it responds when different range of wetting contrast is introduced is a major concern of this study. Despite the fact that numerous experimental and numerical studies on wetting and anisotropic wetting have been reported, only few of them focused on the effects of wettability contrast on liquid droplet. Our proposed numerical approach would offer less complicacy to investigate the above-mentioned effects on wetting in comparison with the available studies on this topic.

1.1.3 Present State of the Problem

Liquid droplets on chemically patterned surfaces with alternating hydrophobic/hydrophilic stripes exhibit an anisotropic wetting behavior [8]. Inspired by the biological materials, e.g., rice leaf and lotus leaf, advanced manufacturing and nano/macro fabrication has made it possible to develop chemically/geometrically heterogeneous surfaces with tunable wettability. Morita et al. experimentally fabricated a monolayer chemically patterned surface by photolithography and observed a strong wetting anisotropy [9]. They investigated anisotropic wetting on micropatterned surfaces of macroscopic droplet of varying diameter where they found a strong wetting anisotropy but a decrement if the liquidphilic area is decreased. In a numerical study, the partial wetting and

the effects of volume and drop size on the chemically heterogeneous surfaces were examined by Brandon et al. [10]. In their study, the utilized different sized droplet to observe the effect on apparent contact angle. Through volume adjustment, they examined its impact on receding and advancing contact angle. Jansen et al. focused mainly on the stripe configuration and demonstrated the nature of pattern which is favorable for a droplet to exhibit strongly elongated shape and numerically studied droplet evolution as a function of varying stripe wettability as well as width [11-12]. The effect of wettability contrast on sessile droplets on micro-striped surfaces was studied for high, intermediate, and low wettability contrast [13]. In their numerical study on drop shape and energetics on micro patterned surfaces, Chatain et al. introduced normalized energy as a function of volume [14]. He et al. proposed a three-dimensional model for anisotropic wetting behavior on striped surfaces by implementing finite element simulation [15]. They proposed a 3-D modeling of a spreading droplet which is found to be reliable for analyzing the three-phase contact line. In another work, they analyzed anisotropic wetting on chemically striped surface where they proposed a modified method to analyze contact angle hysteresis by measuring advancing and receding angle [53].

Although a few numerical studies have been reported on the wetting behavior of liquid droplets on chemically patterned surfaces, there is still a considerable scope for improved prediction and approximation of wetting behavior for designing such surfaces with tunable wettability. Therefore, in this proposed study, a numerical analysis will be carried out to investigate the shape and movement of the three-phase contact line, droplet energetics, and the stability of liquid droplets for varying configuration of the chemical stripe-patterned surfaces.

1.1.4 Research Gap and Our Approach

Theoretical modeling and numerical simulation are still in the early phases of development for forecasting the anisotropic wetting properties of engineered solid surfaces, despite recent breakthroughs in experimental testing. Theoretical investigations, on the other hand, primarily rely on a thermodynamic analysis to simplify the computation process [16,17].

Li et al. [18] investigated the impact of surface geometry on contact angle (CA), contact angle hysteresis (CAH), free energy (FE), and free energy barrier and provided a thermodynamic model to theoretically analyze the anisotropic wetting behavior of superhydrophobic grooved surfaces (FEB). Theoretical framework of Shi et al. [19] for forecasting CA based on the Gibbs free energy incorporates the effects of unilateral force and area constraints. However, there are still only a few theoretical models for anisotropic wetting since they are based on an oversimplified two-dimensional (2-D) architecture of engineered surfaces [18,20,21]. Modeling the spreading process of a 3-D droplet is a dilemma and limited in number for the uncertainty of the final droplet shape after the simulation process.

In our approach, we offer a 3-D model to mimic the spreading of a droplet cross chemically heterogenous surfaces (parallel stripes with alternate wettability) by using Surface Evolver [22], a widely used tool for both resolving the issues assessing the shape and three-phase contact line of a droplet. Our suggested model is less complicated and produces results with excellent accuracy compared to current numerical methods, which are complex and need a lot of computer resources.

1.1.4 Objectives of the Present Study

The main objectives of the present study are as follows:

i. To numerically examine the anisotropic wetting of water droplets on chemically patterned substrates (hydrophobic/hydrophilic stripes) by analyzing the shape, distortion, and movement of the three-phase contact line.
ii. To study the energetics and stability of the liquid droplets for varying geometric configuration and wettability of the chemical striped micro-pattern for a range of volume of liquid droplets.

iii. To study the effect of wettability contrast on micro-striped surfaces by introducing stripes with wettability of different ranges.

The present study is expected to provide a reliable guideline for the prediction of wetting behavior on chemical-stripe patterned surfaces to facilitate the design of such surfaces with controlled wettability.

1.2 Background of the Study

1.2.1 Interface

The geometric surface separating two fluid domains is referred to as an interface. According to this definition, an interface is smooth and devoid of any thickness (i.e., has no roughness). However, the reality is more complicated, the line separating two immiscible liquids is somewhat hazy, and the separation of the two fluids (water/air, water/oil, etc.) depends on molecular interactions between the molecules of each fluid and on Brownian diffusion (thermal agitation). The diagram in figure 1.2.1 (a) represents the interface between two fluids more accurately from a microscopic perspective. However, in engineering applications, the interface's macroscopic behavior is the main concern. Thus, we can consider figure 1.2(b) instead of figure 1.2(a) where the interface is represented by a mathematical surface without thickness and the contact angle is exclusively specified by the tangent to the surface at the contact line.

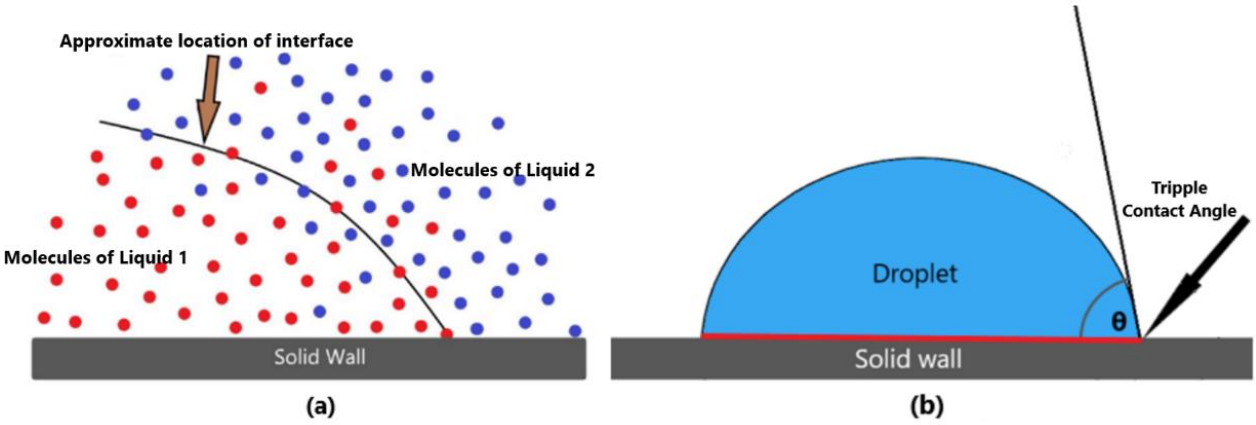

Figure 1.2.1 : (a) Schematic view of an interface at molecular size ; (b) : Macroscopic view of the interface of a droplet

1.2.2 Surface Tension

Surface tension is the fundamental property of the surface of a liquid that allows it to resists an external force due to the cohesive nature of its molecules. Ideally, this property determines the shape of liquid droplet. We can infer from our daily experience that water drops behave distinctly and take diverse forms on various surfaces. In contrast to wax-coated surface, where water tends to acquire a spherical shape, glass surface allows water to spread uniformly. Water drenches tissue paper or cotton cloth, yet a lotus leaf exhibits water-repelling qualities. Insects frequently float and glide on water in nature as if they were resting on a surface with a tight, elastic skin or film. Surface tension, a result of molecular interactions at the interface, can explain the phenomena listed above.

Let's think about a liquid-gas interface (figure 1.2.2 (a)). In a pure liquid, each molecule interacts with its neighbors on both sides as they are attracted to one another, resulting in zero net cohesive force. Majority of these interactions are Van der Waals attractive interactions for organic liquid and hydrogen bonds for polar liquid (i.e., water). However, the molecules exposed at interface experience otherwise. In one half of the space, they interact with molecules of the same liquid (cohesive force), while in the other half, they do so with molecules of a different liquid or gas (adhesive force). Due to the low densities of gases, there are fewer interactions and less attraction than on the liquid side meaning cohesive force being larger than adhesive force, there a dissymmetry in the interactions locally, which results in an excess of surface energy directing inward of the bulk liquid creating an internal pressure. At the macroscopic scale, a physical quantity called “surface tension” has been introduced in order to take into account this molecular effect.

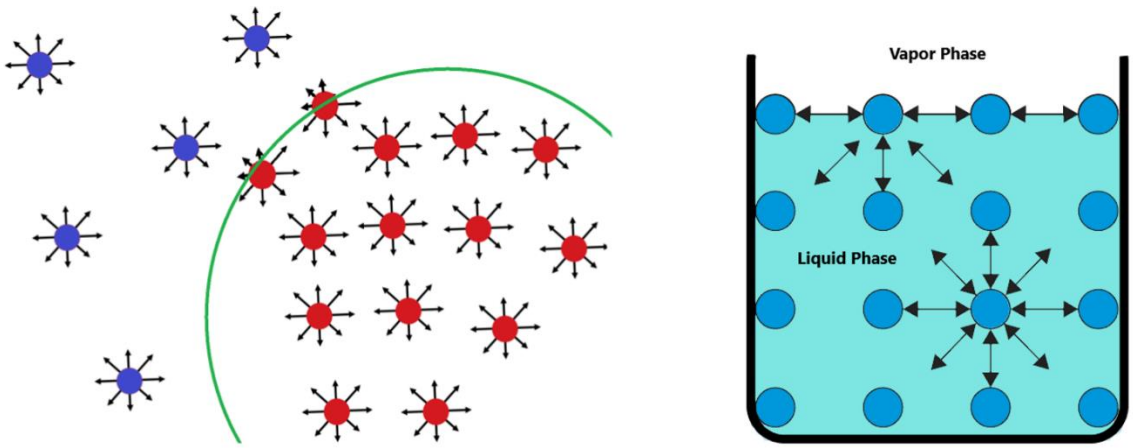

Fig 1.2.2 (a): A schematic view of molecules near an air/water interface. Force imbalance at interface generating surface tension.

With the aid of the molecules' cohesive energy, surface tension can be computed. If U is the total cohesive energy per molecule, a rough estimate of a molecule's energy surplus at the interface is $\frac{U}{2}$. Surface tension is a direct measure of this energy excess, and if δ is a characteristic molecular dimension and δ^2 the associated molecular surface area, then the surface tension is approximately

$$\gamma \approx \frac{U}{\delta^2}$$

The significance of surface tension for liquids with high cohesive energy and small molecular dimensions is illustrated by this relationship. As surface tension arises due to cohesive interactions between the molecules in the liquid at surface, intermolecular hydrogen bonds between water molecules are weaker than metallic bonds of mercury molecules leading to a high cohesive force and high surface tension for mercury. Another result of this approach is that a fluid system will always act to minimize surface area since the larger the surface area, the more molecules there will be at the interface and the more cohesive energy imbalance there will be. The molecules at the interface are constantly seeking out other molecules to balance their interactions. As a result, interfaces usually adopt a flat profile in the absence of additional forces, and when this is not

possible due to volume or boundary constraints, they adopt a rounded form, generally that of a sphere.

The same principle holds true when a liquid comes into touch with a solid. The interface is just the solid surface at the contact of the liquid. Van der Waals forces cause molecules in the liquid to be drawn toward the interface. If there are substantial attractive forces acting on the solid, resulting in a liquid-solid interface with negative surface energy, the solid is said to be wetting or hydrophilic (or lyophilic for non-water liquids). If the attractions are weak, the interface energy is positive, and the solid is nonwetting or hydrophobic (or lyophobic).

The Gibbs model is a useful technique for defining the interfacial surface tension and for further elaborating on the concept of surface tension.

The presence of an interface influences generally all thermodynamic parameters of a system. To consider the thermodynamics of a two-component system (V^{α} and V^{β}) system with an interface, we divide that system into three parts: The two bulk phases with volumes V^{α} and V^{β}, and the interface "σ".

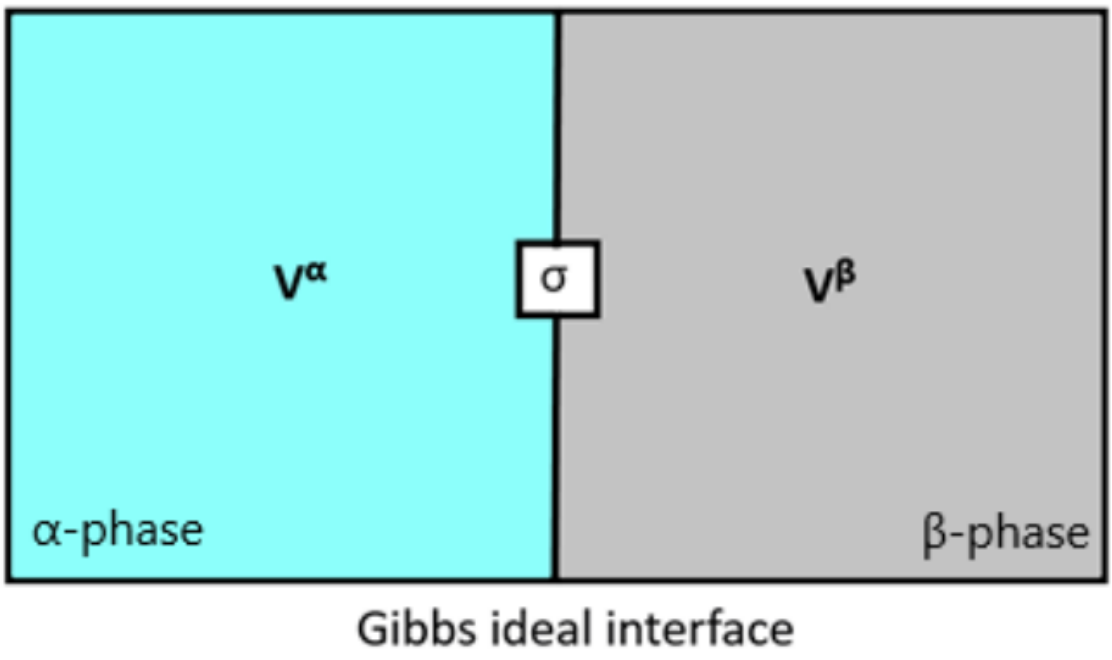

Fig 1.2.2 (b): the two phases α and β are separated by an ideal interface "σ" which is infinitely thin

The Gibbs dividing plane, assumed as an ideal interface is an infinitesimally thin boundary layer, to act as a barrier between the two phases α and β**.**

According to Gibbs model, the interface is ideally thin ($V^{\sigma} = 0$) and the total volume is

$$V=V^{\alpha}+V^{\beta} \tag{1.1}$$

Considering the internal energy U, the number of molecules of the substance N, the entropy S and chemical potential μ, these quantities can be written as a sum of three components. For i = α, β, σ these quantities can be split into their corresponding components for {(U^{i} to U^{α}, U^{β} & U^{σ}); (N^{i} to N^{α}, N^{β} & N^{σ}); (S^{i} to S^{α}, S^{β} & S^{σ}); (μ^{i} to μ^{α}, μ^{β} & μ^{σ})} one of bulk phase α, one of bulk phase β, and one of the interfacial regions σ.

$$U=U^{\alpha}+U^{\beta}+U^{\sigma}$$

$$N=N^{\alpha}+ N^{\beta} + N^{\sigma}$$

$$S = S^{\alpha}+S^{\beta}+S^{\sigma}$$

According to the first and second laws of thermodynamics, a change in the internal energy of a two-phase system is

$$dU=TdS -PdV + \Sigma\mu^{i}dN^{i} + dW \tag{1.2}$$

Here, dW is the work done on the system without expansion work PdV. It contains the surface work γdA. The TdS terms stands for the change in internal energy due to entropy change (i.e., Heat flow). The $\mu^{i}dN^{i}$ term considers the energy change caused by a change in the composition. PdV term corresponds to the volume- work of the two phases. Splitting the total internal energy of the system into three phase components:

$$dU=dU^{\alpha}+dU^{\beta}+dU^{\sigma} = TdS^{\alpha} + \Sigma\mu^{\alpha}dN^{\alpha} -P^{\alpha}dV^{\alpha} TdS^{\alpha} + \Sigma\mu^{\beta}dN^{\beta} -P^{\beta}dV^{\beta}+TdS^{\sigma} + \Sigma\mu^{\sigma}dN^{\sigma} - P^{\sigma}dV^{\sigma}$$

Since the interface is infinitely thin($V^{\sigma}=0$) it cannot perform volume work.

$$V = V^{\alpha} + V^{\beta} + V^{\sigma}$$

$$V = V^{\alpha} + V^{\beta} + 0$$

$$V = V^{\alpha} + V^{\beta}$$

$$dV = dV^{\alpha} + dV^{\beta}$$

$$dV^{\alpha} = dV - dV^{\beta}$$

Now, substituting $dV^{\alpha} = dV - dV^{\beta}$, the equation simplifies as:

$$dU = TdS - P^{\alpha}dV - (P^{\beta} - P^{\alpha})\, dV^{\beta} + \Sigma\mu^{\alpha}dN^{\alpha} + \Sigma\mu^{\beta}dN^{\beta} + \Sigma\mu^{\sigma}dN^{\sigma} + \gamma dA \quad (1.3)$$

Considering F as Helmholtz energy of a system, the change in Helmholtz energy dF is:

$$dF = -SdT - PdV + \Sigma\mu^{i}dN^{i} + dW \quad (1.4)$$

For a two-phase system having an interface it follows that

$$dF = dF^{\alpha} + dF^{\beta} + dF^{\sigma} = -SdT - P^{\alpha}dV - (P^{\beta} - P^{\alpha})\, dV^{\beta} + \Sigma\mu^{\alpha}dN^{\alpha} + \Sigma\mu^{\beta}dN^{\beta} + \Sigma\mu^{\sigma}dN^{\sigma} + dW$$

$$= dF^{\alpha} + dF^{\beta} + dF^{\sigma} = -SdT - P^{\alpha}dV - (P^{\beta} - P^{\alpha})\, dV^{\beta} + \Sigma\mu^{\alpha}dN^{\alpha} + \Sigma\mu^{\beta}dN^{\beta} + \Sigma\mu^{\sigma}dN^{\sigma} + \gamma dA$$

Here γdA contains the surface work. We assume a closed system, so there is no exchange of materials ($dN^{i} = 0$). Thus $dN^{\sigma} = -dN^{\alpha} - dN^{\beta}$. Having constant temperature ($dT = 0$) and volume($dV=0$), the equation becomes

$$dF = -(P^{\beta} - P^{\alpha})\, dV^{\beta} + \Sigma(\mu^{\alpha} - \mu^{\sigma})\, dN^{\alpha} + \Sigma(\mu^{\beta} - \mu^{\sigma})\, dN^{\beta} + \gamma dA$$

At equilibrium, with constant volume ($dV=0$), temperature ($dT=0$) and constant amounts of material ($dN=0$), Helmholtz energy is minimal. At minimum, the derivatives with respect to all independent variables must be zero that follows

$$\mu = \mu^{\alpha} = \mu^{\beta} = \mu^{\sigma}$$

simplifying the equation,

$$dF = -(P^{\beta} - P^{\alpha})\, dV^{\beta} + \gamma dA \qquad (1.5)$$

This equation allows us to define the surface tension based on thermodynamics:

$$\left(\frac{\delta F}{\delta A}\right)_{T,V} = \gamma \qquad (1.6)$$

As per equation (1.6), the surface tension tells us how the Helmholtz energy of the system changes when increasing the surface area while keeping the temperature and the total volume constant.

The Gibbs energy G is usually more important than Helmholtz energy F because its natural variables as T and P are constant in most applications. For the Gibbs energy, change of free energy dG can be written as follows:

$$dG = -SdT - V^{\alpha}dP^{\alpha} + V^{\beta}dP^{\beta} + \Sigma\mu^{i}dN^{i} + \gamma dA$$

Assuming that the interface is flat (planar) we have the same pressure in both phases $P^{\alpha} = P^{\beta} = P$ and we get,

$$dG = -SdT - VdP + \Sigma\mu^{i}dN^{i} + \gamma dA \qquad (1.7)$$

from this equation it is also possible to give a definition of the interfacial tension as the change of Gibbs free energy of the system keeping the temperature and pressure constant, which is equivalent to the previous definition:

$$\left(\frac{\delta G}{\delta A}\right)_{T,P} = \gamma \qquad (1.8)$$

1.2.3 Contact Angle and Wetting Phenomena

Contact angle is a quantitative measure of the wettability of a surface by a liquid. When an interface exists between a liquid and a solid, the angle between the surface of the liquid and the outline of the contact surface is described as the contact angle. Geometrically, this angle is formed by a liquid at the three-phase contact boundary where a liquid, gas and solid intersect (Fig 1.2.3 (a)). Different liquids spread across a horizontal plate depending on the characteristics of the solid surface and the liquid itself. In reality, it depends also on the third constituent, which is the gas or the fluid surrounding the drop. Contact angle is determined by the surface tensions of the three constituents The infamous Young equation (1.10) gives us a clear understanding of how contact angle and surface tension are related, dictating the behavior and structure of liquid droplets.

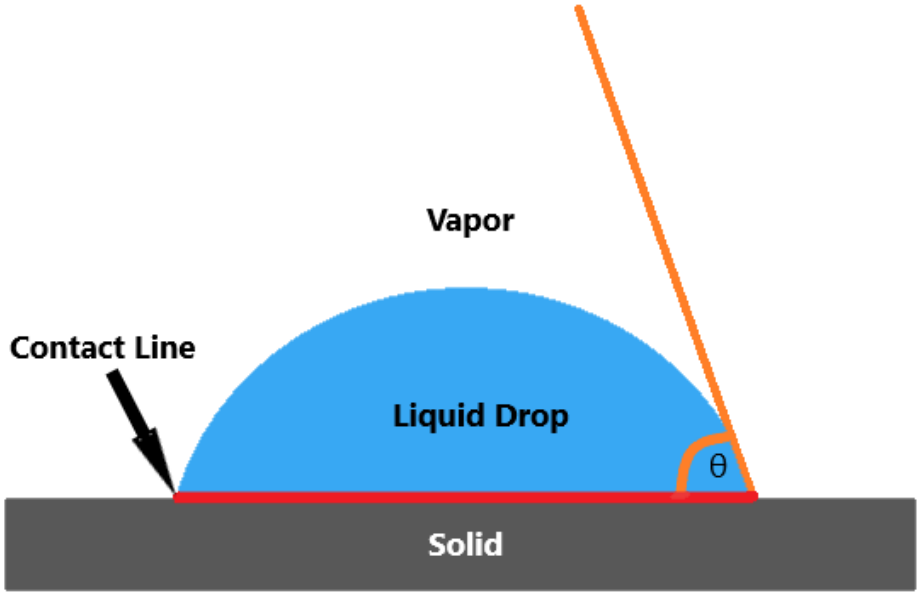

Fig 1.2.3 (a): Three-phase contact line and contact angle of a liquid drop on a smooth solid surface

The intersection of three interfaces involving three different materials, as we already know from prior discussion, makes up a three-phase contact line. Thomas Young proposed [23] treating the contact angle (θ) of a liquid with a surface as the mechanical equilibrium of a drop resting on a plane solid surface under the restrains of three surface tensions at the three-phase contact.

$$\gamma_{lv}\cos\theta = \gamma_{sv} - \gamma_{sl} \qquad (1.9)$$

Here γ_{sv} , γ_{sl} and γ_{lv} are, respectively, the solid–vapor, solid– liquid and liquid–vapor interfacial force per unit length of the contact line, (i.e. surface tension), and θ is the Young's contact angle, figure 1.4.1

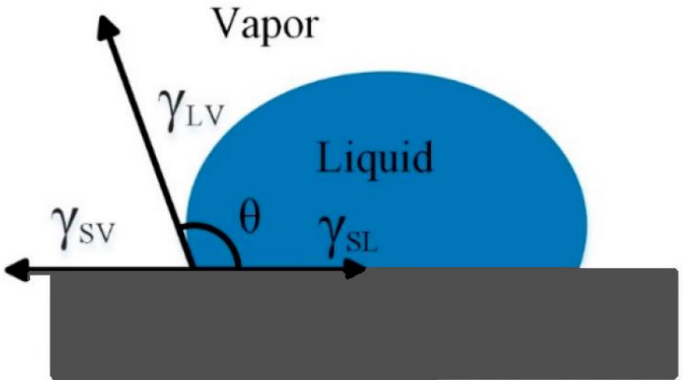

Fig 1.2.3 (b): Interfacial tension forces acting on the contact line resulting Young's contact angle for a liquid droplet on a smooth solid substrate.

This relation is called Young's law and is very useful to understand the behavior of a drop. Particularly, it demonstrates that the surface tensions of the three elements determine the contact angle. For a droplet on a solid, the contact angle is given by the relation

$$\cos\theta = \frac{\gamma_{sv}-\gamma_{sl}}{\gamma_{lv}} \qquad (1.10)$$

Young's law can be more rigorously derived from free energy minimization. Consider a sessile droplet large enough for the effect of the triple line to be neglected. The change of free energy due to a change in droplet size can be written as:

$$dF = \gamma_{sl}\, dA_{sl} + \gamma_{sv}\, dA_{sv} + \gamma_{lv}\, dA_{slv} = (\gamma_{sl} - \gamma_{sv} + \gamma_{lv} \cos\theta)$$

where θ is the contact angle. At mechanical equilibrium dF = 0 and

$$\gamma_{sl} - \gamma_{sv} + \gamma_{lv} \cos\theta = 0$$

which is identical to the Young's law.

This angle is known as Young or equilibrium contact angle θ. If gravity can be neglected, the rest shape of a drop on a perfectly smooth surface will then be a spherical cap of suitable volume and with a contact angle equal to the Young's contact angle as shown in Figure 1.2.3 (b)

On a smooth surface depending on the nature of solid surface, liquid and the surrounding fluid/gas there are two possible outcomes: either the liquid forms a droplet which is referred to as partial wetting, or the liquid forms a thin film, in which case the horizontal dimension of the film depends on the original volume of liquid (figure 1.2.3 (c)). For example, water spreads like a film on a very clean and smooth glass substrate, whereas it forms a droplet on a plastic substrate. In the case of partial wetting, there exists the three-phase contact line or the triple line where all three phases come together.

As suggested by De Gennes [8], we can define a spreading parameter $S = \gamma_{sv} - (\gamma_{sl} + \gamma_{lv})$ which is the energy cost per unit area in wetting a dry substrate with a liquid film. If $S > 0$, it is energetically favorable for the liquid phase to spread indefinitely, to wet as large as a solid area as possible. If $S < 0$, the liquid will only wet a finite area, and form an angle to the solid substrate.

When a liquid does not totally wet the solid, it forms a droplet on the surface. Two situations can occur: if the contact angle with the solid is less than 90°, the contact is said to be "hydrophilic" if the liquid has a water base, or more generally "wetting" or "lyophilic". In the opposite case of a contact angle larger than 90°, the contact is said to be "hydrophobic" with reference to water or more generally "not wetting" or "lyophobic".

Youngs equation can categorize the wetting conditions into several intervals.

- When contact angle is 0^0 or very close to 0^0, the liquid spreads completely over the surface of the solid which is referred to as complete wetting.

- Then comes the partial wetting where contact angle ranges from 0^o to 90^o. The solid is said to be hydrophilic. The lower the contact angle from 90^o, the more the solid is hydrophilic.
- Un-wetted or hydrophobic surfaces arises when the contact angle is lying between 90 and 180 degrees. With contact angle increasing from 90°, hydrophobicity rises. For water, the surface is defined as superhydrophobic surface when the contact angle exceeds 150^o degrees.
- At 180^o, the surface is called completely un wetted having no physical contact with the liquid and surface.

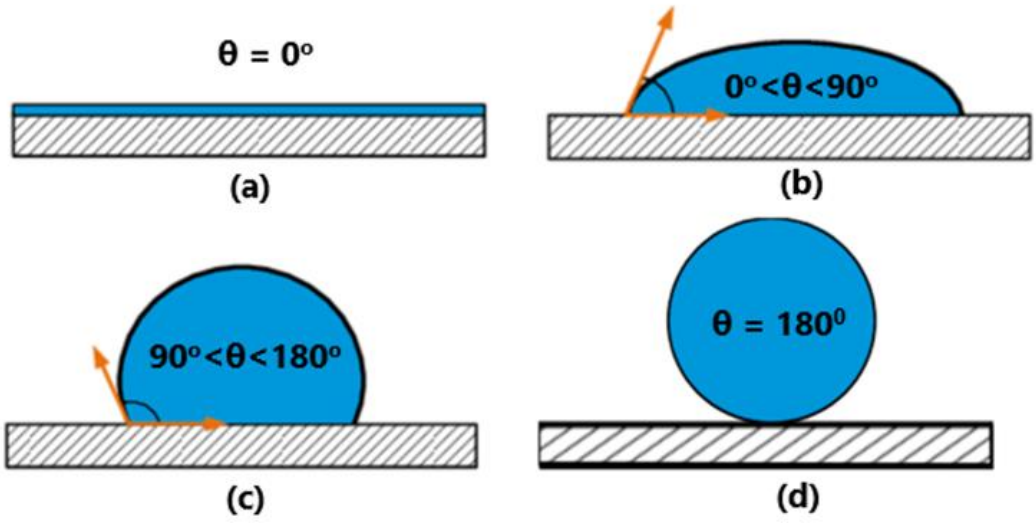

Fig 1.2.3 (c): The contact angle of a drop on a solid surface with various wetting conditions.

1.2.4 Wetting on Rough Surfaces

Previously, wetting on ideal surfaces, which are uniformly smooth solid, were only considered. However, in reality, actual surfaces are not completely smooth (Figure 1.2.4 (b)). A liquid droplet in equilibrium on a solid will have a different contact angle depending on the roughness or texture of the surface. Considering the topography of the substrate, surface energy balance determines the equilibrium configuration of the rough or textured surfaces. In this section, several possible configurations available for a droplet on a textured surface will be introduced in brief.

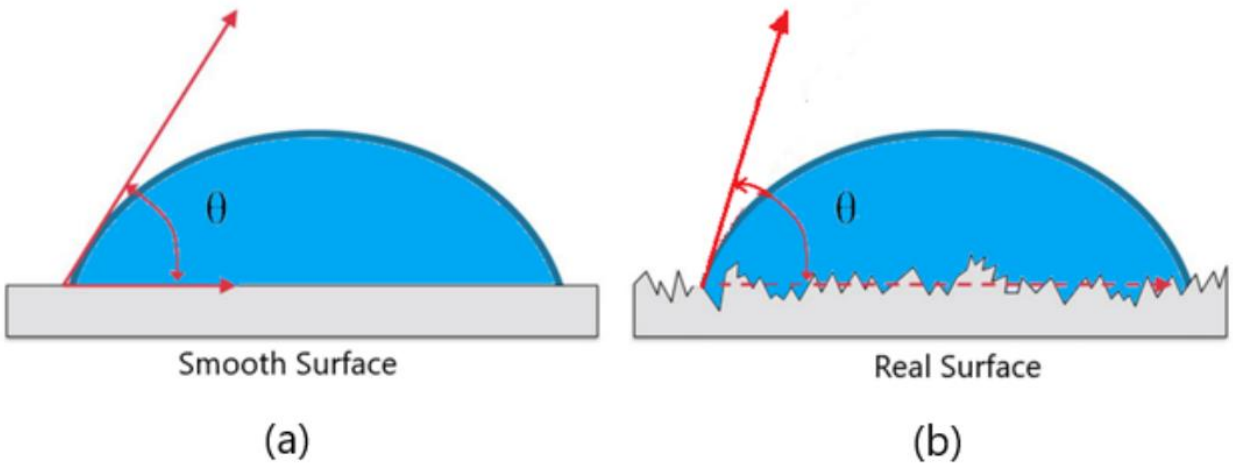

Fig 1.2.4 : Liquid droplet having different contact angle on (a)smooth surface ; (b) real surface

1.2.4.1 Wenzel State

Roughness of the solid wall modifies the contact between the liquid and the solid. Wenzel's study on wetting on rough surfaces [24] is fundamental in chemical and physical properties of a solid surface contribute to its wetting behavior. He observed that a 'rough' surface will store more surface energy per unit area rather than a smooth one, and how this will affect its equilibrium contact angle.

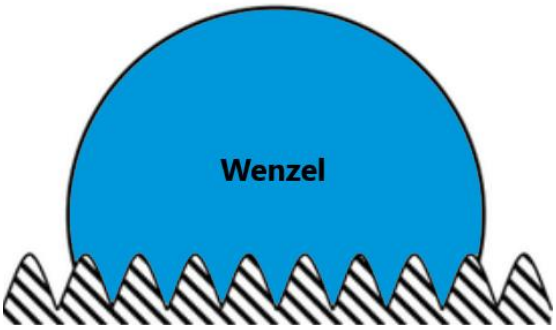

Fig 1.2.4.1 (a): Wenzel state of a liquid droplet residing on rough surface filling the grooves

Suppose that θ_W is the contact angle with the rough surface and θ the angle with the smooth surface (in both cases, the solid, liquid, and gas are the same). Assuming the size of the roughness is very small, so that the molecules of the liquid are macroscopically interacting with a plane surface but microscopically with a rough surface. Suppose a very small displacement of the contact line (fig. 1.2.4.1(b)).

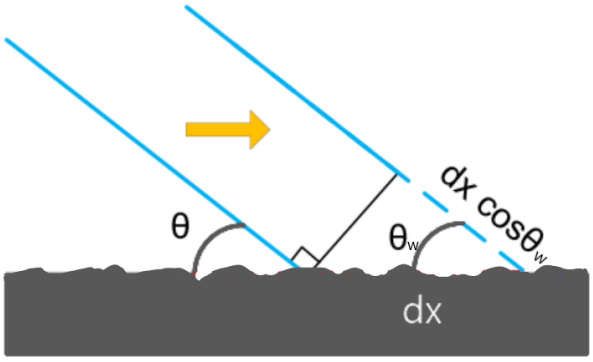

Fig 1.2.4.1 (b): Interface contact on a rough surface

Then the work of the different forces acting on the contact line is given by

$$dW = (\gamma_{sl} - \gamma_{sv})r\,dx + \gamma_{lv}\cos\theta_W\,dx$$

where *r* is the roughness, i.e., the ratio between the real surface area with the corresponding ideally smooth surface area, considering r > 1(for smooth surface), the change in energy is

$$dE = dW = (\gamma_{sl} - \gamma_{sv})\,r\,dx + \gamma_{lv}\cos\theta_W\,dx$$

Assuming an equilibrium state of the liquid drop after the small perturbation *dx*, it finally stops at a position where its energy is minimum, so that

$$\frac{dE}{dx} = 0$$

$$\gamma_{lv}\cos\theta_W = (\gamma_{sl} - \gamma_{sv})r$$

$$\cos\theta_W = r\cos\theta \qquad (1.5.2)$$

Hereby, it emerges from eq. (1.5.2) that in Wenzel state, the roughness actually increases the contact angle and thereby the wettability for the already hydrophobic surface ($\cos\theta < 0$), but decreases it for hydrophilic surfaces ($\cos\theta > 0$).

A drop will adopt a stable condition on a rough surface, giving it the option to switch between two states. The drop can fill the roughness structures as shown in Figure 1.5.2(a) and the state is called Wenzel state. Otherwise, the drop will find it difficult to penetrate the roughness structures because of the capillary forces of the liquid, and the effect is referred to as the Cassie-Baxter state which is discussed in the next section.

1.2.4.2 Cassie-Baxter state

The notion of roughness effecting the contact angle was extended by Cassie and Baxter in 1944 when they focused on porous mediums, where liquid does not penetrate the grooves on rough surface and leaves air gaps [25]. In this state the air is trapped in between the roughness structures, and thereby providing the drop to sit on the composite surface made of solid and air.

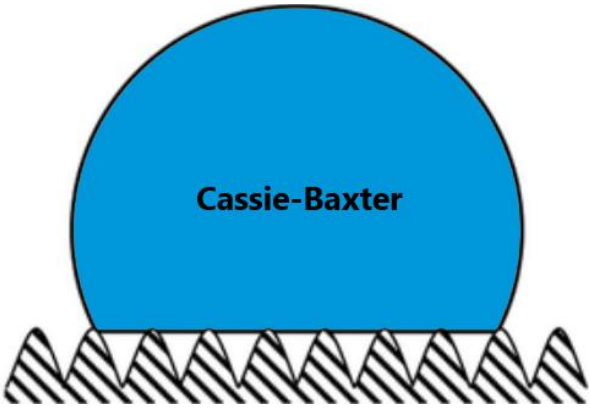

Fig 1.2.4.2: Cassie-Baxter state of a liquid droplet sitting on rough surface

As a matter of fact, the Cassie-Baxter apparent contact angle, θ will be equal to the average between the substrate contact angle θ and the contact angle with the air trapped between the solid protrusions θ_{air} =180°.

$$\cos\theta_{CB} = f_{sl}\cos\theta + f_{lv}\cos\pi$$

$$= f_{sl}\cos\theta - f_{lv}$$

The weights f_{sl} and f_{lv} are the fraction of the drop base in contact with the solid substrate f_{sl} and trapped air f_{lv} . This equation can be written as:

$$\cos\theta_{CB} = f_s \cos\theta - (1- f_s)$$

$$= f_s \left[\frac{(\gamma sv - \gamma sl)}{\gamma lv}\right] +1]-1$$

Here, 'f_s' is the Cassie roughness factor which represents the fractional contact area between the water and the solid surface. For a perfectly smooth surface, 'fs' will be equal to 1. And under these conditions Cassie-Baxter equation reduces to Young's equation.

1.2.4.3 Metastable State

There is a specific type of composite wetting condition that has been observed in which some liquid penetrates the cavities but does not reach the asperity's bottom. (Figure 1.5.4) As a result, there is still room between the bottom of the cavity and the base of the droplet. This intermediate wetting state is referred to as Cassie-Baxter composite or metastable state [26,27].

Fig 1.2.4.3: Liquid droplet in metastable state filling a small portion of the groove

1.2.5 Isotropic and Anisotropic Wetting

From previous discussion, we can recall that a liquid droplet, on a smooth homogeneous surface, tries to minimize its surface area to attain a spherical shape. In terms of contact angle (CA), measuring from any direction, it remains constant at the triple contact line. When it is identical when measured in any direction, the surface is said to be isotropic in its wettability. Due to isotropic geometry and chemical composition, there is no difference in the contact angle (CA) measured in any direction. On the contrary, when a liquid contact line comes into touch with the physical or chemical heterogeneity present in solid surfaces, anisotropic wetting happens. In case of anisotropic wetting, droplet shows distinct contact angles from particular directions while spreading or in movement on the surface. This includes both static (different static CAs in different directions) and dynamic (different sliding angles and directional movement) properties of droplet motion.

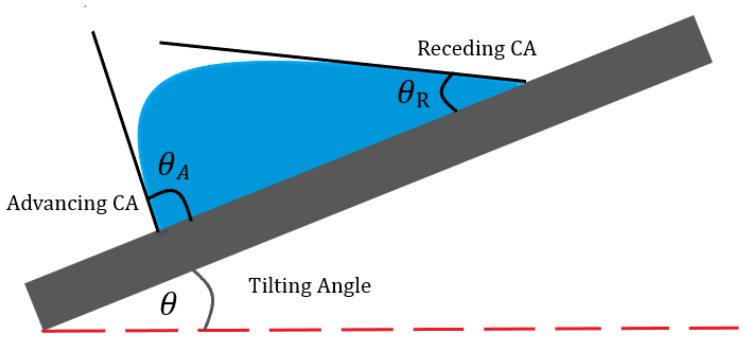

Fig 1.2.5.1: advancing and receding angle of a droplet

Liquids on inhomogeneous surfaces or structures exhibit anisotropic wetting behaviors as opposed to wetting of liquids on homogeneous surfaces because of driving forces created in particular directions. On a solid surface, external forces balance the forces acting on a stationary droplet. An imbalance of these external forces causes the driving force to surpass the resistance of the stationary droplet that initiates anisotropic wetting. Movement of the liquid droplet is obstructed by the resisting force F_R which originates from the contact angle hysteresis.

$$F_R \sim \pi R\gamma(\cos\theta_R - \cos\theta_A)$$

Where, R is the droplet radius, γ denotes liquid's surface tension, θ_R and θ_A depicts advancing and receding contact angle respectively. The outcome is that decreased contact angle hysteresis (CAH) encourages droplet directional mobility.

Talking about the direction of measuring/viewing the droplet and its contact angle, two particular different perspective of view can explain the anisotropic wetting clearly. First one is perpendicular view (orthogonal view), in the grooves perpendicular direction (fig 1.6). Contact angle measured from this view is called perpendicular / orthogonal contact angle $\theta_{\perp}$. the second one is parallel view along the groove's parallel direction and angle measuring from this angle is called parallel contact angle $\theta_{//}$.

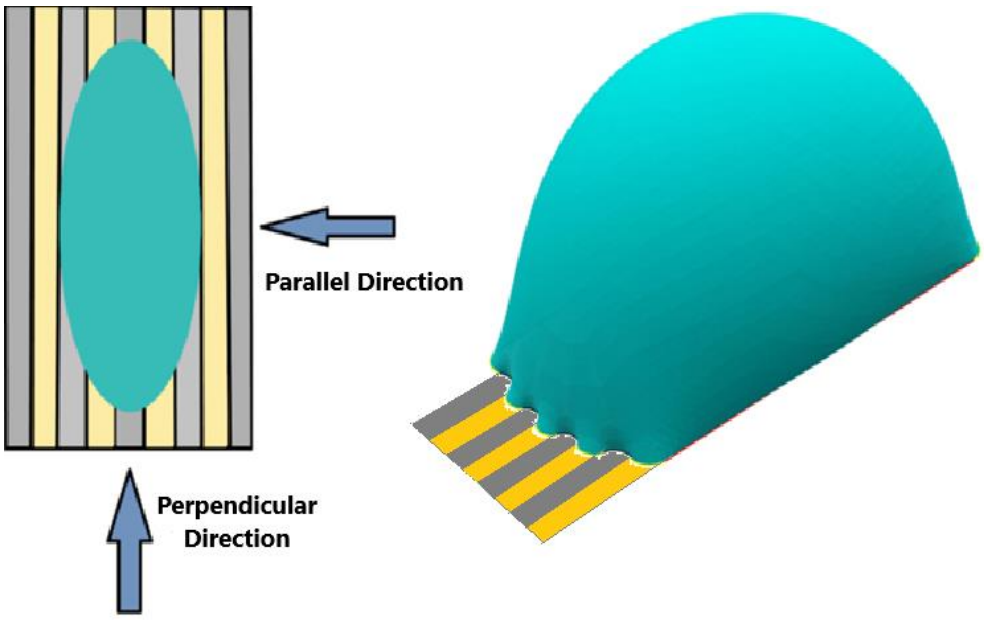

Fig 1.2.5.2: Parallel and Perpendicular viewing direction

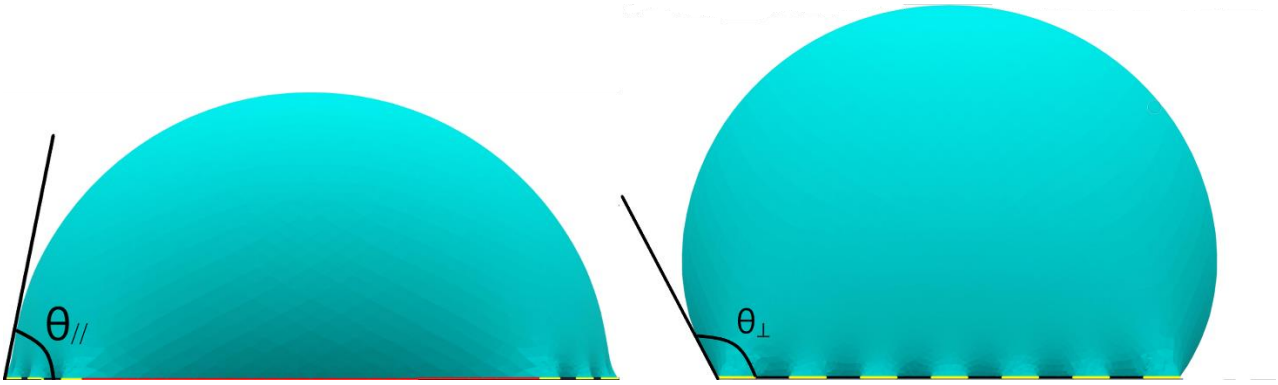

(a) (b)

Fig 1.2.5.3: (a) Parallel Contact Angle (b) Perpendicular Contact Angle

In general, either non uniform surface wettability (chemical heterogeneity) or asymmetrical geometric shapes (structural heterogeneity) of the solid surface results in for anisotropic wetting of a liquid droplet. This heterogeneity creates asymmetric energy barrier in different directions lead to anisotropic wetting phenomena of liquids. Due to this surface energy difference, liquid droplets on chemically heterogeneous surfaces tend to flow from side with lower to side with greater surface energy. In case of physical heterogeneity, the three-phase contact line is pinned at the edge of the pillar/groove edges when encounter a change in structural morphology and it goes perpendicular to the pillars or grooves due to the micro-grooved structures. The contact line pinned at the edge of the pillar due to the increase in surface energy. Because of this, a far higher energy barrier must be surpassed perpendicularly as opposed to expanding in the grooved direction or in the parallel direction. Thus, a liquid droplet spreading along the grooves was favored, producing an extended form. Detailed theory of anisotropic wetting on chemically heterogeneous (striped) will be discussed in the next section as out research is very much related to it.

Additionally, Combination of chemical and structural anisotropy can help us obtaining as well as comprehending unique and complex anisotropic wetting on natural and artificial surfaces as well as their applications.

1.2.6 Wetting on Chemically Striped surface

Liquid droplet on chemically inhomogeneous solid surfaces will be focused in our study. From mathematical point of view, this scenario exactly resembles the Cassie-Baxter model. For simplicity, we analyze the case of a solid surface consists of two different materials having alternating stripes. If θ_1 and θ_2 are the contact angles for each material at a macroscopic size, and f_1 and f_2 are the surface fractions of the two materials (fig. 1.2.6) and θ be the apparent contact angle, then the energy to move the interface by dx is:

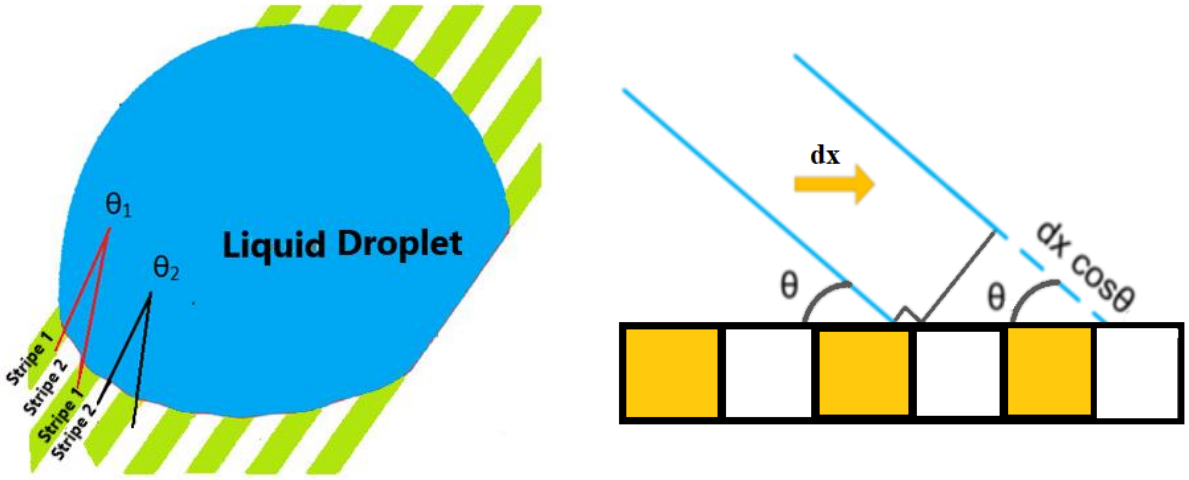

(a) (b)

Fig 1.2.6: (a)Liquid droplet on chemically stripe patterned surface with different surface energy and contact angle; (b) interface contact and movement on chemical stripe-pattern surface

$$dE = dW = (\gamma_{sl} - \gamma_{sv})_1 f_1\, dx + (\gamma_{sl} - \gamma_{sv})_2 f_2\, dx + \gamma_{lv} \cos\theta\, dx$$

at equilibrium, dE = dW = 0; thus, comparing with Young's angle it follows:

$$\cos\theta = f_1 \cos\theta_1 + f_2 \cos\theta_2;\ \text{where } f_1 + f_2 = 1$$

1.9 Outline of the Thesis

The primary goal of this dissertation is to establish a computational approach for analyzing liquid droplet anisotropy in wetting behavior residing on chemically striped surface with alternating (hydrophilic/hydrophobic) wettability. It focuses on developing a numerical method to examine the energetics, shape and wetting phenomena of liquid droplet based on wettability contrast and its implications on anisotropic wetting.

Chapter 01 elucidates the fundamental concepts and physics of wetting. Discussion related to wettability, surfaces, energy and other key parameters have also been elaborated through proper theoretical and mathematical approach. Final part of this chapter offers the purpose, motivation and potential of this research.

Chapter 02 reviews most pertinent experimental studies as well as several recent literatures on numerical wettability outcomes.

Following that, in **Chapter 03**, detailed modeling and formulation of computational approach have been discussed. Based on surface morphology and liquid droplet physics, a numerical methodology has been developed to simulate liquid droplet's shape on alternating (hydrophilic/hydrophobic) wettable surface. An open-source interactive program "Surface Evolver" that studies surface related phenomena taking into account surface tensions and related energies has been used as a numerical tool in our study. This chapter also provides a thorough description of the precise steps involved in this computation approach.

In **Chapter 04**, major findings from this study have been thoroughly documented and discussed. Finally, in **Chapter 05**, conclusions from each of the chapters are summarized and future recommendations are suggested.

Chapter 02

Literature Review

Researchers have long been intrigued by the possibility of using surfaces with unique wettability. This interest has intensified with the development of manufacturing and fabrication techniques (micro/nano), since man has developed the capacity to produce surfaces with unique types of wettability in accordance with his needs. However, in nature, these types of surfaces with chemical or physical roughness are frequently present for controlling the interactions between solids and liquids. Lotus leaf has become archetypes for its distinctive behavior such as superhydrophilicity and self-cleaning properties [29,30]. The papillose epidermal cells, which produce asperities or papillae, are what give leaves their rough texture. As a result, it exhibits distinctive quality of self-cleaning due to its contact angle with water of over 160^{o} and critical sliding angle of less than 5^{o} [31].

Lotus leaf is not the only member in nature to shows this kind of properties. Micro structured papillae on rice leaves are positioned parallel to the rice leaf edge, allowing droplets to roll easily in this direction and pin along the perpendicular one thus making the surface similar to lotus leaf [32]. However, it is different form lotus leaf from the viewpoint of their arrangements of micro-papillae with nano-protrusions resulting parallel sliding angle 3^{o} and perpendicular sliding angle $9^{o.}$ Similar to this, the orderly alignment of the leaf veins in bamboo leaves results in elliptical-shaped water droplets. [33].

Not only plants and leaves, animals and insects also exhibit particular wetting properties to adopt in nature. Superhydrophobic nature of butterfly's wings help them from sticking together in contact of water [34]. With hydrophobic bumps and hydrophilic groove channel, Namibian beetles condense for from humid air and direct them to their mouth in desert area [35].

Numerous anisotropic wetting surfaces have been created by adding physical asymmetry or chemical heterogeneity in an effort to mimic the unique anisotropic wettability of biological surfaces seen in Mother Nature. The most used method for surface patterning is photolithography, which creates patterns using the right light source, mask, and photoactive material. This method is used to generate hydrophobic-hydrophilic patterns on variety substrates [36-38].

For effective fog-collection, Bai et al. created superhydrophobic-superhydrophilic surfaces by using a photomask to selectively illuminate UV light [39]. Fabricating patterned surface by inkjet printing technology is a very complex method. Based on basic inkjet printing technique, Zhang et al. created biomimetic superhydrophobic surfaces with micro-sized hydrophilic patterns for water collection [40].

In a different work, Lai et al. achieved ink-regulated adhesion switching on superhydrophobic TiO2 nanotube arrays by site-selective alcohol-based ink patterning, and they showed how the technique might be used for droplet manipulation and gas sensing [41]. On a super hydrophilic surface, Geng et al. produced two-dimensional hydrophobic barriers with an asymmetrical pattern via inkjet printing. Such surfaces with asymmetric chemical heterogeneous patterns may achieve unidirectional liquid spreading [42].

Directional wettability, or the modification of wetting characteristics based on the orientation of the surface, can be produced by anisotropic surface texturing. To incorporate anisotropic liquid behavior on diverse types of surfaces, numerous investigations on directional wettability have been carried out. Bikerman noted the anisotropic behavior of liquid on a surface with parallel grooves, where the droplet was stretched in the direction of the grooves [43]. A relationship between the surface texture parameter and anisotropy was developed by Hitchcock et al. [44]. This parameter measured the relationship between the average amplitude and wavelength of the surface characteristics. By experimentally observing wetting properties on three different types of polymers, Sung et al. demonstrated in 1989 that surface roughness and topology, rather than molecule orientation, are the primary parameters responsible for anisotropic wetting behavior [45]. In addition to experimentally proving the substrate's superhydrophobicity, Chen et al. examined and characterized anisotropic wetting of an inherently hydrophobic PDMS surface modified by parallel microgrooves [46]. They developed a numerical model for the ultimate elongated liquid droplet form, assuming both elliptical and cubic contact lines.

Feng et al. discovered anisotropic behavior in the natural product known as "rice leaf," where a droplet can migrate in a certain direction while maintaining anisotropic dewetting characteristics due to the arrangement of micropapillae on that particular surface.[47]. By aligning carbon nanotubes on a surface, they then mimicked this process. This surface was discovered to have a similar type of droplet unidirectional movement, which provides a foundation for the development of regulated wettability in the future.

By adjusting the surface geometry and roughness, Rahman and Jacobi conducted a series of experiments on the anisotropic wetting, frosting, and melting of parallel rectangular micro-grooved brass surfaces. [48-50]. They machined parallel micro-grooves on the four series of brass alloy surfaces, three of which had constant pillar and groove width and another had constant groove height.[48]. In every case, the measured contact angle hysteresis was substantially smaller along the grooves than it was across them. As a result, the droplet's Cassie wetting behavior, which was caused by a significant variation of advancing contact angles measured between orthogonal and parallel groove orientations, was shown to have wetting anisotropy of contact angle hysteresis in the 7° to 48° range. These effects had been discussed for the static contact angle difference between the orthogonal and parallel directions of the groove in their prior study. [49]. In the absence of chemical alterations, they created the brass surface with parallel rectangular micro-grooves using the same surface processing and roughening processes, but with different geometry for the groove width, pillar width, and pillar height. Droplets having lower parallel contact angle for stretched along the grooves and sunk down the grooves were the main reason for Wenzel droplets having higher rate of elongation ratio, while Cassie droplets had shown almost circular shape, resulting in less anisotropy. Nazia et al. numerically obtained the apparent contact angles showing anisotropic wetting for eight parallelly rectangular micro-grooved brass surfaces with groove parameters variation and compared with the experimental values, which had been found in a good agreement [51]. He et al. proposed a theoretical model for analyzing the sliding behavior based on the concept of adhesion energy [52] where different sliding behavior in parallel and perpendicular direction attributed to the adhesion energy per unit area.

On rough substrates, Patankar et al. considered the modeling of hydrophobic contact angles for wetted and composite contact [54]. They proposed a design to develop a rough superhydrophobic substrate that accounts for multiple equilibrium drop shape. They also studied the anisotropy

wetting of rough surfaces and reported multiple equilibrium shape on a rough surface with parallel grooves [55]. Fixing the number of pillars, they found is convenient to explain the anisotropy effect. In another experimental work, they depending on the formation of droplet, there can be two contact angles and established a design criterion for a robust hydrophobic rough surface. [56]

For alternating wavy and micro-V-grooved rough surfaces, Ikram et al. compared droplet energetics on similar topographic scale and reported that micro-wavy surface offers small stable droplets as well as higher wettability [57]. A journey towards isotropic region for higher intrinsic contact angle is another significant finding of their work.

Anisotropic wetting is significantly influenced by stripes and similar structures. Ellipsoidal-shaped drops appear on stripe bases configurations. Viewing directions are of two kinds for this kind of anisotropy: parallel and perpendicular. An extensive review of germane literature of chemically patterned surfaces have been discussed in previous chapter [8-15, *]. Dupuis et al. investigated droplet dynamics on patterned substrates by exploring the spreading of droplet on chemically and topologically patterned substrates using lattice Boltzmann algorithm [58]. A final result of his work was to model the water collection of Namibian beetles from wind. Azimi et al. proposed a novel continuum model of static and dynamic CAs on micro patterned hybrid surfaces. [59] They offer a slip boundary model based on Navier -Stokes equation to establish a realistic continuum approach to simulate the 3-D contact line dynamics. This proposed model has a good agreement with static and dynamic wetting phenomena observed in experimental studies.

Chapter 03

Computational Approach

3.1 Introduction

The primary goal of this chapter is to provide an in-depth explanation of the computational approach that was used to develop the numerical model to simulate and predict the wetting behavior of three-dimensional liquid droplet on a chemically heterogenous surface having alternating hydrophobic/hydrophilic stripes. The creation of these models enables researchers to analyze properties of the liquid droplet that are difficult or implausible to study through experimental methods The wetting characteristics of liquid droplets for chemically heterogeneous surfaces have been modeled, developed, and analyzed using the interactive and extensively used numerical tool "Surface Evolver," which will be comprehensively covered in the following sections.

3.2 Surface Evolver

Surface Evolver is a public domain software package developed by Professor Kenneth A. Brakke for geometry based supercomputing projects funded by National Science Foundation [22]. It is an interactive, finite-element based application for investigating surfaces that are shaped by surface tension and other energies and are subjected to different constraints. This program uses gradient descent approach to evolve the surface toward minimal energy state. Reducing the system's free energy to create the equilibrium liquid droplet form is the foundation of Surface Evolver's numerical method. The algorithm initiates with a user defined data file(.txt) that contains all mathematical information about the energies, geometry and surface. Then gradually it develops the surface towards a minimum energy state according to the provided information. The surface evolver documentation contains comprehensive information about the theoretical background and simulation techniques employed in this software [61].

3.3 Model Formulation

Our model needs to develop a three-dimensional liquid droplet placed on a surface that is chemically heterogenous with altering hydrophilic hydrophobic stripes. Both the liquid drop and solid surface are exposed to the ambient fluid: in our case which is air. also, we assume that the liquid and the fluid are mutually immiscible. Surface energy (E_s) and gravitational force (F_g) are two that acts on the liquid drop, though whether the latter force will act depends on the size of the droplet. Thus, the total energy of the surface is the sum these two energies: free surface energy (E) and gravitational energy (E_g). However, gravitational effects are not taken into account in our model since the typical research droplets (10 μL or less in volume) are too small to be affected by gravity. This type of sufficiently tiny liquid droplet is called "sessile droplet". Therefore, in this scenario, we merely focus on the surface tension of the liquid and its interaction with the substrate surface. Total interfacial energies can be expressed as follows:

$$E = \iint_{A_{lv}} \gamma_{lv} dA + \iint_{A_{Sl}} \gamma_{sl} dA + \iint_{A_{sv}} \gamma_{sv} dA \tag{3.1}$$

Where, surface tension between the liquid-solid, liquid-gas, and solid-gas phases are indicated by γ_{sl}, γ_{lv}, and γ_{sv}, while A_{sl}, A_{lv}, and A_{sv} designate the interfacial or contact area between liquid-solid, liquid-gas, and solid-gas phases, respectively.

The intrinsic contact angle θ of the surface material can be determined as per Young's equation in equation 1.10 from the horizontal force balancing of tensions at the interface at the three-phase contact line.

$$\gamma_{sv} - \gamma_{sl} = \gamma_{lv} \cos\theta \tag{3.2}$$

From eqn (3.1) and (3.2) we can obtain,

$$E = \gamma_{lv} \left[A_{lv} - \iint_{A_{sl}} \cos\theta \; dA \right]$$

$$E/\gamma_{lv} = A_{lv} - \iint_{A_{sl}} \cos\theta \; dA \tag{3.3}$$

This equation states that to achieve equilibrium drop shape, the free energy (E) of a droplet with constant volume needs to be minimized. It also shows that, since the free energy is minimized with respect to the form of the liquid-air interface, the intrinsic contact angle (θ) is the sole factor that impacts the equilibrium drop shape on a surface. As E/γ_{lv} is minimized throughout the process, in our situation, the only parameter we need to be concerned with is intrinsic contact angle.

3.4 Model Development and Mathematical Description

Surface Evolver (SE) is a simulation tool that moves a liquid droplet closer to the minimal energy state condition, however it is unable to help with model design or development. It needs an initial input file that contains the mathematical formulation of the model. The user must define this model using a .txt file of appropriate format (. fe) by mentioning the vertices, edges and faces chronologically. In three-dimensional co-ordinate system, a vertex is a spatial point that points out the location of the surface on a plane. Changes in the coordinates of the surface lead to surface evolution. On the other hand, and edge is a one-dimensional geometric feature linking two vertices. A facet is a flat triangle having three parallel sides with respect to each other. An ordered collection of three or more edges are defined as face. Then, geometric, energy and volumetric constrains are applied according to the model. In our model, where liquid droplet resides on chemically inhomogeneous surface with alternating hydrophobic/hydrophilic stripes will follow the Cassie-Baxter wetting state that will experience two different interfacial energy domains at base having two different contact angles.

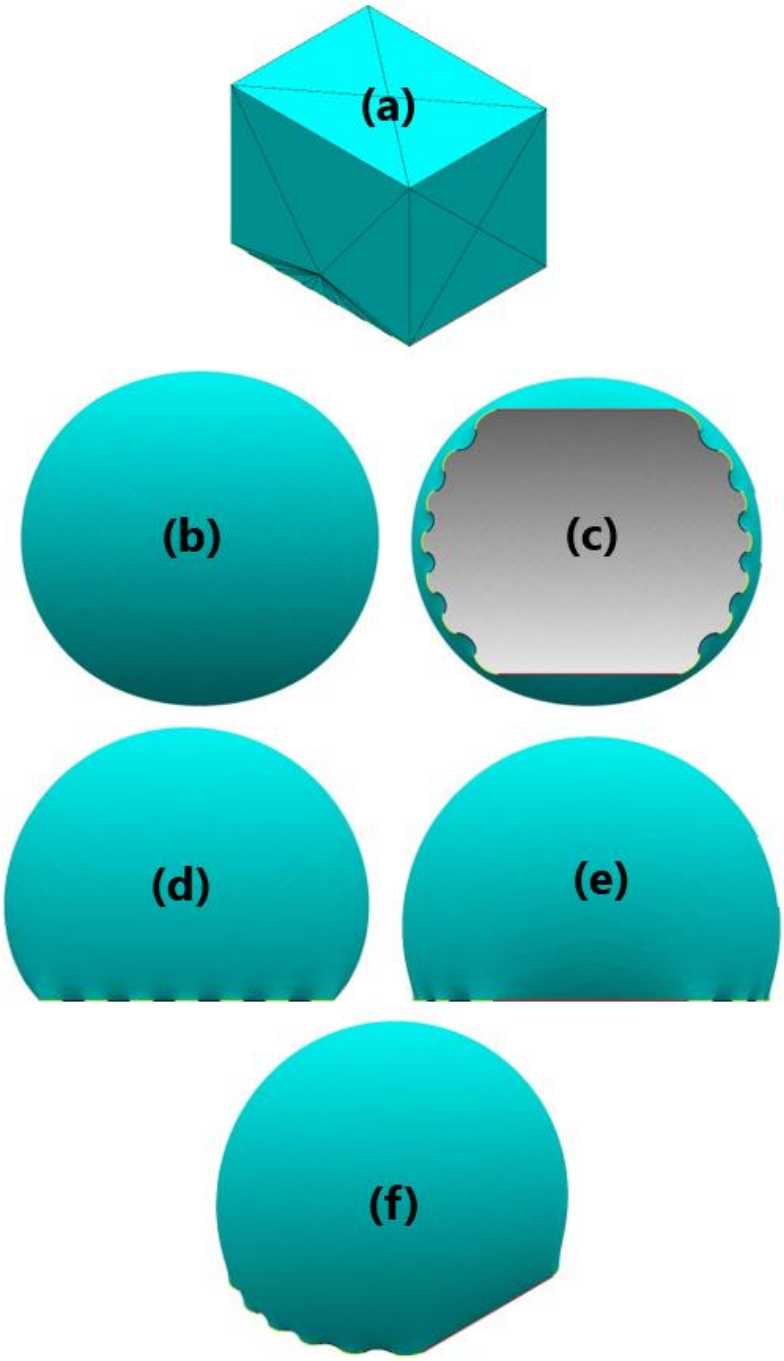

Fig: 3.4.1 (a) initial cube (b) bottom view (c) top view(d) front view (e) side view (f) isometric view of a liquid droplet in surface evolver

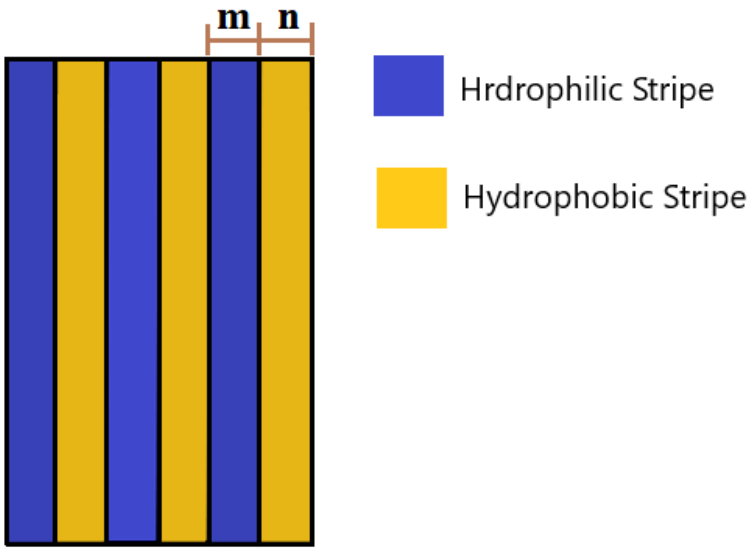

Fig : 3.4.2 : hydrophilic / hydrophobic stripe model

The initial geometry of the droplet comes as a form of a cube with most possible smallest mesh size (fig: 3.4.1 (a)). Simulation process continues with a series of iterations until the energy of the system reaches a desired value that doesn't vary at a large scale anymore. This is the condition of convergence that this algorithm always seeks to fulfill. Constrained vertices keep their position fixed whereas vertices in contact with liquid air interface adjust their position at every iteration step to minimize the energy of the system within given parameters. With successful mesh refinement and iteration steps initial model evolves into desired drop shape.

SE represents bodies by enclosing triangles with facets oriented along the surface normal. According to Brakke, the surface energy is defined as $-\gamma_{lv}\cos\theta$ for the top face of the chemical stripe surface, which corresponds to the material's intrinsic contact angle (θ) [42,43]. There are no restrictions on the vertex coordinates of the surface's striped areas, where the liquid-air contact was seen during the formation of the initial cubical droplets. Only the boundary vertices of the striped are constrained so that the droplet doesn't leave the striped area. As we already know that in Cassie state, droplet will not fully fill the groove cavities whereas, in case of Wenzel wetting, no air-gap will be found inside the asperities. In our case, the Cassie model will be considered for

striped surface. Green's Theorem is applied to the assessment of surface energy at the interface faces of solid-liquid of striped surface, which results in the transformation of a surface integral to a line integral, which is along edges of the three-phase contact line, because of this transformation.

Now, vector field $\vec{w}$ can be determined such that,

$$\iint_{face} T\vec{k} \,.\, d\vec{S} = \int_{edge} \vec{w} \,.\, d\vec{l} \tag{3.4}$$

Where, T is the surface tension per unit length which can be rewritten from Young's equation as:

$$T = -\gamma_{lv} \cos\theta \tag{3.5}$$

Now, from Stoke's theorem, we can say that:

$$Curl\, \vec{w} = T\vec{k}$$

Or, $\nabla \times \vec{w} = T\vec{k}$

$$\begin{bmatrix} \vec{\imath} & \vec{\jmath} & \vec{k} \\ \partial/\partial x & \partial/\partial y & \partial/\partial z \\ w_x & w_y & w_z \end{bmatrix} = T\vec{k} \tag{3.6}$$

So, for the surface energy at a horizontal face in contact with a stripe, $\vec{w} = -T_y\vec{\imath}$ or $\vec{w} = -T_x\vec{\jmath}$ can be utilized like:

For, $\vec{w} = -T_y\vec{\imath}$,

$$\begin{bmatrix} \vec{\imath} & \vec{\jmath} & \vec{k} \\ \partial/\partial x & \partial/\partial y & \partial/\partial z \\ -T_y & 0 & 0 \end{bmatrix} = T\vec{k} \tag{3.7}$$

For, $\vec{w} = -T_x\vec{\jmath}$,

$$\begin{bmatrix} \vec{\imath} & \vec{\jmath} & \vec{k} \\ \partial/\partial x & \partial/\partial y & \partial/\partial z \\ 0 & -T_x & 0 \end{bmatrix} = T\vec{k} \tag{3.8}$$

In this way, contact surface energy in line integral form around three-phase contact line, which is constrained by the surface of each stripe along with its inclined walls, can be attained.

3.5 Meshing and Convergence

Compared to many other finite element programs, Surface evolver differs in that the mesh is changed after each iteration. Determining convergence and the final result's accuracy might be challenging. A triangular tessellation is used by Surface Evolver to represent surfaces, and it can be gradually improved to obtain the necessary level of precision. By iteratively changing vertices within a set of constraints, the Newton-Raphson method is utilized to quickly bring the energy of the surface to a local minimum. Hills, valleys, and passes can be seen on the graph of the energy function, which is reminiscent of a hilly region. Consequently, E, the gradient of the energy function, can be regarded as the steepest upward direction. Up until a local minimum is reached, the Evolver reduces energy by moving downward, or in a negative gradient direction. Iteration, refinement, vertex averaging, and trimming of unusually long edges produced during refinement are the steps of simulation that must be manually entered by the user because Surface Evolver does not automate the simulation process. Starting with a rough mesh, the simulation gradually fine-tunes and averages the vertex counts until it achieves the eventual. Iterations continue until there is little to no energy change in the system. After refining and iterations, vertex averaging is frequently carried out to ensure that the vertices. For the model generation procedure to yield the best results, the simulation phases are set as user-defined Identifiers. Each identifier contains information about the amount of refinement, mesh modification, vertex averaging, and the number of iteration steps necessary for the level of refinement. The simulation's procedures can be carried out using these user-defined identifiers, which facilitates and speeds up completion.

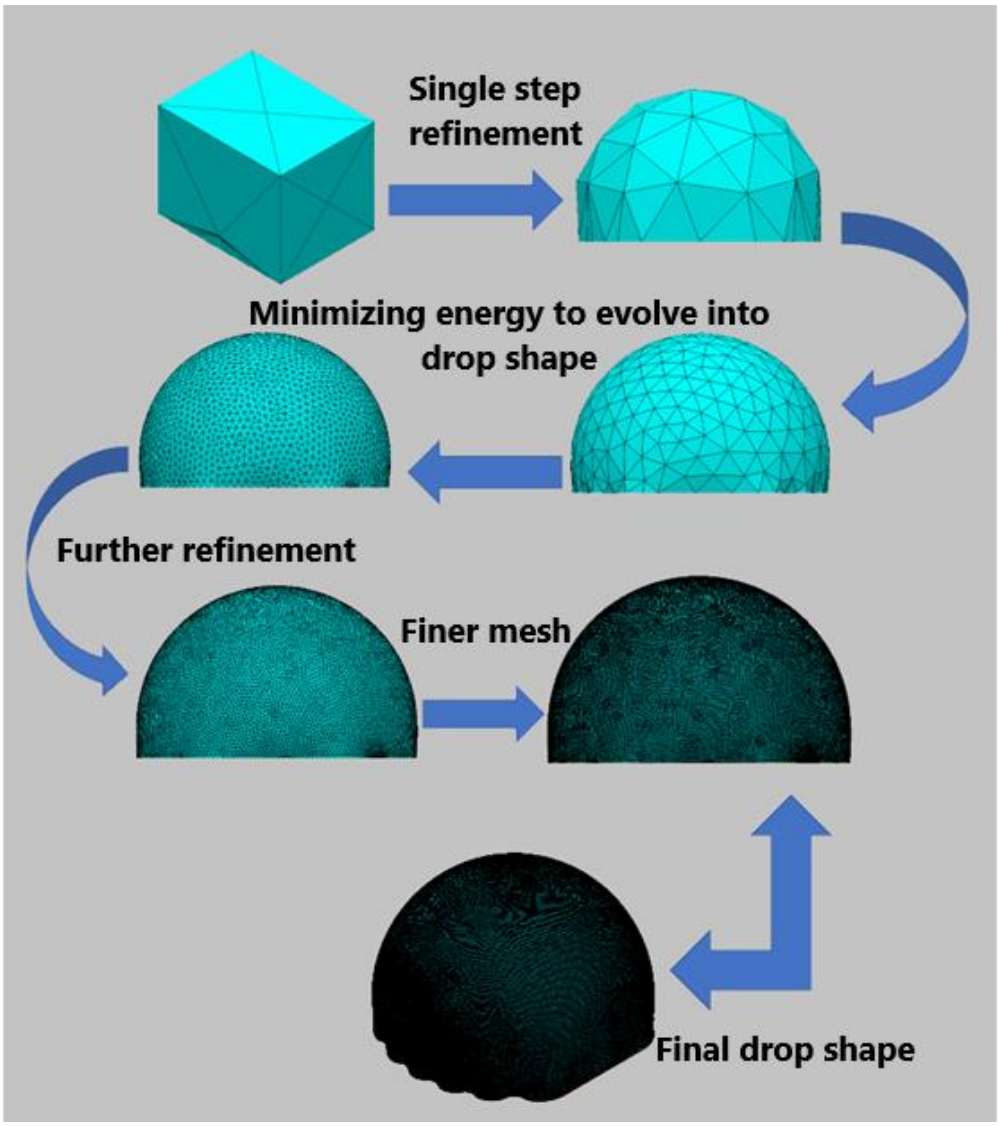

Fig 3.5: Simulation procedure in a chronological order in which droplet approaching towards its ultimate equilibrium shape by attaining minimized energy state by necessary refining and meshing

3.6 Post Processing Operation

Post-processing is required to gather sufficient data once the simulation process in Surface Evolver is complete, particularly contact angles from the equilibrium droplet shape deposited on micro size rough surfaces. The completed droplet's image is first exported as an .eps file and saved in a folder. After being extracted from that particular file, the droplet's image was then saved in jpg format (.jpg file).

The apparent contact angles of the liquid droplets were measured using "ImageJ," a Java-based free and open-source image processing program. This tool was widely used by researchers to calculate the contact angles of droplets.

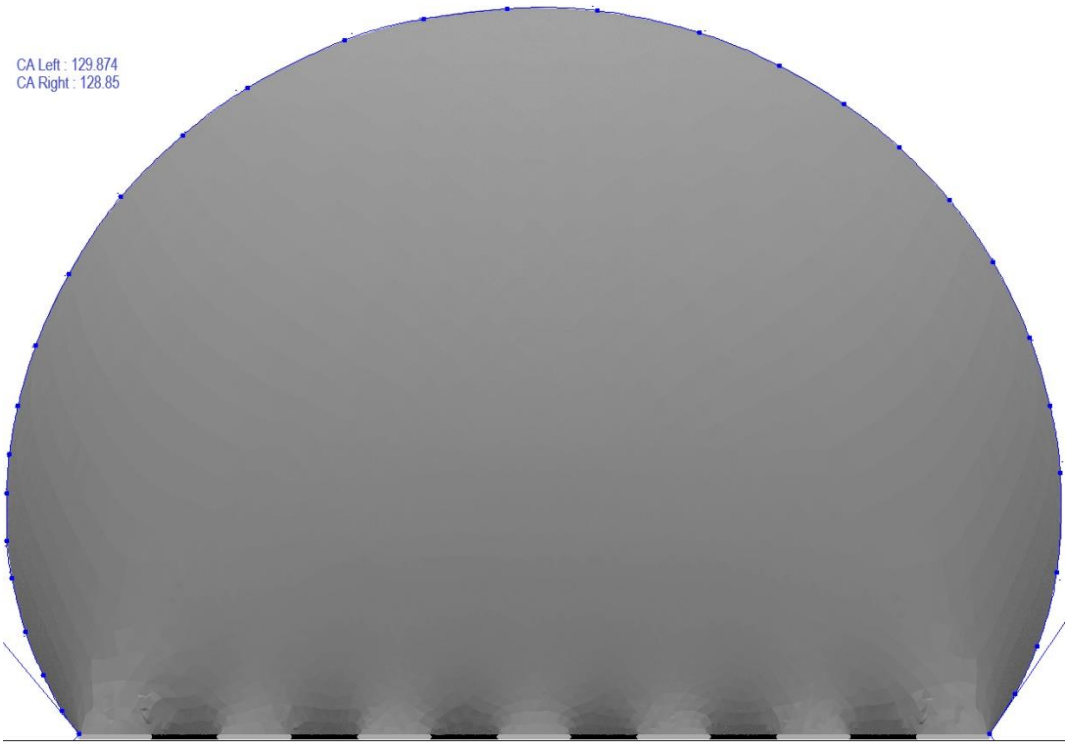

Fig 3.6: Dropsnake plugin to measure contact angle of a droplet in Imagej

3.7 Validation of the Developed Model

The created model was tested against the respective experimental work of Shi et al. [19] on micro-machined parallel grooved surface and Rahman et al. [49] on parallel grooved surface. Droplet on parallel grooved surface is closely analogous to chemically stripe surface if they are at complete Cassie-Baxter wetting State.

Shi et al. fabricated the substrate with intrinsic contact angle 80^o and considered Cassie-Baxter wetting having parallel grooves that are considered to have 180^o as contact angle. They used 2 μL of water droplet for the study.

Rahman et al used brass surface having intrinsic contact angle of 67.5^o and volume of droplet was 5 μL. They also investigated Wenzel wetting as a result of pillar's aspect ratio (D_g/W_g) effect, but in our simulation, they were ignored due to our methodology.

Results found in our model are in good agreement with the experimental works. The SE model findings showed a maximum variation of 2% Shi et al. experimental data Table 3.8.1 There is a visible consistent deviation (6-10%) from Rahman et al. experimental data Table 3.8.2 because, in that experiment groove depth played a huge role on contact angle. Also, there were metastable state of droplets. But in our simulation, droplet is considered totally in equilibrium perfect Cassie-Baxter state. Red values in parenthesis indicates the deviation of our numerical result from experimental investigation.

Table 3.8.1: Validation of the developed model using the experimental data of Shi et al. [19]

Volume	Pillar Width (μm)		Θ_{phobic}	Θ_{philic}	Exp. Perpendicular angle	Exp. Parallel Angle	Perpendicular angle from present simulation	Parallel angle from present simulation
	Philic	Phobic						
2 μL	50	100	80	180	138 ±4	109±2	140.53 (1.83%)	110.5 (1.37%)
	75	100	80	180	137±3	105±3	138.72 (1.26%)	106.2 (1.14%)
	100	100	80	180	136±5	102±4	134.32 (1.32%)	104 (1.96%)
	125	100	80	180	131±6	100±3	130.07 (0.7%)	101.6 (1.6%)
	150	100	80	180	128±4	98±4	127.08 (0.72%)	100 (2.04%)

Table 3.8.2: Validation of the developed model using the experimental data of Rahman et al. [49]

Sample Width (μm)			Intrinsic contact angle	Exp. Perpendicular angle	Exp. Parallel Angle	Numerical Perpendicular angle	Numerical Parallel angle
Groove Width	Pillar Width	Groove Depth					
130	80	67	67.5	144.88	124.02	155.12 (7.06%)	115.5 (6.86%)
130	110	67	67.5	145.66	85.2	157.71 (8.27%)	83.23 (2.26%)
130	187	67	67.5	142.94	115.51	154.85 (8.33%)	110.48 (4.35%)
130	112	67	67.5	145.66	85.2	155.01 (6.42%)	85.36 (0.187%)

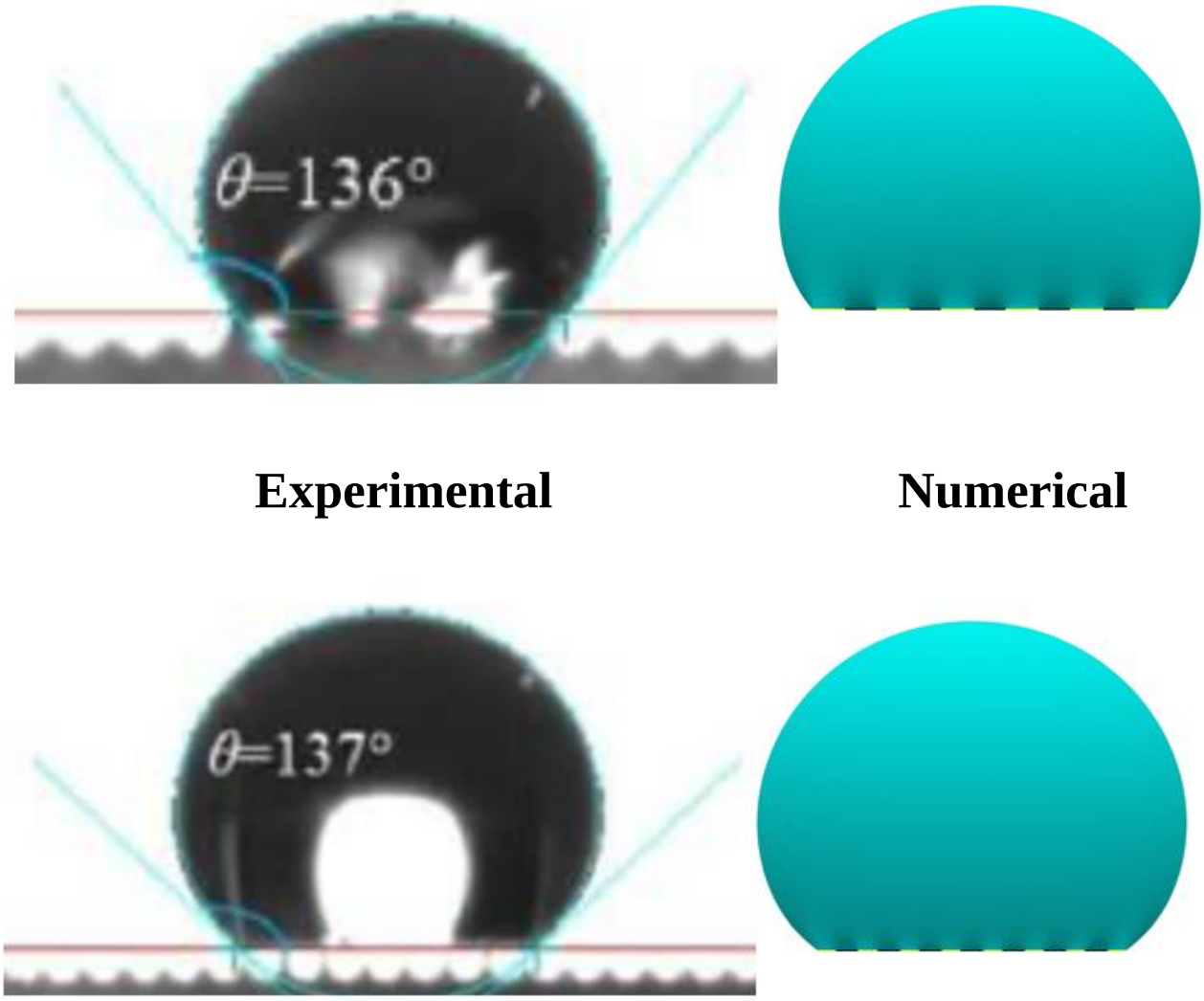

Fig 3.7: Validation of numerical results from SE of Shi et al. [19]

Chapter 04

Result and Discussion

4.1 Introduction

Depending on the morphology of a surface wetting physics and state differ from one to another. In a smooth ideal surface, depending on the surface energy, wetting may occur fully, partially or leave it in an un-wetting state with a distinct contact angle. However, in real, uneven and rough surfaces liquid behaves otherwise. In that case, contact angle doesn't have a unique value rather it depends on the viewing orientation. If measurement of contact angle remains independent of this viewing orientation, it is referred to as "isotropic" wetting. Otherwise, it is known as "anisotropic wetting". Anisotropic wetting offers two distinct kind of viewing angle: parallel angle or side view or view along the groove direction and perpendicular angle or front view or view across the groove direction. Anisotropy happens when some asperity, roughness or oriented geometrical morphology is introduced in a surface such as micro pillar, micro groove, chemical stripe patterned, circular or V groove etc. In such cases, the angles are not equal rather perpendicular angle is greater than parallel angle. Difference between these two angles is known as degree of anisotropy.

Our area of research interest lies in anisotropic wetting. To be more specific, we are interested in chemically inhomogeneous surface comprised of alternating wettability. Chemically striped surface offers a strong anisotropy depending on the hydrophilic and hydrophobic portion's characteristics. Physically it is analogous to microgrooved surface where liquid is in Cassie-Baxter state of wetting. However, microgroove possesses more roughness factor due to height and sharp edges compared to chemically striped surface.

A significant number of experimental and numerical studies have been reported regarding anisotropy wetting on microgrooved and chemically striped surface, very few of them focused-on wettability contrast and how it affects wetting of a surface. In this study we will focus on numerical

analysis of wettability on chemically stripe patterned surface having a wide range of wettability contrast. We analyzed our studies using a numerical tool "Surface Evolver "– a program designed for exploring surface related phenomena [22].

We considered Hydrophilic Angle, $\theta^{o}_{philic} = 80^{o}$, Hydrophobic Angle, $\theta^{o}_{phobic} = 100^{o}, 140^{o}, 180^{o}$; Hydrophilic Stripe width, m = 75 µm , 100 µm , 125 µm ; Hydrophobic Stripe width, n = 100 µm. Considered wetting conditions are mentioned below Table 4.1.

Table 4.1 The wetting scenarios considered in the present study

Case	Hydrophilic Angle, θ^{o}_{philic}	Hydrophobic Angle, θ^{o}_{phobic}	Hydrophilic Stripe Width, m (µm)	Hydrophobic Stripe Width, n (µm)
(i)	80	100	75	100
(ii)	80	100	100	100
(iii)	80	100	125	100
(iv)	80	140	75	100
(v)	80	140	100	100
(vi)	80	140	125	100
(vii)	80	180	75	100
(viii)	80	180	100	100
(ix)	80	180	125	100

We focused on the energetics, stability, anisotropy, shape and spreading of droplet under various geometrical and morphological configurations surface. For this purpose, a varied number of stripe configurations (9,11,13,15,17) have been considered in our numerical simulations. Figure () depicts Moreover, a comparison with microgrooved surface have been carried out to analyze the roughness effect.

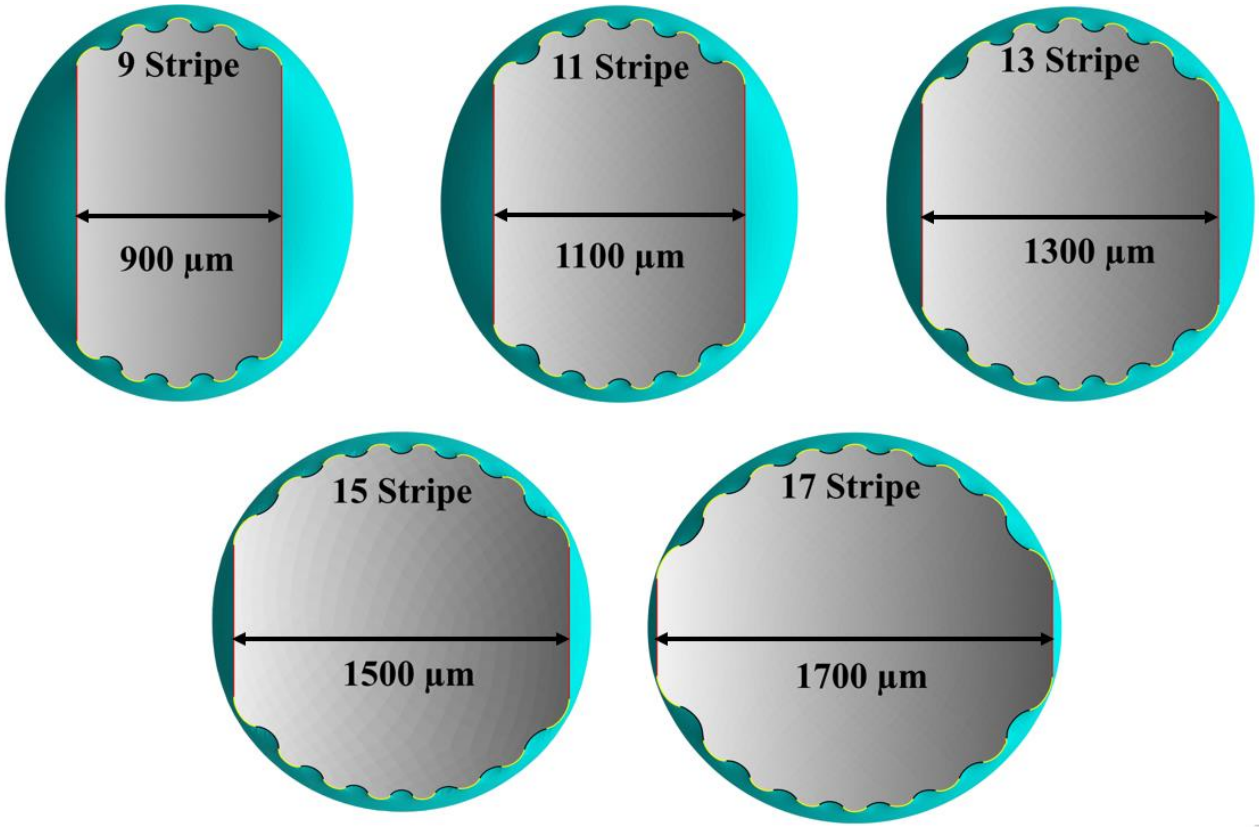

Fig 4.1.1: droplet of volume 2 µL on five different stripe configurations (9,11,13,15,17)

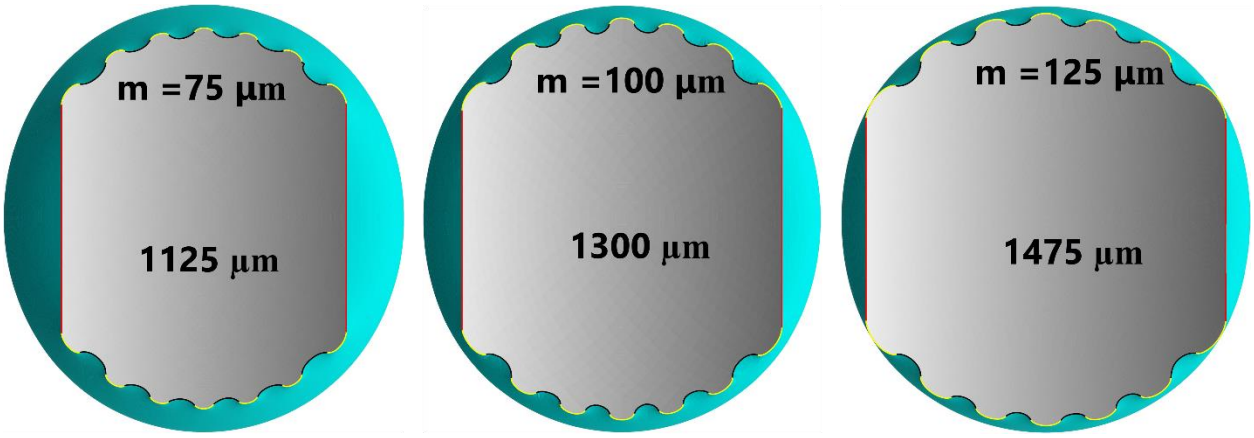

Fig 4.1.2: droplet of volume 2 µL on different hydrophilic stripe configurations (75 µm, 100 µm, 125 µm)

4.2 Analysis of Droplet Energetics

Interfacial energy, potential energy, and line tension are supposed to make up the majority of a system's free energy. However, potential energy and the effects of the line tension have little bearing on the overall system energy. Thus, the system's total free energy may therefore simply comprise the interfacial energies. The circumstances under which a stable equilibrium wetting state develops are determined by the interfacial energy of the contact surface between a solid substrate and a liquid droplet.

In order to fully understand the energetics of droplets, it is necessary to understand how the shape and energy of a liquid droplet change in respect to its size or volume and the roughness of its surface. Our area of interest is chemically striped surface with alternating wettability. If the surface is smooth enough, the three-phase contact line deforms according to the intrinsic contact angle only showing no anisotropy but in a patterned surface with different surface energies the three-phase contact line exhibits a wave like shape where convex and concave parts are located on hydrophilic and hydrophobic stripes respectively.

We can announce the surface energy that needs to be decreased to achieve an equilibrium droplet shape as follows based on our prior study of energetics:

$$E = \gamma_{lv} [A_{lv} - \iint A_{sl} \cos\theta \, dA] \quad (4.1)$$

For a droplet of constant volume, we can use this term to study stability on a surface on patterned surfaces that we already discussed in pervious chapter. However, normalized energy is the most practical when examining this dimensionless energy for all metastable drops of varied volumes. The previously mentioned interfacial surface energy can be written in the following manner as a normalized form if V signifies the volume of the liquid droplet. [14].

$$E_{norm} = E/\gamma_{lv} (V^{2/3}) \quad (4.2)$$

Normalized energy on a smooth flat surface is unaffected by droplet size and intrinsic contact angle. Fig 4.2(a) represents the unchanged normalized energy on flat surface having intrinsic

contact angle 70^o and 140^o. Fig 4.2(b) & 4.2(c) shows the bottom, side and isometric view of the droplets of different size and volume. For a specific intrinsic contact angle (θ) of 70° (hydrophilic) and 140° (hydrophobic), normalized energy has a fixed value of 4.84 and 7.58, respectively, for all droplet volumes on smooth flat surfaces, as illustrated in Figure 4.2(a). From this graphical illustration, it is clear that normalized energy value will be higher for larger intrinsic contact angles, i.e., lower surface energy will represent higher normalized energy value. Figure 4.2(b) and 4.2(c) depict the scenario of droplet spreading on both of these hydrophilic and hydrophobic flat surfaces for two different droplet sizes 1 μL, and 3 μL).

All numerical calculations from the Surface Evolver simulation assume that the water-air interface's surface tension is 0.072 N/m at 25°C. However, in chemically striped surface having different surface energy doesn't exhibit volume independency rather it hits a minimum value. Details of this analysis will be discussed in the next section.

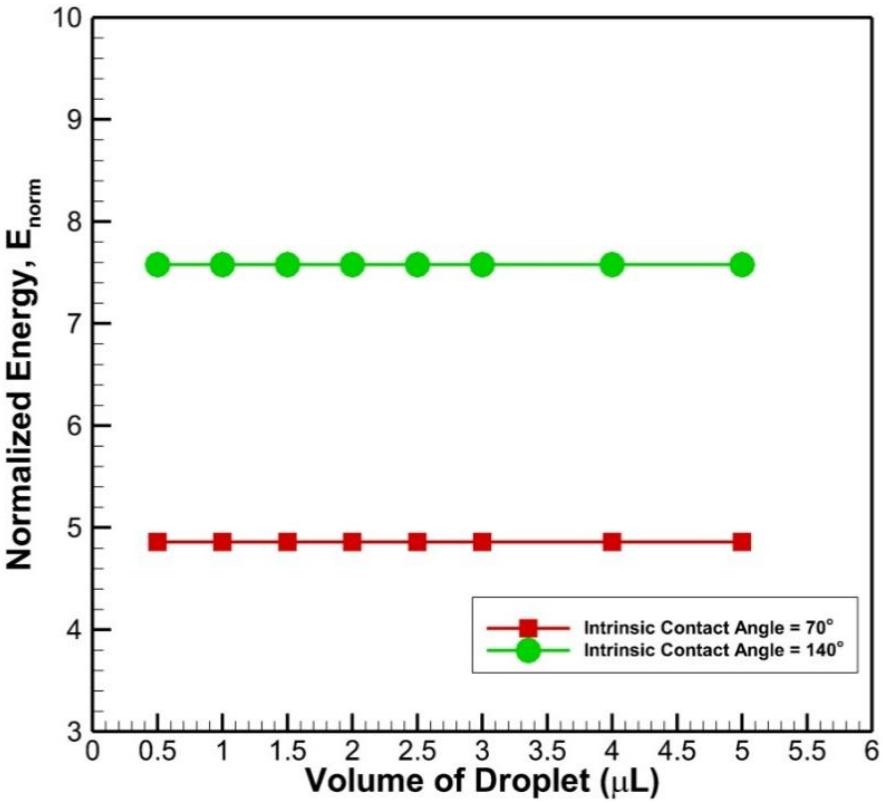

Fig 4.2(a): Normalized energy value of a sessile liquid droplet with the variation of droplet volumes on hydrophobic (intrinsic contact angle, θ = 140°) and hydrophilic (intrinsic contact angle, θ = 70°) smooth flat surfaces

Intrinsic Contact Angle: 70º	
Front View	Bottom View
 1 µL	 1 µL
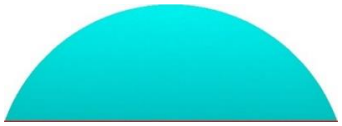 3 µL	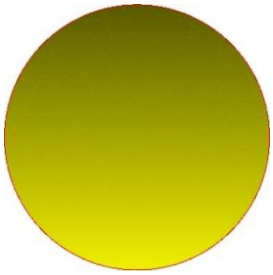 3 µL

Fig 4.2 (b) : Front and bottom views of equilibrium water droplets of 1 µL and 3 µL for hydrophilic smooth flat surfaces for intrinsic CA = 70º

Intrinsic Contact Angle : 140^{o}	
Front View	Bottom View
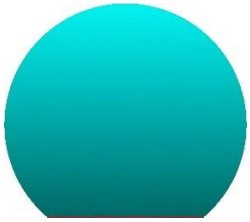 1 µL	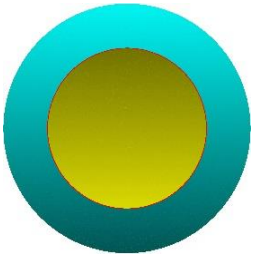 1 µL
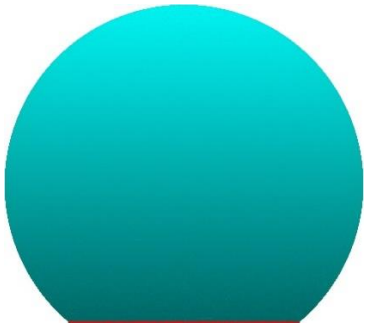 3 µL	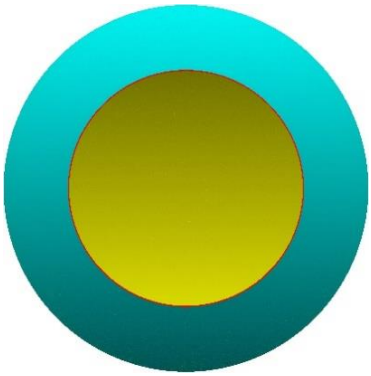 3 µL

Fig 4.2 (c) : Front and bottom views of equilibrium water droplets of 1 µL and 3 µL for hydrophobic smooth flat surfaces for intrinsic CA = 140^{o}

4.2.1 Effect of Droplet Volume on Droplet Energetics

For a fixed wetting condition and constant volume total free energy (E) shows local minima at every different striped configuration and a lowest value among them to specify a stable state on a specific configuration [15]. However, total free energy € grows continually with droplet volume. The total energy € and normalized energy (E_{norm}) of the droplets are displayed as a function of droplet volume in fig 4.2.1.1 It illustrates a typical run of a droplet on 13 stripes with hydrophilic angle, θ_{philic}= 80, hydrophobic angle θ_{phobic}= 100,140 and 180 having both hydrophilic and hydrophobic stripe width 100 µm.

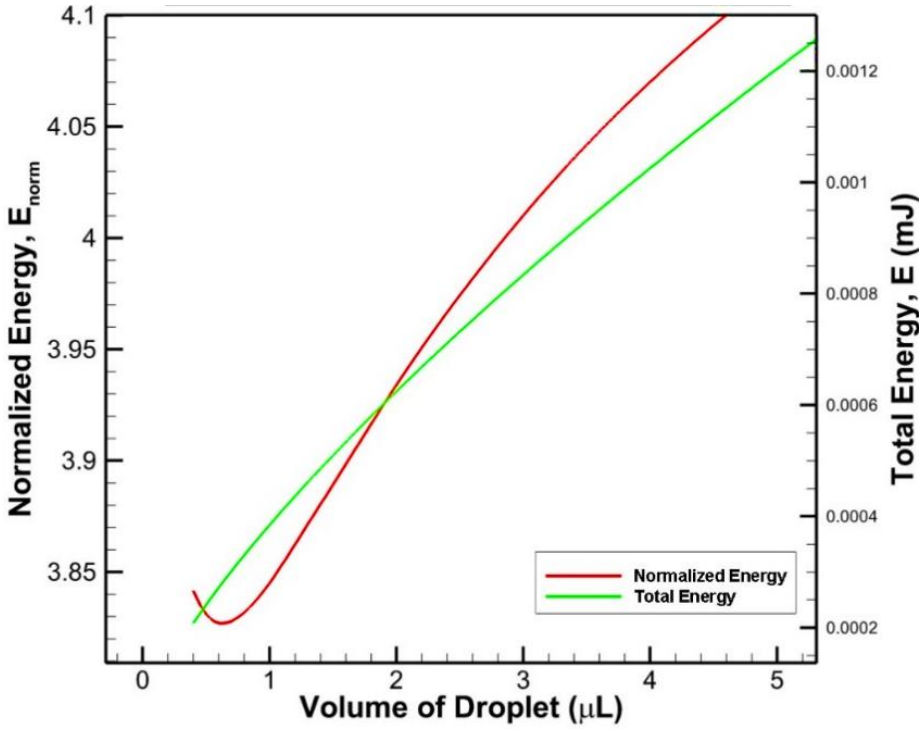

(a)

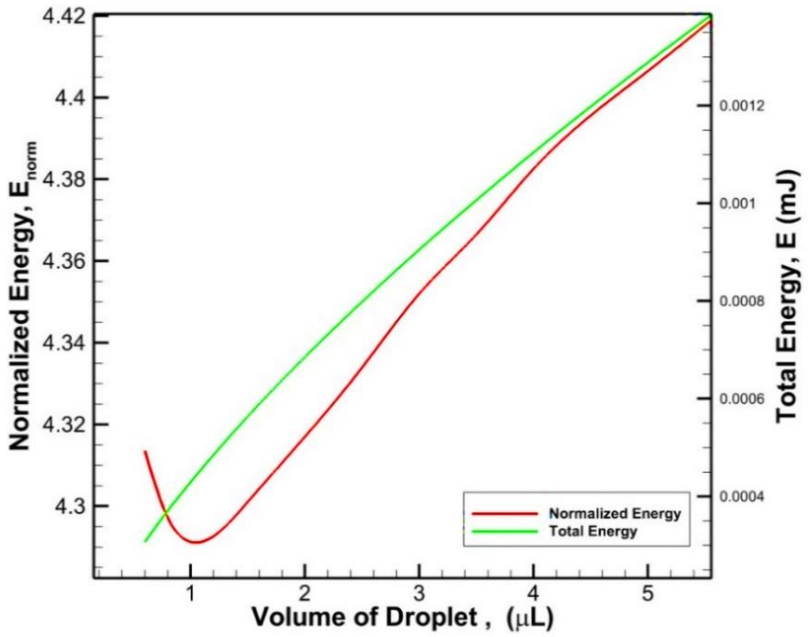

(b)

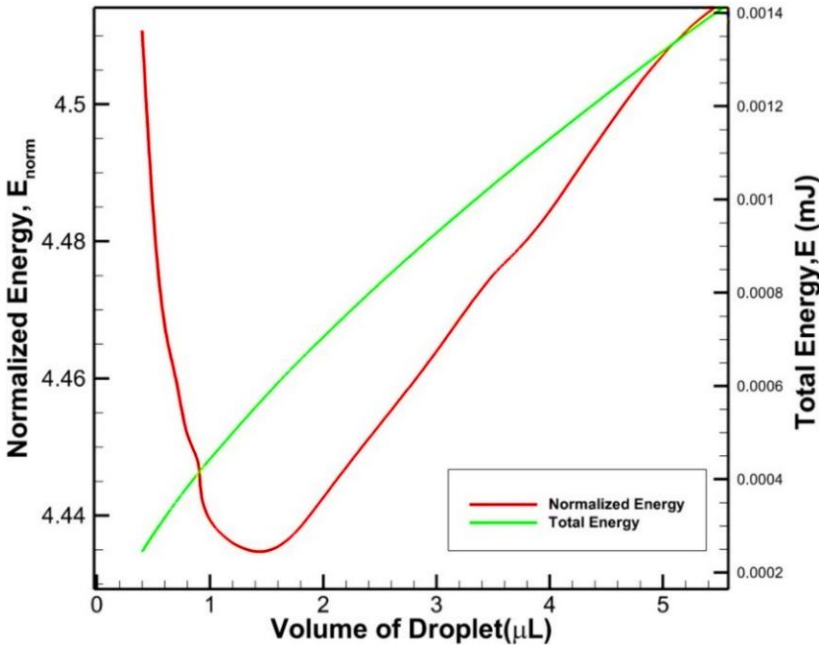

(c)

Fig 4.2.1.1: Total and Normalized energy of a droplet on 13 Stripes; $\theta_{philic} = 80^o$;(a) $\theta_{phobic} = 100^o$; (b) $\theta_{phobic} = 140^o$ (c) $\theta_{phobic} = 180^o$; m= 100 µm; n=100µm

In contrast to total free energy (E), the normalized energy (E_{norm}) for each of the wetting configurations reaches a minimum at a specific volume [14]. Fig 4.2.1.2 illustrates the normalized energy (E_{norm}) of liquid droplet residing on 9,11,13,15 and 17 stripes with hydrophilic angle, θ_{philic}= 80^o and hydrophobic angle, θ_{phobic}= 100^o,140^o and 180^o respectively to introduce wettability contrast. Hydrophilic surface width m=75 µm,100 µm and 125 µm and hydrophobic stripe, n = 100 µm. thus, in our study there exists 9 different wettability configurations.

It is noticeable form the graph and table that, the volume where minimum E_{norm} exhibits, it increases with number of stripes. So, from the perspective of stability, the system becomes more stable if the volume and number of stripes are decreased [15]. This trend is followed by every wettability configuration in our study. For example, minimum E_{norm} increases from 3.869 to 3.877 from 9 stripes to 17 stripes configuration when $\theta_{philic} = 80^o$; $\theta_{phobic} = 100$; m=75 µm, n = 100 µm.

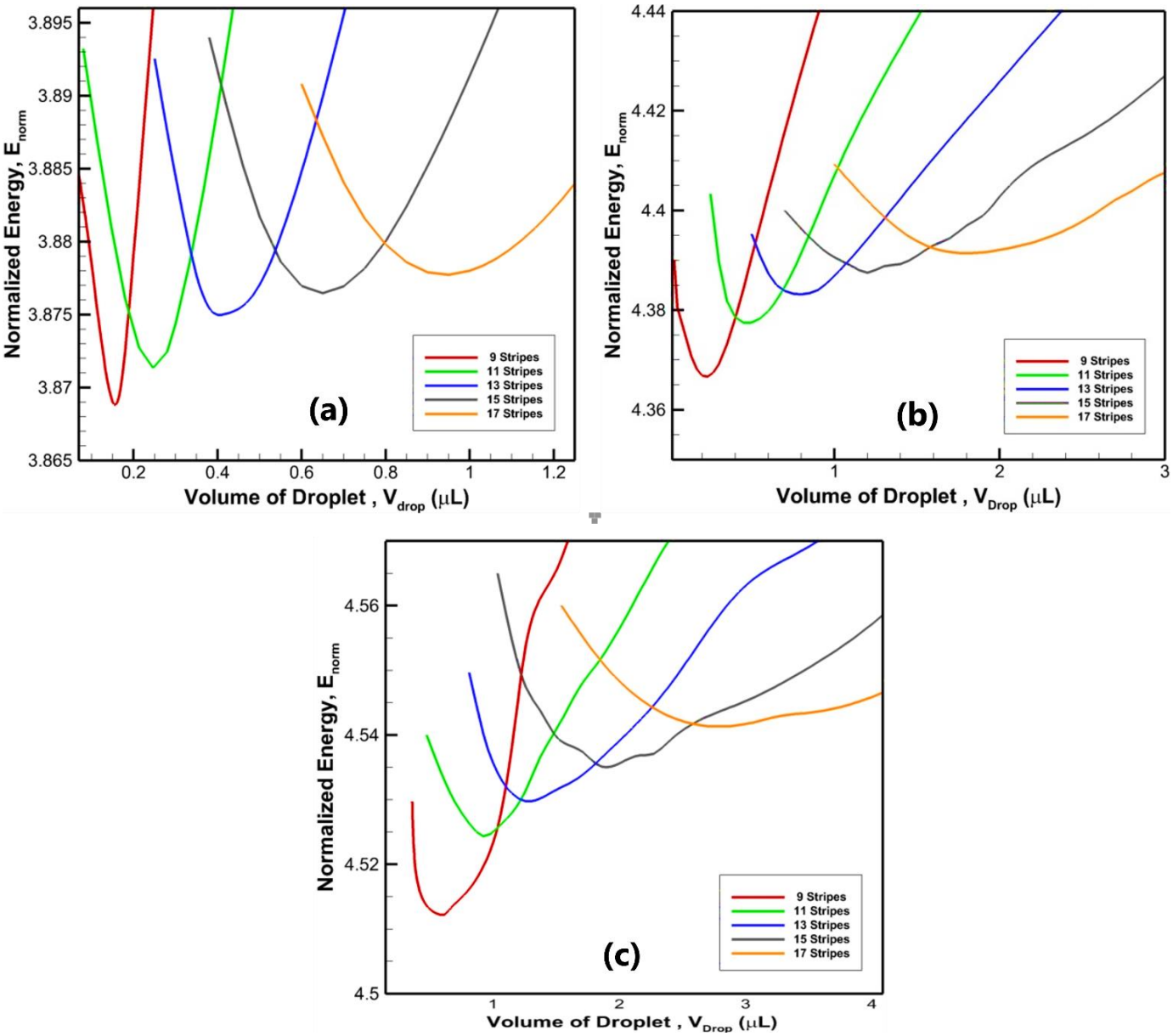

Fig 4.2.1.2: Normalized energy of droplet with on 9,11,13,15,17 Stripes; $\theta_{philic} = 80^o$;(a) $\theta_{phobic} = 100^o$; (b) $\theta_{phobic} = 140^o$ (c) $\theta_{phobic} = 180^o$; m= 75 μm; n=100 μm

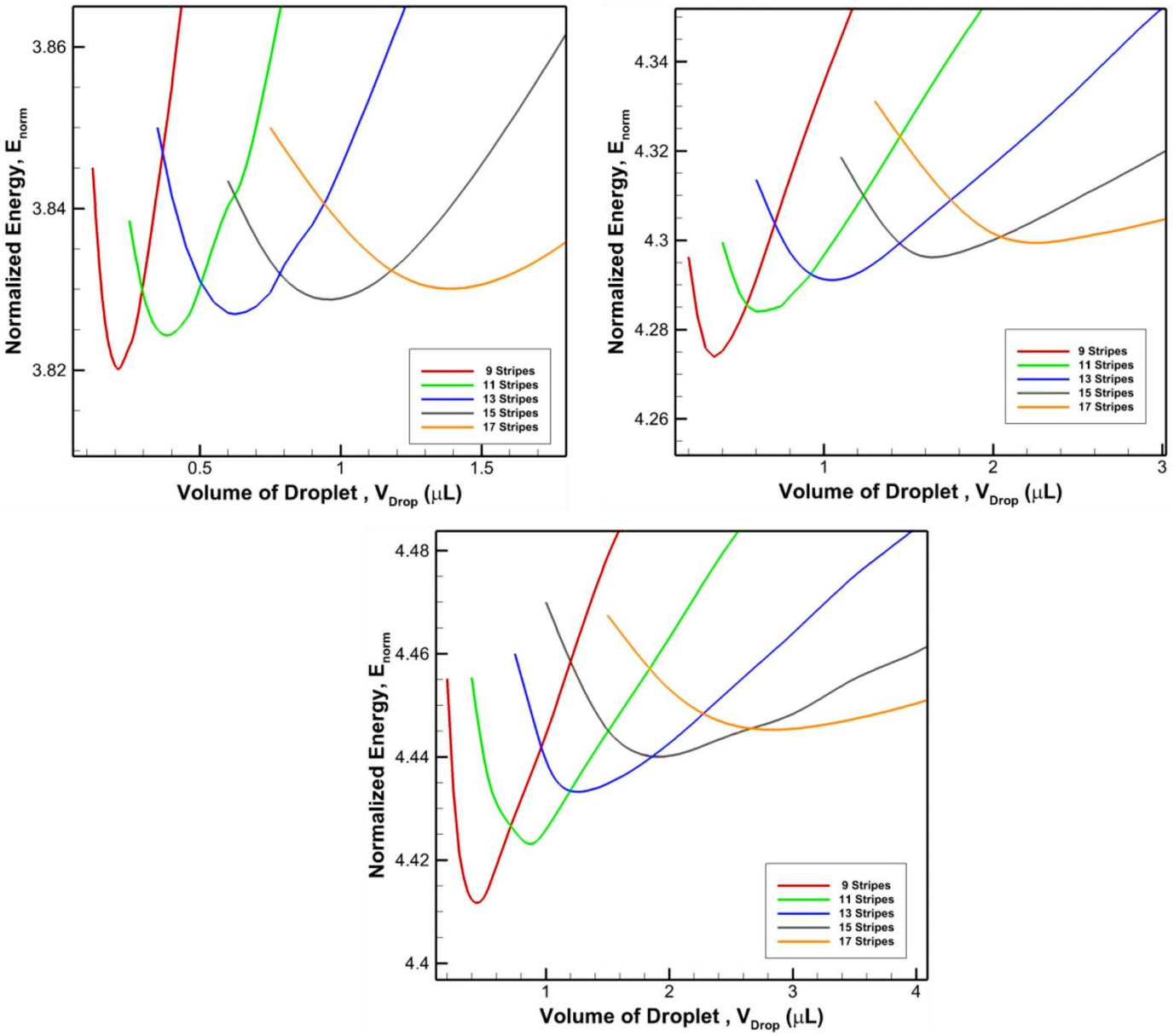

Fig 4.2.1.3: Normalized energy of droplet with on 9,11,13,15,17 Stripes; $\theta_{wet}=80^0$; $\theta_{phobic}=180^0$; m=100 µm; n=100µm

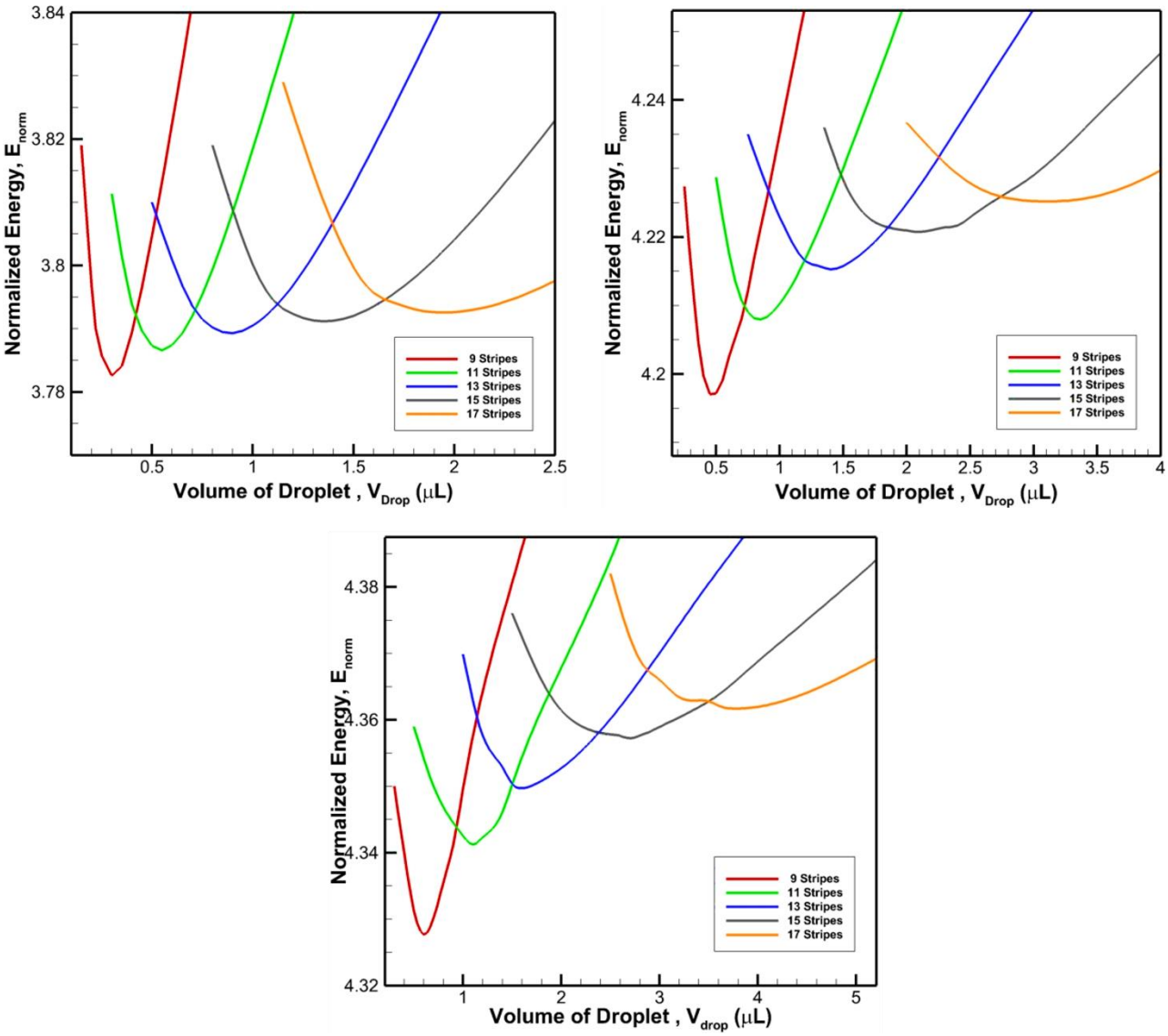

Fig 4.2.1.3 :Normalized energy of droplet with on 9,11,13,15,17 Stripes; $\theta_{wet}=80^0$; $\theta_{phobic}=180^0$; m=125 μm; n=100μm

In our simulation process, the total number of stripes are not confined to a fixed numeric value of width. As a result, while droplet has more stripes beneath, it encompasses more surface area experiencing more hydrophilic and hydrophobic portion compared to lower stripe configuration. To achieve a stable equilibrium state, droplet with higher volume needs higher striped configuration. Anjan et al for surfaces with parallel microgrooves reported this kind of situation [60].

In our study, all configuration shows similar trend. For instance, at m = 75 µm, 100 µm and 125 µm, the most stable cases were found having normalized energy (E_{norm}) and volume 3.869 and 1.5 µL, 3.82 and 0.22 µL and 3.785 and 0.25 µL respectively. All of them were sitting on 9 striped configurations. Here, at m=125µm, droplet contains lowest energy but highest volume.

Since the boundary contact line is fixed in case of narrow stripes a liquid droplet has two ways to adjust within its excess volume: spreading in the parallel direction or adjustment of volume by deforming its height and shape. In this case, they contain excess energy at an unstable state as with higher volume and with the help of excess energy to surpass energy barrier they will try to spread perpendicularly and wet next stripe [11,12].

Apart from equilibrium state at a specific volume for a wetting configuration, there exists numerous nonequilibrium /metastable droplet. The only equilibrium drop possess an equilibrium shape; rest of the drops have non equilibrium drop shape due to no equilibrium position of the triple line.

At non equilibrium position, there acts an additional elastic energy ($E_{elastic}$) at the three-phase contact line that can be written as follow [13]:

$$E_{elastic} = \frac{1}{2} k_e (x-x_0)^2$$

Where, k_e is the elastic constant of the triple line and *x* and *xo* are the constrained and equilibrium positions of the triple line, respectively. With more elastic energy present, metastable instances have greater normalized energies than stable cases do. For lower volume droplet maintain a good profile of spreading and wet the patterned surface across the parallel direction.

4.2.2 Effect of Hydrophilic Stripe Width and Hydrophobic Contact Angle on Energetics

Wettability contrast and hydrophilic stripe dimension have significant effects on energetics and equilibrium contact angle of stable droplets. Since in our study, hydrophilic contact angle (θ_{philic} $=80^{o)}$ and hydrophobic stripe width n = 100 µm are constant, we are going to observe how droplet energetics respond and behave for variable hydrophilic stripe width m and hydrophobic contact angle $\theta_{phobic.}$

Normalized energy (E_{norm}) of the most stable state decreases with increasing hydrophilic stripe width [53]. On a fixed wetting condition, small m (hydrophilic stripe) and is preferable to attain big equilibrium contact angle. Whereas wider m is preferable to attain more stable state according to the principle of minimum energy. Cases we consider in our study, shows similar trend of result.

For θ_{phobic}=100, normalized energy of liquid droplet at 9 stripe configuration possesses 3.869, 3.82 and 3.785 for hydrophilic stripe width 75 µm,100 µm and 125 µm respectively Fig 4.2.2.1. With wider hydrophilic stripe, liquid droplet gets more in contact with a surface with higher surface free energy (lower intrinsic contact angle) what is preferable for spreading. With increasing stripe width m, volume of droplet also increases to cover the stripes area. In this case it increases from 0.15 µL to 0.25 µL to attain equilibrium state. We have to keep in mind that, all the values that the graph and table contain, they are at most stable state. They possess the minimum energy as per to their configuration. So, a system becomes more stable if the hydrophilic stripe width is increasing compared to hydrophobic stripe leading to a low dry fraction area for a droplet.

With a constant hydrophilic angle and stripe width, if the hydrophobic angle is increased gradually, minimum normalized energy of the most stable droplet on a given stripe configuration increases. For a 13-stripe configuration, this value is 3.875,4.383 and 4.529 showing an increasing trend. Increasing in hydrophobic angle means at the hydrophobic stripe portion, the droplet faces more hydrophobicity which leads the three-phase contact line to evolve inward. Surface energy difference between two opposite portion increases that leads the droplet to contain more energy at equilibrium state. It is also noticeable that to adjust the excess energy droplet has to attain more

volume in same stripe configuration for higher hydrophobic angle. Volume increases from 0.4 µL to 0.1 µL in this configuration.

From our simulation graph and data analysis this can be said that now, lower hydrophobic angle is preferable for the system to reach a more stable state. Whereas large hydrophobic angle is preferable to achieve large equilibrium contact angle.

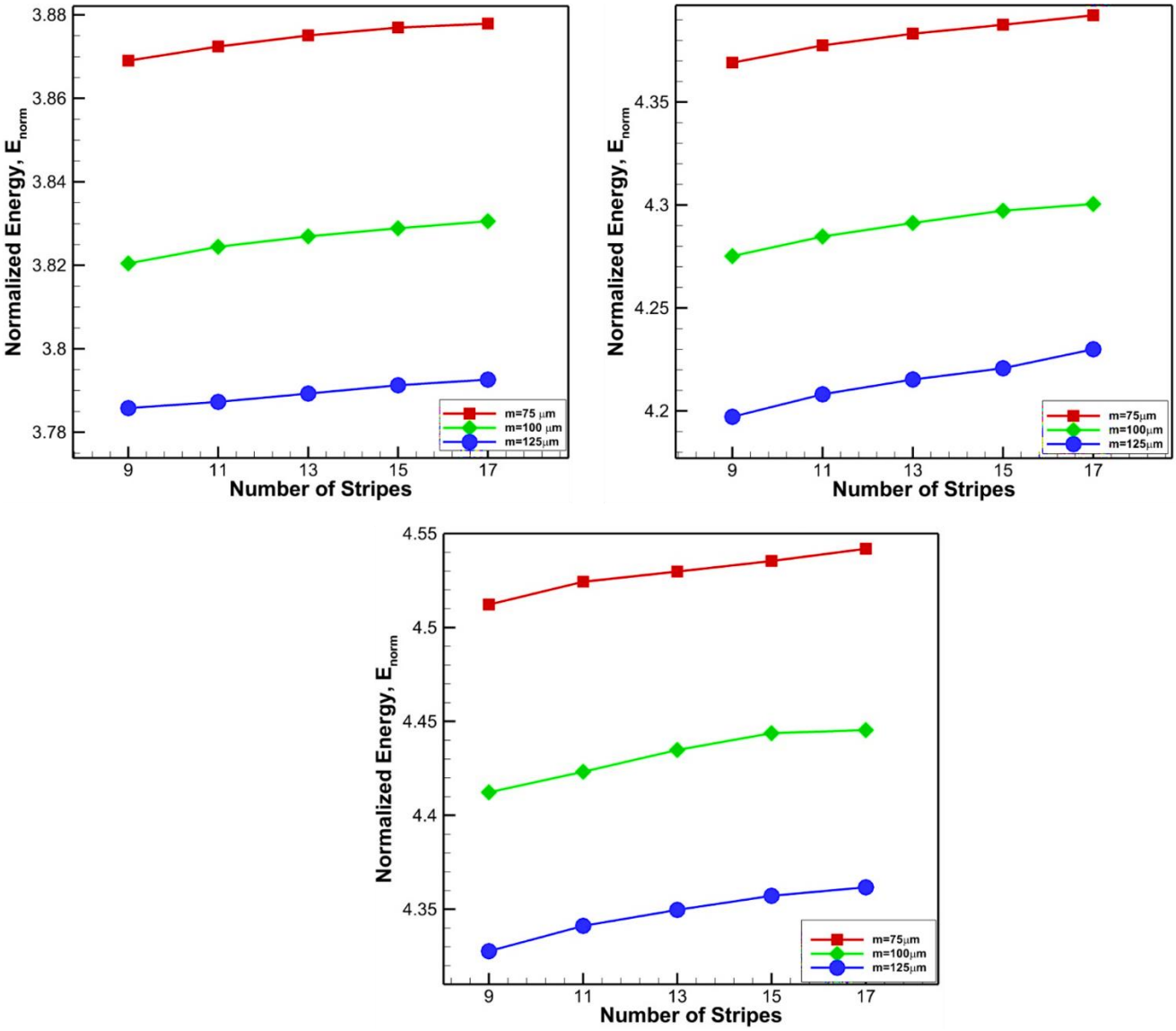

Fig 4.2.2.1 :Normalized Energy as a function of Number of stripes and θ_{phobic} =140°

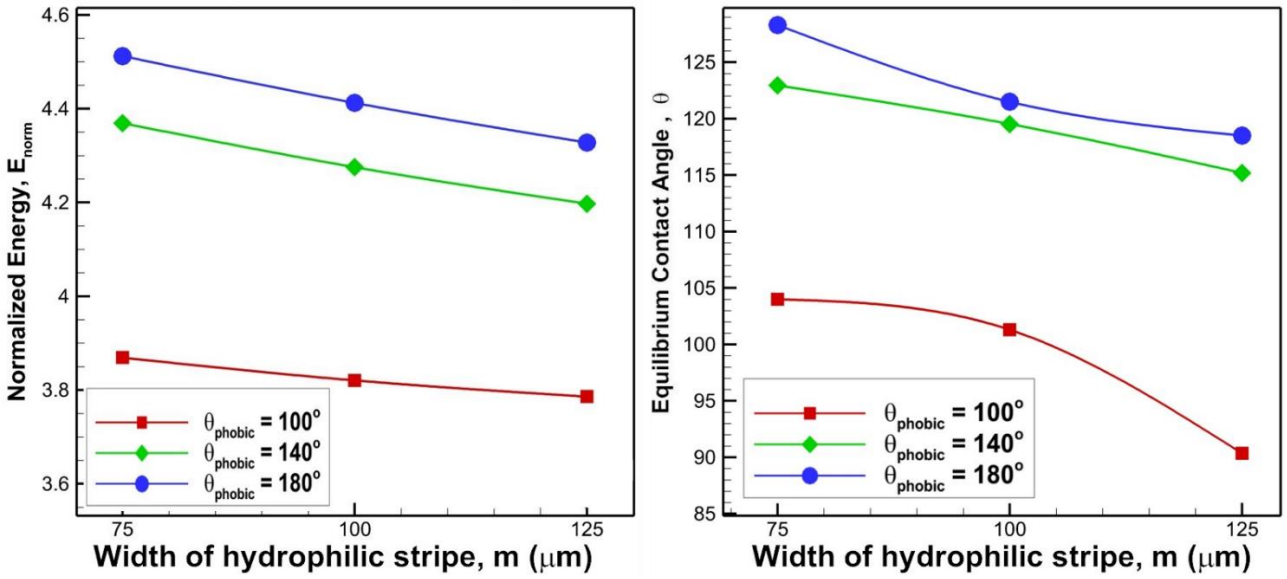

(a) **(b)**

Fig 4.2.2.2 : Change of (a) normalized energy(E_{norm}) ; (b) equilibrium contact angle (θ) with hydrophilic stripe width m for 9 stripes ; θ_{philic} =80° and hydrophobic stripe width n = 100μm

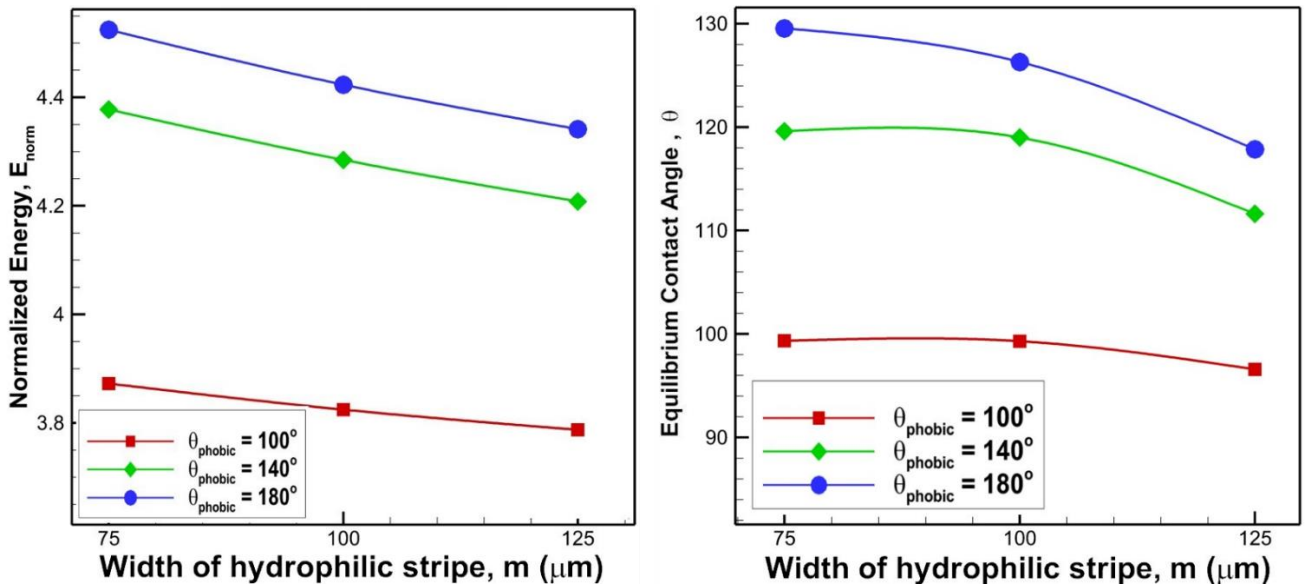

(a) **(b)**

Fig 4.2.2.3: Change of (a) normalized energy(E_{norm}) ; (b) equilibrium contact angle (θ) with hydrophilic stripe width m for 11 stripes ; θ_{philic} =80° and hydrophobic stripe width n = 100μm

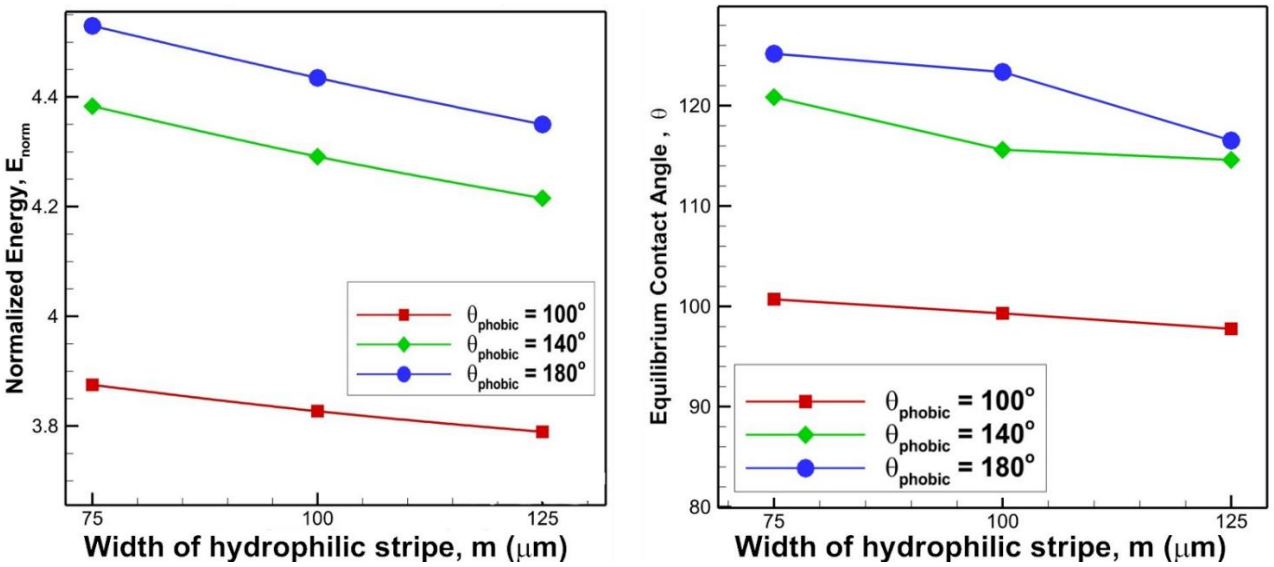

(a) **(b)**

Fig 4.2.2.4 : Change of (a) normalized energy(E_{norm}) ; (b) equilibrium contact angle (θ) with hydrophilic stripe width m for 13 stripes ; θ_{philic} =80° and hydrophobic stripe width n = 100μm

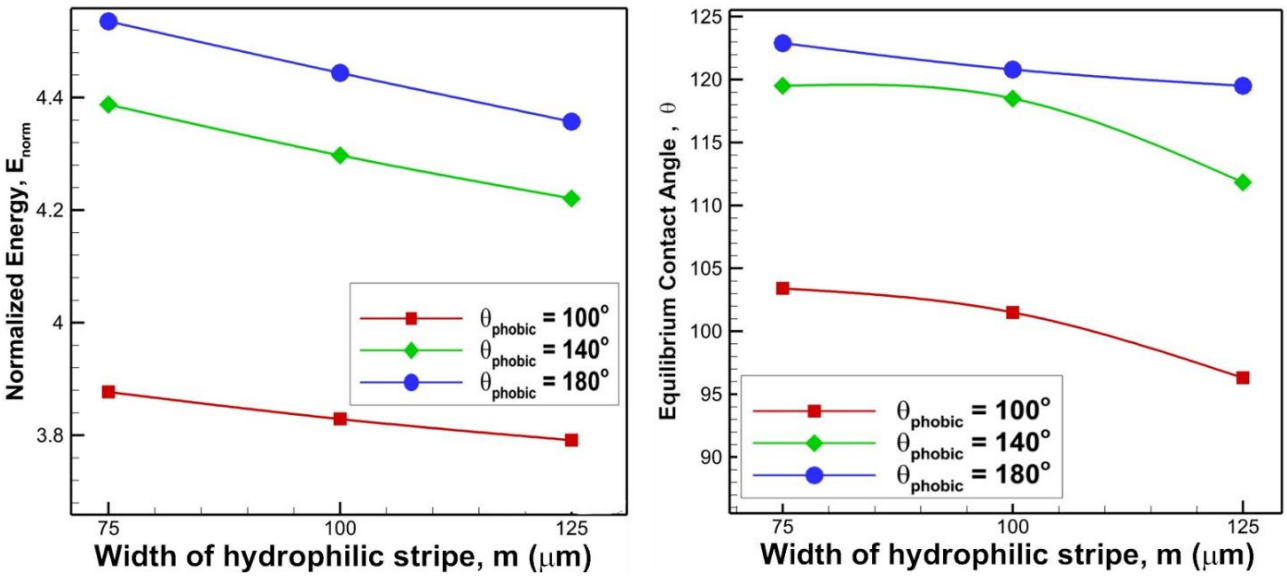

(a) **(b)**

Fig 4.2.2.5: Change of (a) normalized energy(E_{norm}) ; (b) equilibrium contact angle (θ) with hydrophilic stripe width m for 15 stripes ; θ_{philic} =80° and hydrophobic stripe width n = 100μm

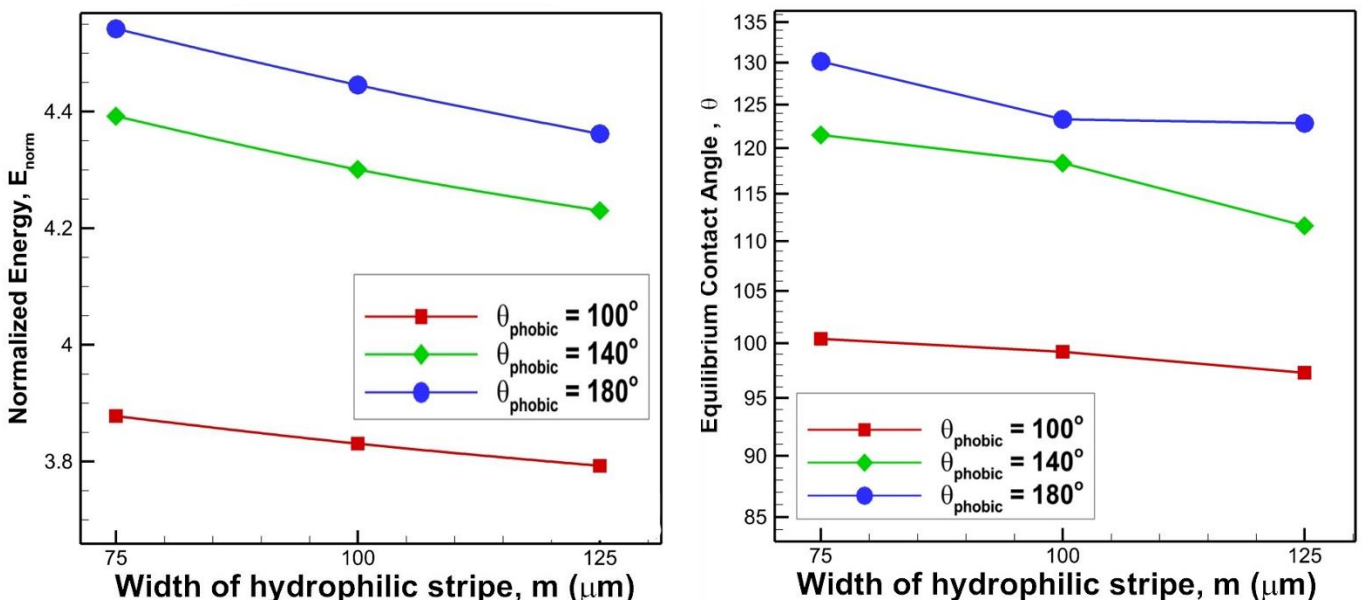

(a) **(b)**

Fig 4.2.2.6 : Change of (a) normalized energy(E_{norm}) ; (b) equilibrium contact angle (θ) with hydrophilic stripe width m for 17 stripes ; θ_{philic} =80° and hydrophobic stripe width n = 100μm

4.2.3 Combined Effect of Hydrophilic Stripe and Hydrophobic Contact Angle

Discussion and results from previous sections indicate that we need higher hydrophilic stripe width and lower hydrophobic angle would to attain the most stable state. But combinedly it cannot be exclusively said that we have to take as big as hydrophilic stripe width and as much as lower hydrophobic stripe to create an absolute stable configuration. Let's look at fig 4.2.3. We can see that, as per previous discussion, normalized energy of the green line configuration should not cross the black one. As black dot dash is having θ_{phobic} = 180° and m=125μm; whereas green solid line is having θ_{phobic}= 140° and m=75 μm. This figure is for droplets on 11 stripe configurations.

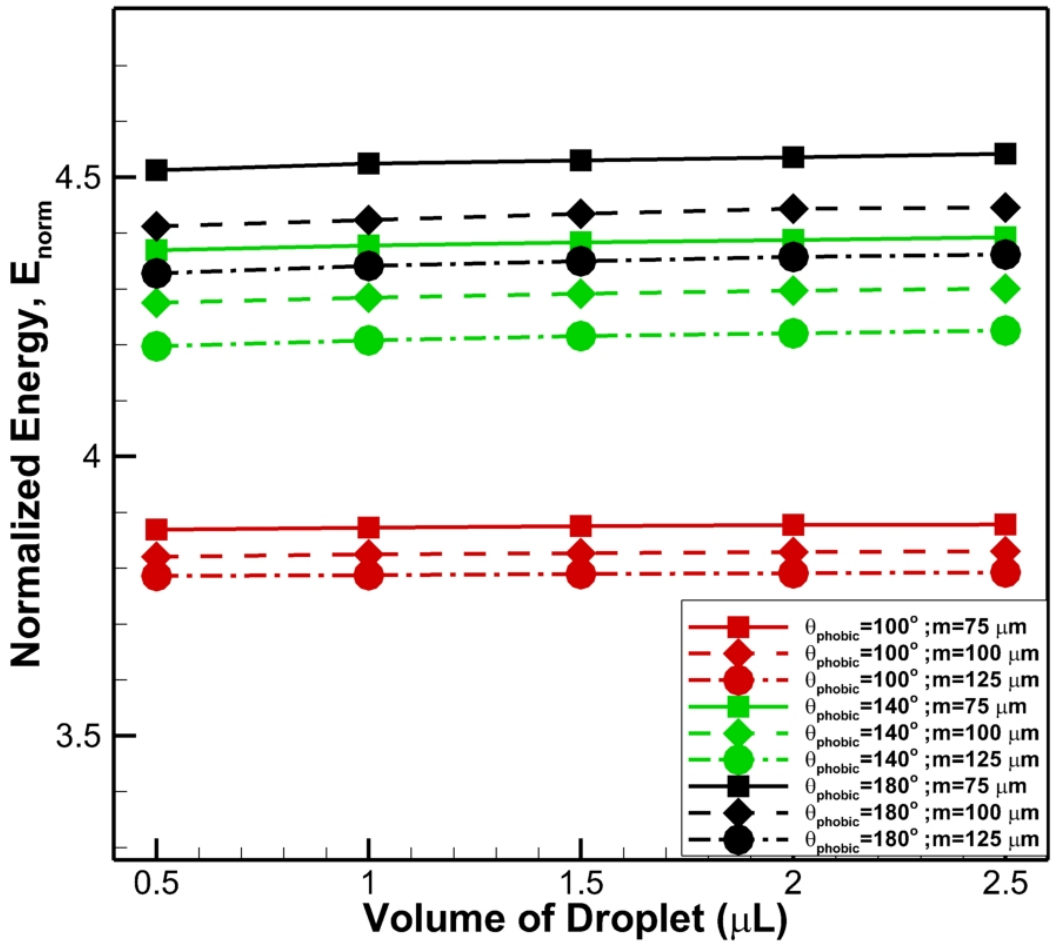

Fig 4.2.3: Combined effect on stability of hydrophilic stripe m and hydrophobic angle θ_{phobic}

This is ambiguous as which parameter is dominant cannot be determined. Sometimes hydrophilic stripe could play more vital role to lower the energy or sometimes θ_{phobic} can be dominant enough to surpass that energy.

4.3 Analysis of Contact Angle

The apparent contact angle provides an indication of how wet the surfaces are that the liquid droplet is put on. According to the value of contact angle, the shape of droplet and morphology of the surface can be assumed easily. This analysis focuses on the observation of contact angle for different surface configuration and wettability contrast. Additionally, degree of anisotropy will be discussed in this section to find out the insights of anisotropic wetting of a surface at different wetting conditions.

4.3.1 Effect of Volume on Contact Angle

The consequences of wettability contrast are not often reported, despite the fact that experimental and numerical investigations of the wettability of surfaces with chemical stripes have garnered a lot of attention. In case of anisotropic wetting, we have to take care of parallel and perpendicular angles observing from two distinct sides of the droplet. It seems, as the size of the droplet (volume) increases, parallel angle remains nearly constant but perpendicular angle is showing an increasing trend because of the constrained contact line [53].

In our study, volume of the droplet ranges from .01 µL to 6 µL. it is noticeable that, in every case, perpendicular angle is always bigger that parallel angle thus leading to a non-spherical shape of droplet. Having alternating stripes, the droplet spread along the parallel stripe as both end is fixed that doesn't allow it to spread over next stripe. As a result, perpendicular angle is always larger than parallel angle [11,12].

At a very low value of volume, it is possible for a droplet to equal both angles (visibly seen at 15 and 17 stripe configuration). But with increasing volume perpendicular angle increases very fast. From our graph, for example, we can observe that, for a 13-stripe configuration with $\theta_{phobic}=140^{o}$ & m= 75 µm, perpendicular angle increases from 104.8 degree to 125.6 degree for a change in volume from 0.5 µL to 1 µL. However, for parallel angle, it always saturates at a particular value, in this case 88.2^{o} that satisfies the modified Cassie-Baxter equation. Changes of angle in higher volume is much less than changes in small volume as at higher volume, the droplet adjusted its

excess volume and height due to the pinning effect and energy surplus at three-phase contact line. This trend is observed at all wetting conditions and configurations in our simulation. Following graphs illustrates the statement very well and it also agreed with the report Jansen documented [11]. In the next section we will discuss the effect of hydrophilic stripe width m and hydrophobic angle θ_{phobic} on contact angle.

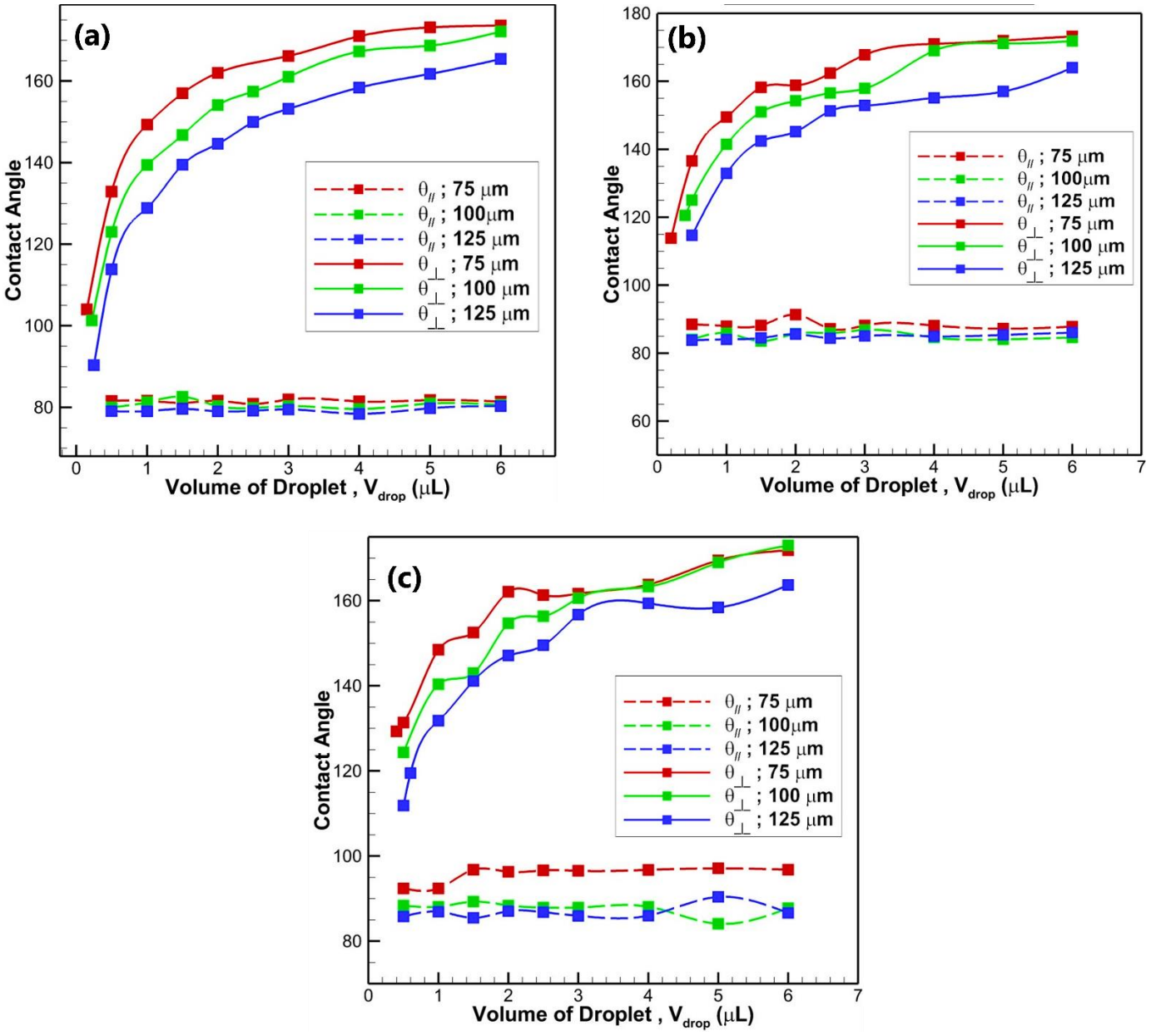

Fig 4.3.1.1: variation of parallel and perpendicular contact angle as a function of volume droplet for 9 stripe configurations at (a) $\theta_{phobic} = 100^0$,(b) $\theta_{phobic} = 140^0$, (c) $\theta_{phobic} = 180^0$;n = 100 µm

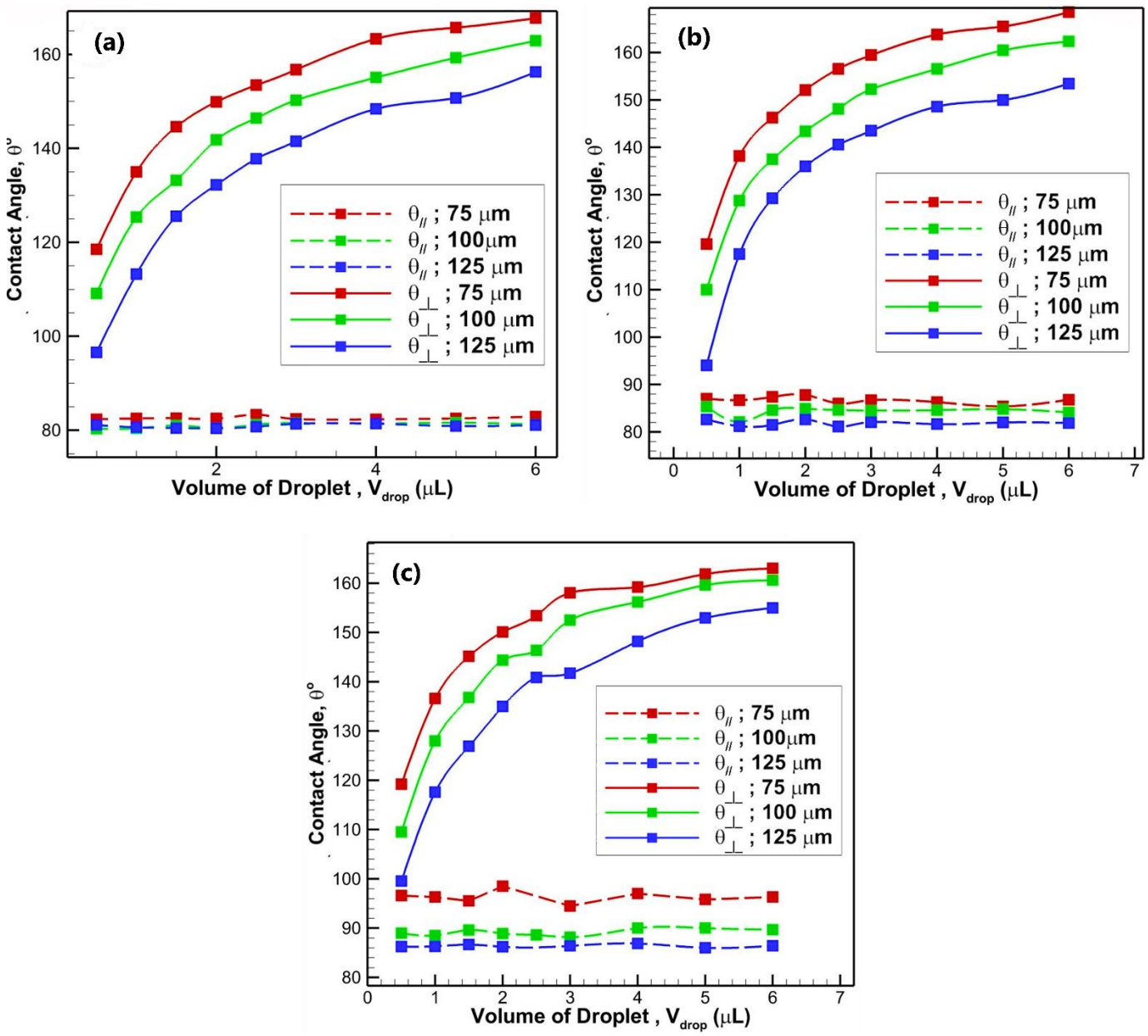

Fig 4.3.1.2: variation of parallel and perpendicular contact angle as a function of volume droplet for 11 stripe configurations at (a) $\theta_{phobic} = 100^0$,(b) $\theta_{phobic} = 140^0$, (c) $\theta_{phobic} = 180^0$;n = 100 μm

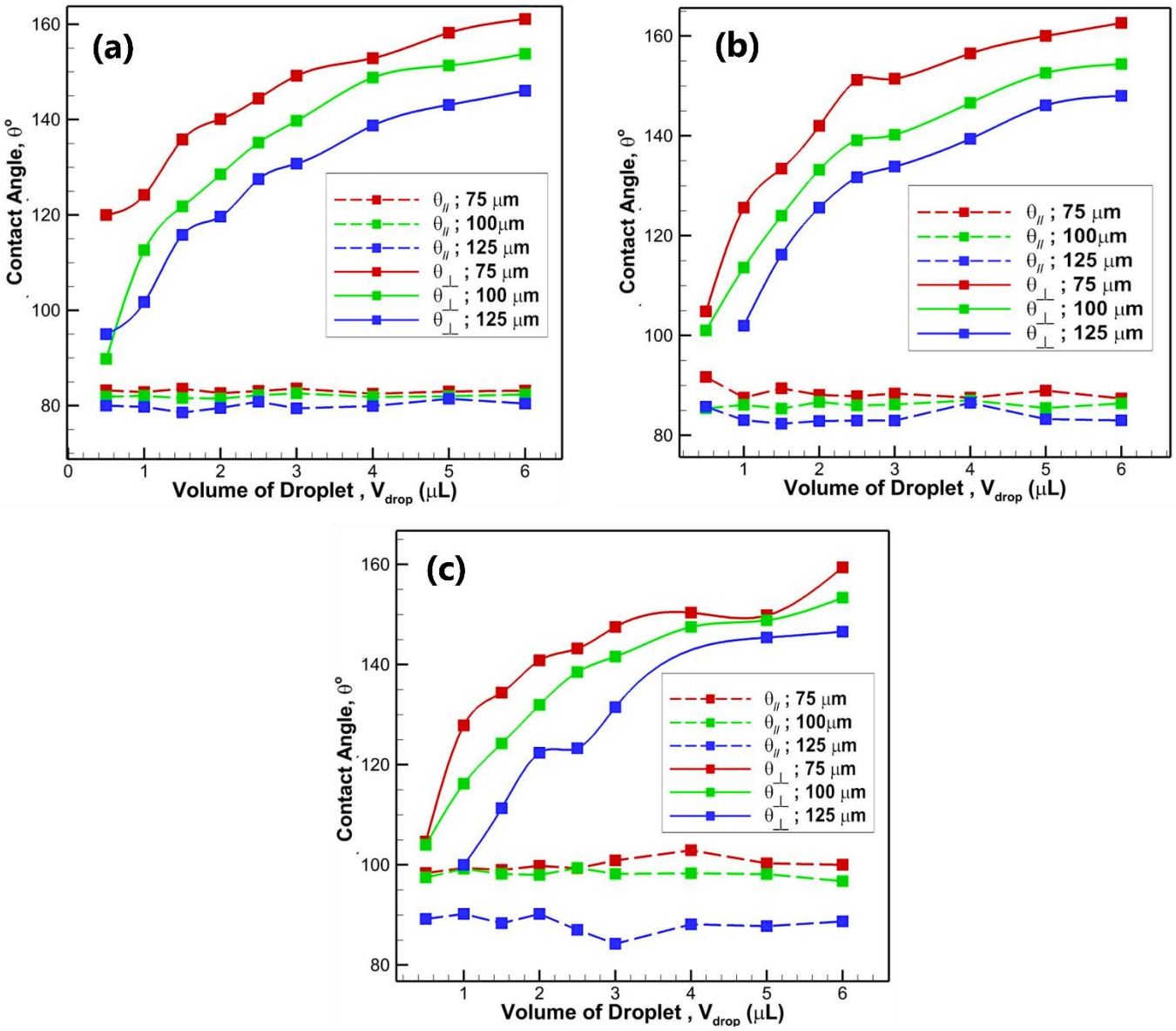

Fig 4.3.1.3: variation of parallel and perpendicular contact angle as a function of volume droplet for 13 stripe configurations at (a) $\theta_{phobic} = 100^0$,(b) $\theta_{phobic} = 140^0$, (c) $\theta_{phobic} = 180^0$;n = 100 μm

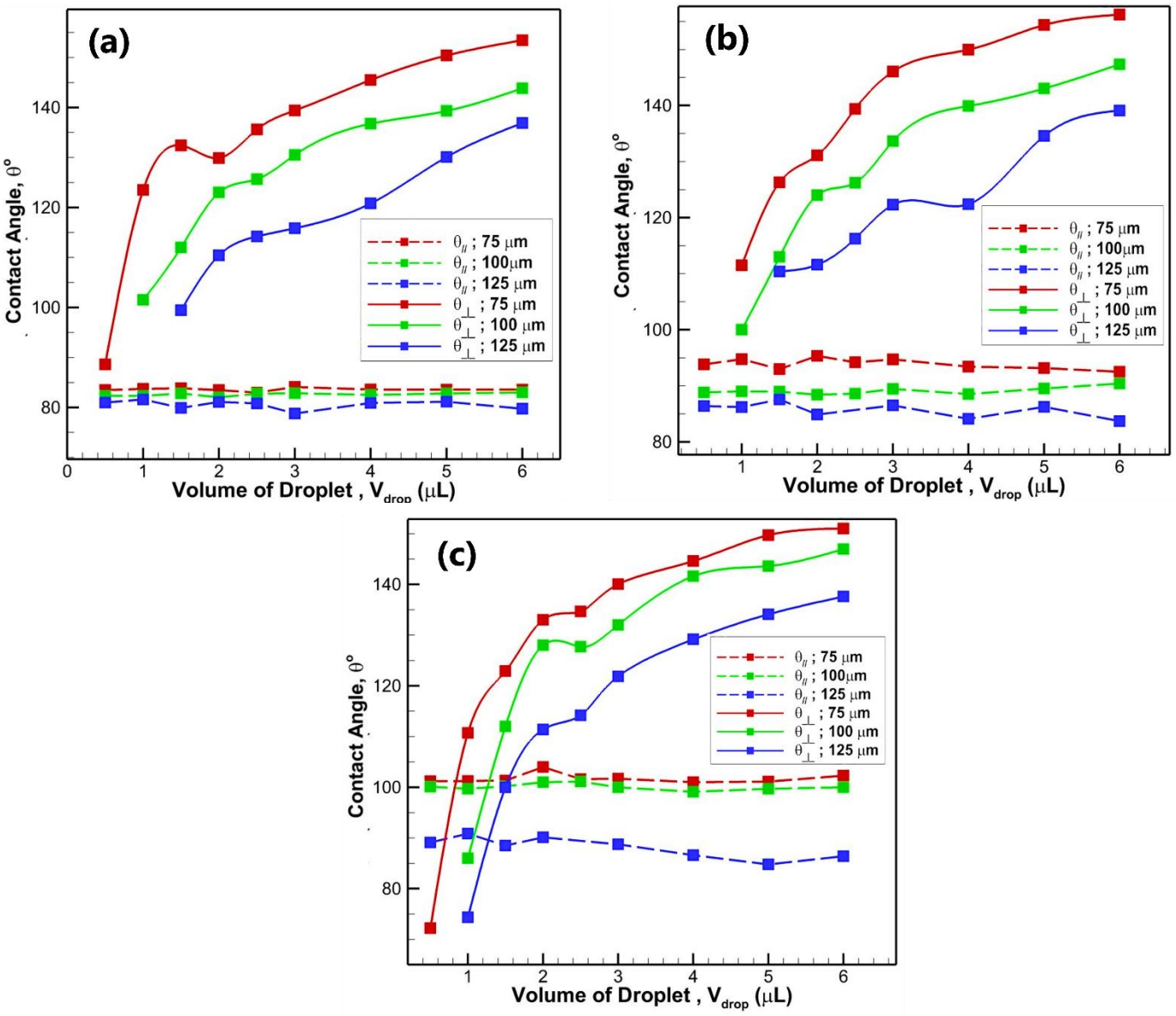

Fig 4.3.1.4: variation of parallel and perpendicular contact angle as a function of volume droplet for 15 stripe configurations at (a) $\theta_{phobic} = 100^0$,(b) $\theta_{phobic} = 140^0$, (c) $\theta_{phobic} = 180^0$;n = 100 μm

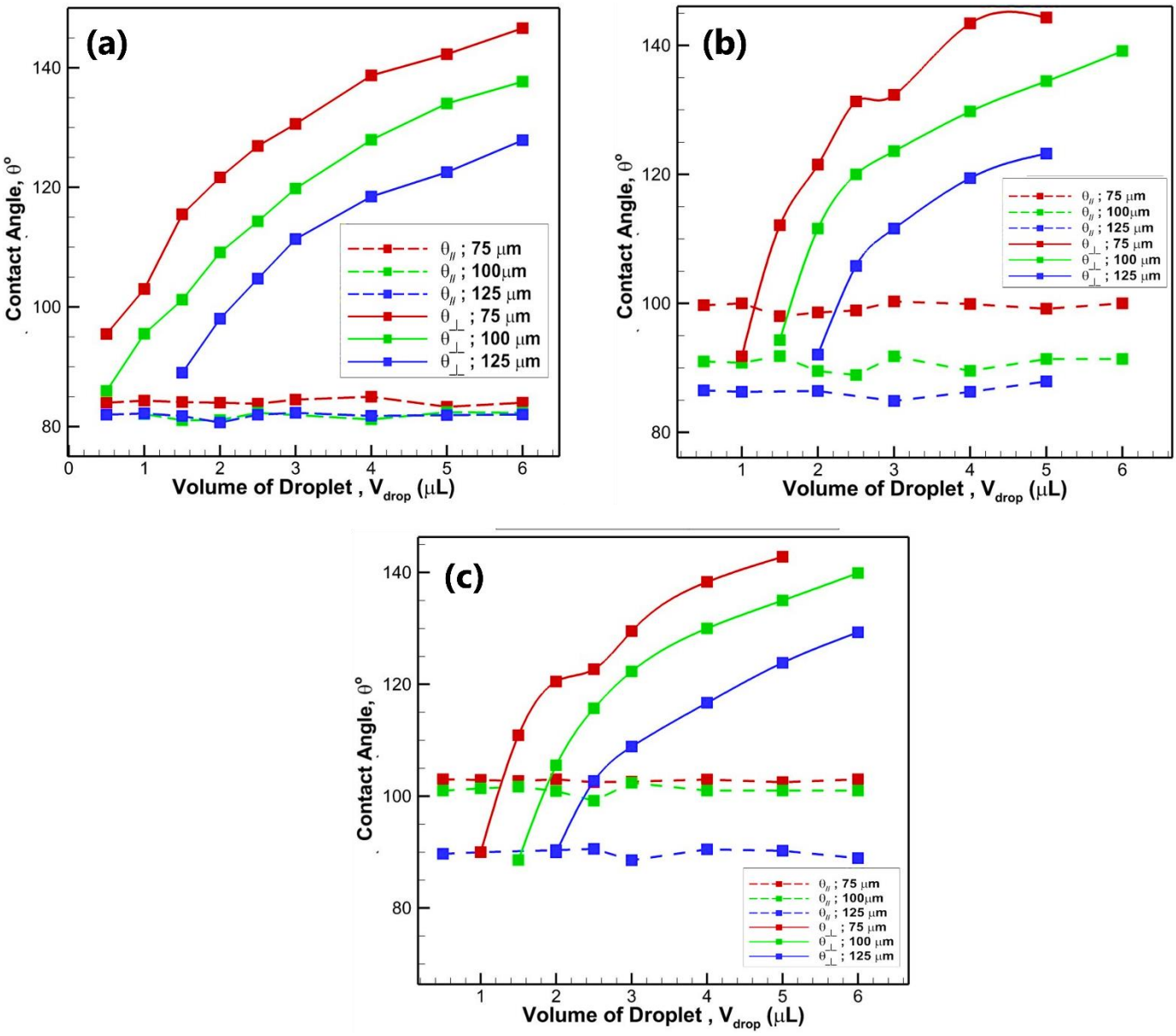

Fig 4.3.1.5: variation of parallel and perpendicular contact angle as a function of volume droplet for 9 stripe configurations at (a) $\theta_{phobic} = 100^0$,(b) $\theta_{phobic} = 140^0$, (c) $\theta_{phobic} = 180^0$;n = 100 μm

4.3.2 Effect of Hydrophilic Stripe Width on Contact Angle:

For a droplet, hydrophilic stripe is congenial for it to spread along parallel direction. From earlier discussion, we observe that droplet always prefer to sit on odd number of stripes having hydrophilic stripe at boundary. In our study, hydrophobic stripe width, n is always constant having a value of 100 µm but varying the hydrophilic stipe width have a significant effect on energy, contact angle and elongation.

From our previous discussion, we already know that, wider hydrophilic stripe helps a droplet to spread more along the stripe. Both parallel and perpendicular angle are observed to be decreasing with increasing hydrophilic stripe width.

Shi et al. [] in his experiment used 2 µL droplet to investigate effect of contact angle with increasing hydrophilic stripe width on geometrically patterned surfaces. They found both contact parallel and perpendicular angle to be decreasing with increasing hydrophilic stripe width.

Our simulation shows same trend with around 2% error with parallel angle value and deviation in perpendicular angle at m = 100 µm deviation obtaining 133,128 and 111.4 degree for perpendicular angle and 102, 99.2 and 88.5 degree for parallel angle. The deviation happens may be metastable condition of the droplet at that configuration. Every wettability contrast follows the same.

Simulation from Jansen et al. [11] also have a good agreement with this. With wider stripe, droplet gets more total area and hydrophilic portion for spreading. During volume adjustment, stretching of the droplet happens that decreases height. That's why both angle shows decreasing trend.

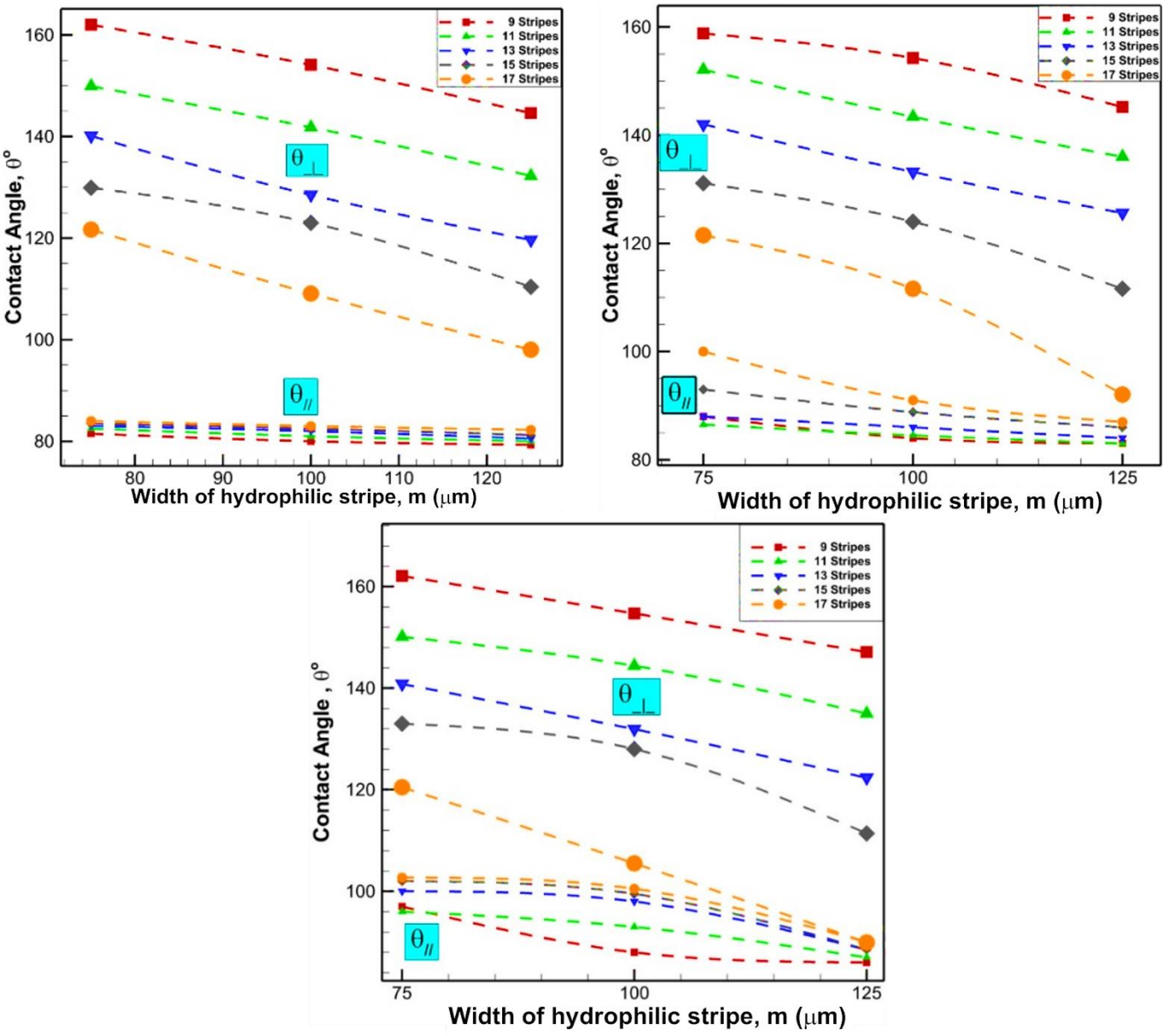

Fig 4.3.2: Contact angle decrement (parallel and perpendicular) as a function of hydrophilic stripe width, m

4.3.3 Effect of Hydrophobic Stripe Angle on Contact Angle:

Parallel angle $\theta_{//}$ increases if the hydrophobic stripe angle θ_{phobic} is increasing gradually. From graph, we observe that no matter what the hydrophilic stripe width is, with increasing θ_{phobic} , parallel angle $\theta_{//}$ shows a growing trend. It is also noticeable that, at 17 stripe configuration, value of parallel angle is always larger than of its smaller stripe configuration. Following graph is done for 2μL droplet volume having $\theta_{philic} = 80^{o}$ and n = 100 μm.

Total % of hydrophobic portion ($\frac{x.n}{y.m+x.n}$) beneath the droplet is always higher in 17 stripe configurations as our droplet doesn't have the restriction of residing on a fixed numeric value of width. As a result, when θ_{phobic} increases, droplet faces more hydrophobic area thus more energy barrier along stripe border. Strong pinning effect exists here that the droplet feels the tendency to move inward thus increasing its height. As a result, parallel angle is increasing significantly when stripe number and θ_{phobic} both increases.

For instance, from our simulation, for m= 75 μm,100 μm and 125 μm, the hydrophobic portion increases from 9 stripes to 17 stripes :51.61% to 52.34%; 44.44% to 47.06% and 39.03% to 41.56% respectively. Thus, increasing parallel angle with stipe numbers. This increasing value has a good agreement with the explanation and simulation result with Bliznyuk et al [12]. He proposed volume rearrangement explanation to explain this increase in parallel angle.

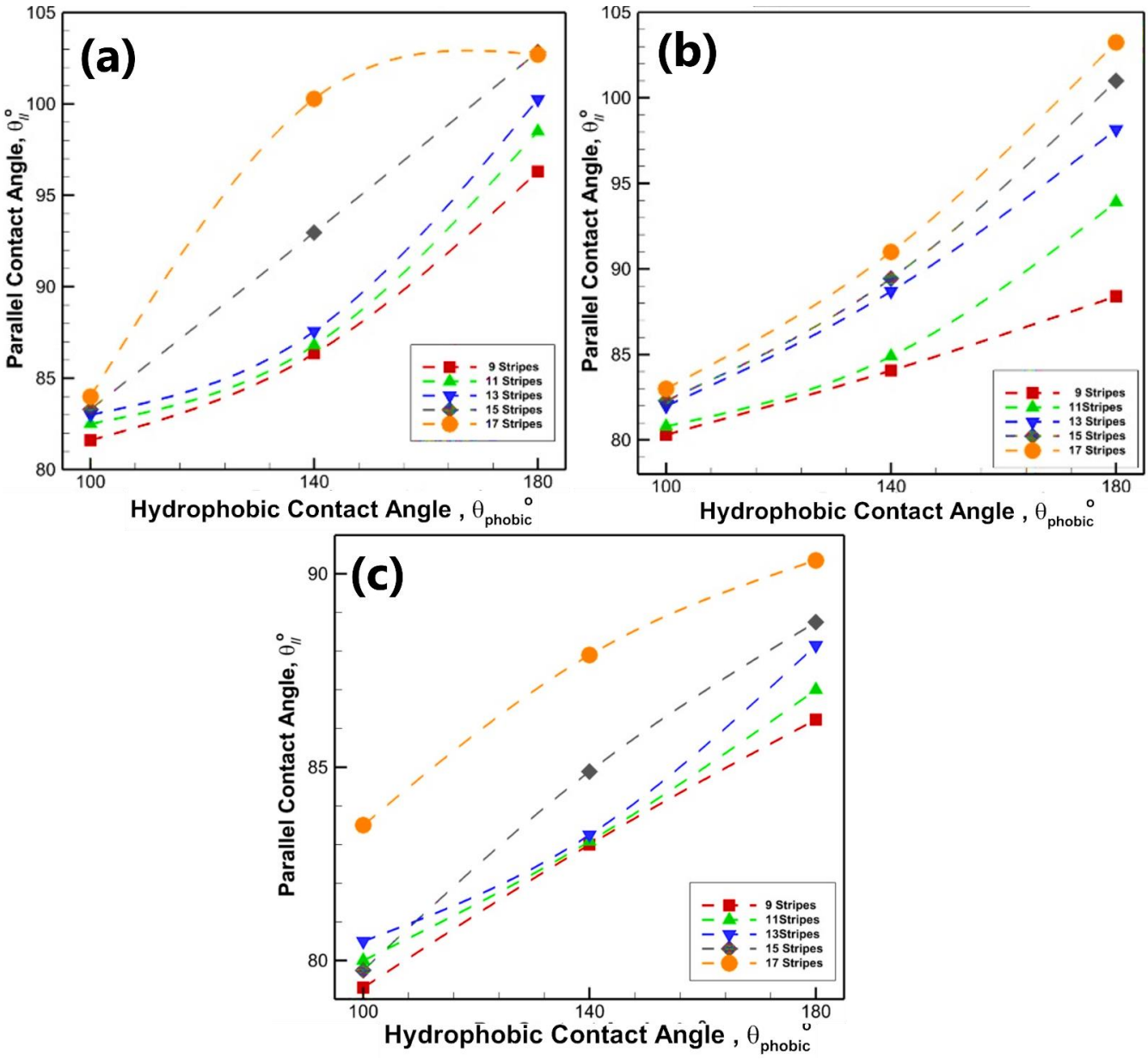

Fig 4.3.3: effect of Hydrophobic stripe contact angle θ_{phobic} on parallel contact angle of droplet

4.4 Degree of anisotropy

In anisotropy wetting, angles measured form two spectacular direction have different values. The difference between perpendicular and parallel angle is referred to as degree of anisotropy $\Delta\theta$. In stripe configuration, we have already discussed that, parallel contact angle remains nearly constant and perpendicular angle increases with increment in volume.

Within a constant volume, parallel angle increases and perpendicular angle is decreases if the number of stripes is increased. Jansen in his study, proved that, when a fixed amount of volume wets the next stripe is spreads more and as a result perpendicular angle decreases significantly [12]. Same trend has been observed in our simulation. Following table is showing the changes in parallel and perpendicular angle of a droplet with 2 µL volume. Here θ_{philic} =80º; m=100 µm; n=100 µm.

Table 4.4.1: Effect of Hydrophobic Contact Angle on Degree of Anisotropy

Number of Stripes	**Θ_{phobic} = 100**		**Θ_{phobic} = 140**		**Θ_{phobic} = 180**	
	Parallel	Perpendicular	Parallel	Perpendicular	Parallel	Perpendicular
9	80.312	154.1	84.25	154.25	88.4	154.7
11	80.5	141.8	84.9	143.4	93.9	144.4
13	81.5	128.5	86.7	133.2	98.3	131.9
15	82	123	88.4	124	101	128

This table shows that the contact angle in perpendicular direction is decreasing significantly whether there is an increment in parallel angle which agrees with Jansen's findings [11,12]. Thus, the degree of anisotropy decreases with increasing stipe number.

Following table shows the change of angle with change in hydrophilic stripe width (volume 2 µL, Θ_{phobic} = 100). From our previous discussion, wider hydrophilic angle is congenial for a drop to

spread along the stripe. As a result, parallel and perpendicular both angle is decreasing. But compared to perpendicular angle, the change of parallel angle is very low due to the strong pinning effect at the edge. Degree of anisotropy thus decreasing very sharply when hydrophilic stripe width is increasing.

Table 4.4.2: Effect of Hydrophilic Stripe width on Degree of Anisotropy

Number of Stripes	**m = 75**		**m = 100**		**m = 125**	
	Parallel	Perpendicular	Parallel	Perpendicular	Parallel	Perpendicular
9	81.6	162	80.3	154.1	79.0	144.6
11	82.5	149.9	80.5	141.8	80.4	132.3
13	81.6	140.1	81.5	128.5	79.5	119.7
15	81.5	129.9	82.0	123	79.3	110.4
17	82.1	121.7	82.5	109.1	82.7	98.0

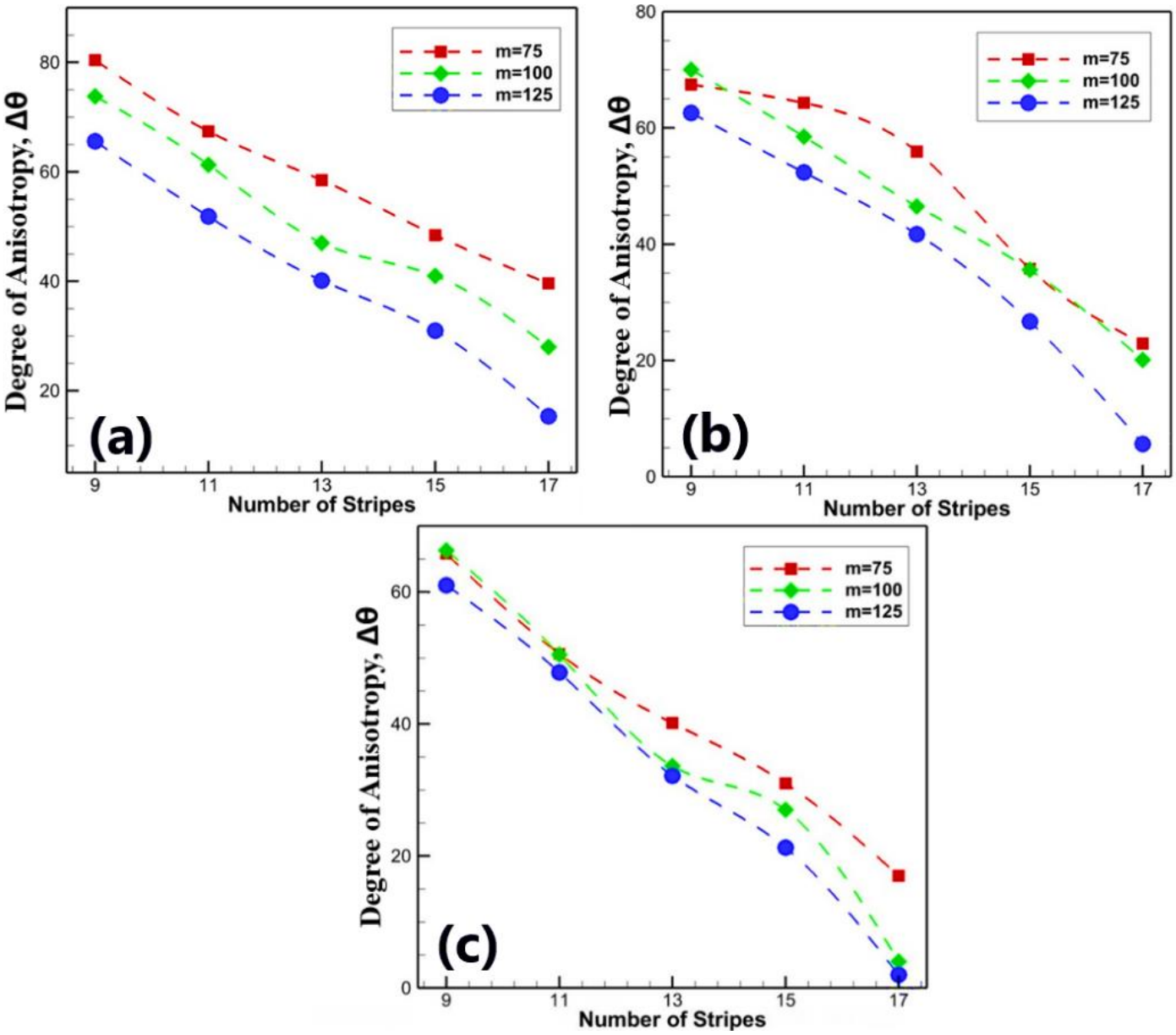

Fig 4.4.3: degree of anisotropy on 9,11,13,15,17 stripe configuration as a function of hydrophilic stripe width m, $\theta_{philic} = 80^o$; $\theta_{phobic} = 180^o$

4.5 Distortion of Liquid Droplet

On a microgrooved or striped surface, droplet prefers to spread along the parallel groove than to perpendicular side due to high energy barrier on boundary leading to an elongated shape of the droplet. Morita et al. defined distortion of a droplet as ratio of length (L) to width(W) or length of major axis to minor axis [9]. The mechanism of droplet distortion follows only an advancing contact line that is towards the parallel or y direction of the droplet. Because of heavy energy barrier in perpendicular or x direction, distortion occurs toward the parallel groove/stripe. Low surface tension liquid distorted easily whereas high surface tension liquid scarcely distorted (water) with increasing volume, degree of distortion increases [12]. In our case, we used only water (high surface tension liquid) On the other hand, Elongation is defined as the ratio of length to width from bottom view [11]

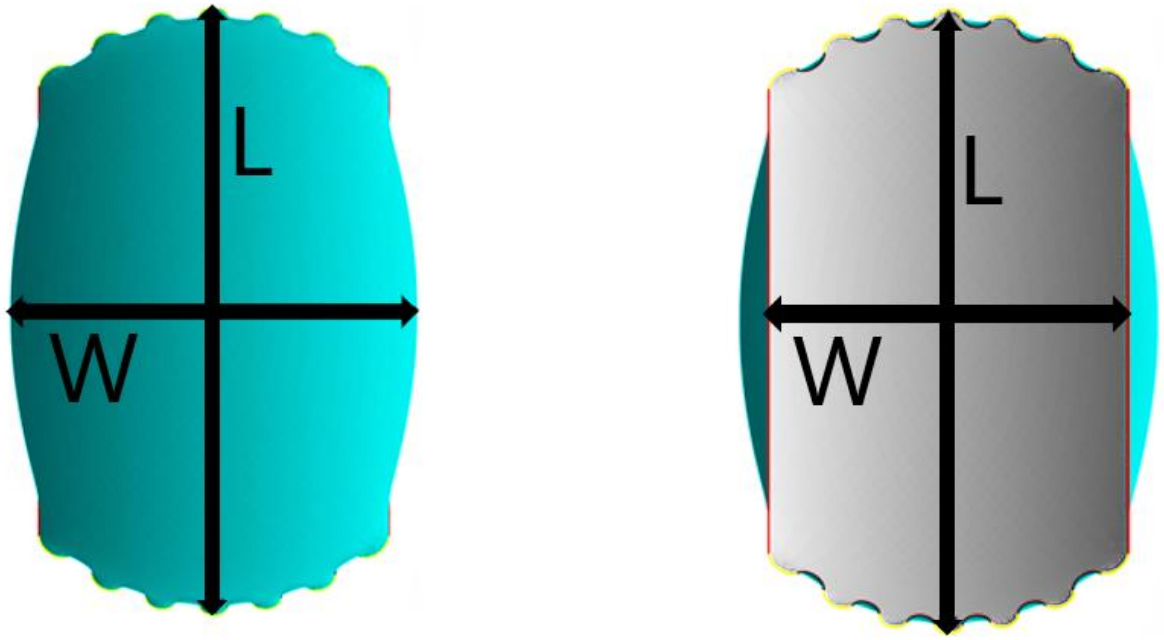

Fig 4.5.1 distortion and elongation from top view(left) and bottom view(right)

On a given number of striped configurations, distortion value is always higher for low hydrophobic angle as the droplet needs to overcome less energy for spreading. As both are ration of L/W; value of elongation is always larger than distortion as the width is fixed in the bottom. According to Morita [9], distortion increases with volume. Our simulation shows the same trend. However, in our study, it always becomes near unity where the normalized energy is lowest which corresponds to the most stable state. It is interesting to observe that, this is independent of wettability contrast, width of hydrophilic stripe and stripe numbers. We found this result may be because our choice of hydrophilic angle is 80^o which is near the hydrophobic area thus less spreading expected in more hydrophilic surface. Interestingly, may be due to the same reason, elongation shows same trend, becomes unity near equilibrium state.

High degree of distortion results in achieving low contact angle due to the overall hydrophilic nature of the surface. In rough surfaces, while Wenzel wetting occurs, the height of the droplet decreases due to the wetting in the rough structures. But in Cassie-Baxter or chemically stripe patterned surfaces, droplet height remains larger resulting in a higher contact angle.

With increasing hydrophilic stripe width, value of distortion & elongation should be increased [11-13]. On a fixed stripe- pattern, wider hydrophilic stripe offers high surface energy to the droplet and is congenial for spreading into the parallel direction. On geometric rough surface, for it is referred to as the aspect ratio effect and at critical point the transition between Wenzel and Cassie-Baxter happens. But in our cases, as there is no groove for the drop to sink in or base is not constrained under fixed a numeric value of width, when either no. of stripe or width of stripe is increased, this trend is not followed due to wider base width of droplet.

Solid line in the figures indicates the distortion whether dash dot line is for elongation of the spreading droplet. Red, Green and Blue lines are for $\theta_{phobic} = 100^o$; $\theta_{phobic} = 140^o$; $\theta_{phobic} = 180^o$ wetting condition. Long dash of black line indicates no distortion. Intersection points of black dash line and other curves are indicating the equilibrium droplets.

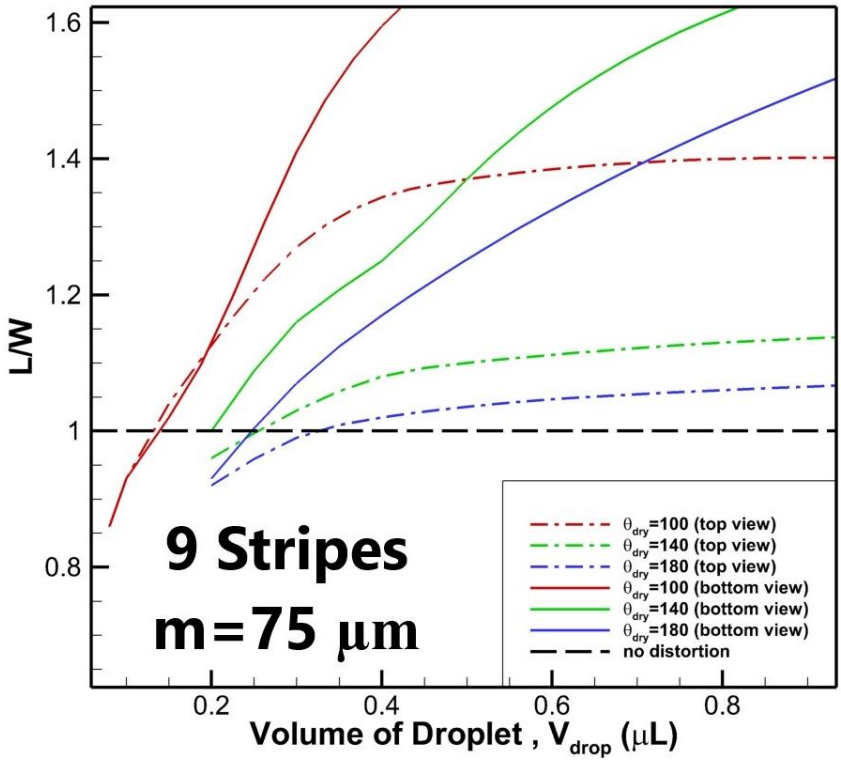
1.6
1.4
1.2
1
0.8
L/W
9 Stripes
m=75 μm
θdry=100 (top view)
θdry=140 (top view)
θdry=180 (top view)
θdry=100 (bottom view)
θdry=140 (bottom view)
θdry=180 (bottom view)
no distortion
0.2
0.4
0.6
0.8
Volume of Droplet , Vdrop (μL)

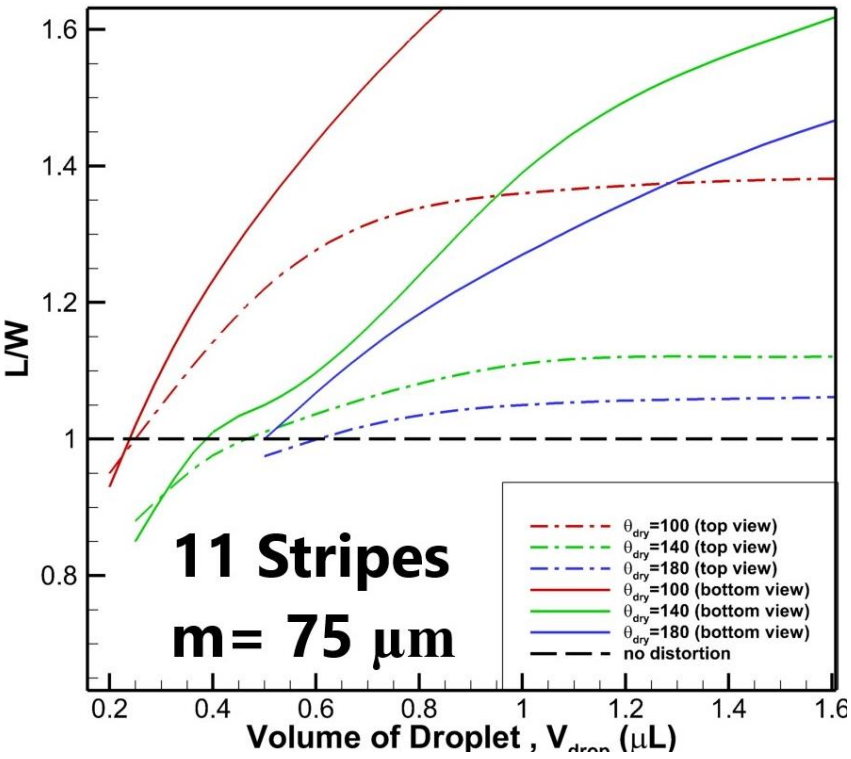
1.6
1.4
1.2
1
0.8
L/W
11 Stripes
m= 75 μm
θdry=100 (top view)
θdry=140 (top view)
θdry=180 (top view)
θdry=100 (bottom view)
θdry=140 (bottom view)
θdry=180 (bottom view)
no distortion
0.2
0.4
0.6
0.8
1
1.2
1.4
1.6
Volume of Droplet , Vdrop (μL)

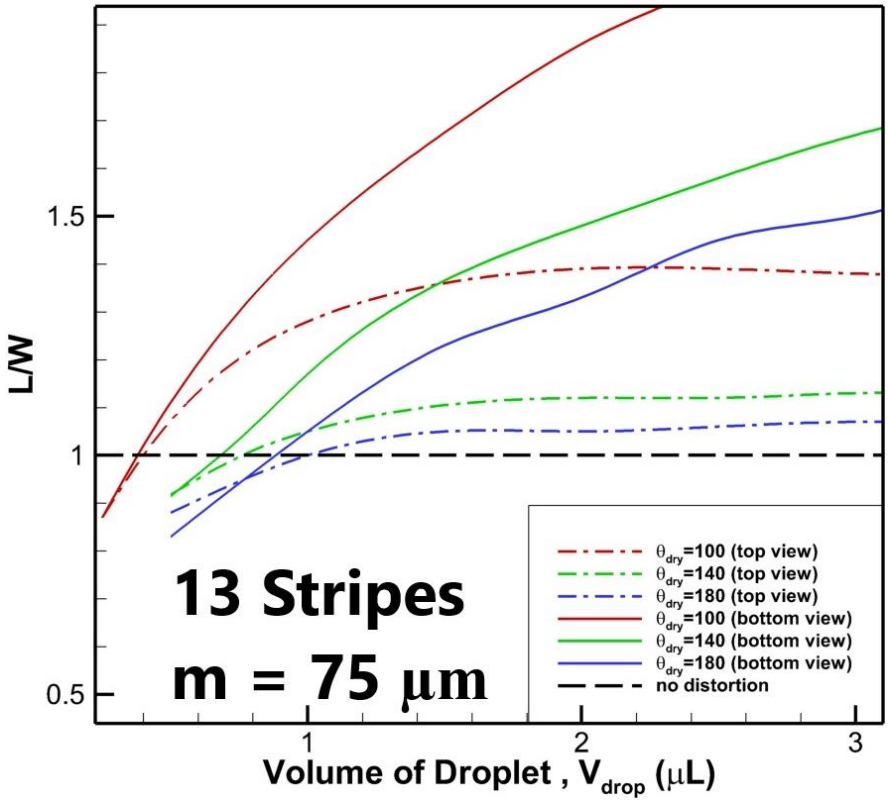
L/W
1.5
1
0.5
1
2
3
Volume of Droplet , V_{drop} (μL)
13 Stripes
m = 75 μm
θ_{dry}=100 (top view)
θ_{dry}=140 (top view)
θ_{dry}=180 (top view)
θ_{dry}=100 (bottom view)
θ_{dry}=140 (bottom view)
θ_{dry}=180 (bottom view)
no distortion

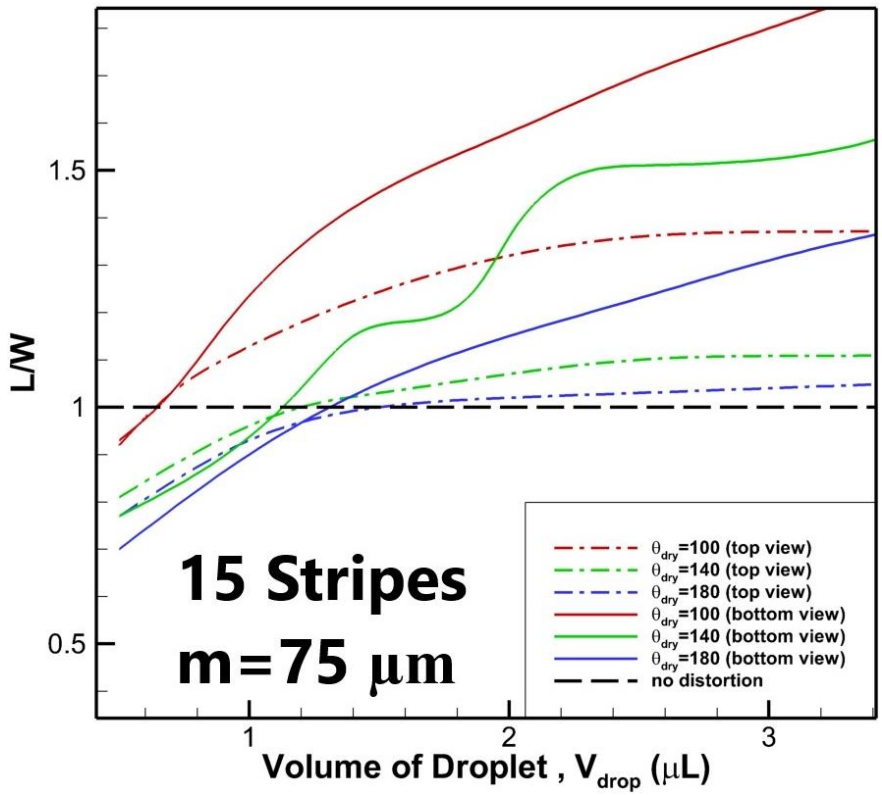
L/W
1.5
1
0.5
1
2
3
Volume of Droplet , V_{drop} (μL)
15 Stripes
m=75 μm
θ_{dry}=100 (top view)
θ_{dry}=140 (top view)
θ_{dry}=180 (top view)
θ_{dry}=100 (bottom view)
θ_{dry}=140 (bottom view)
θ_{dry}=180 (bottom view)
no distortion

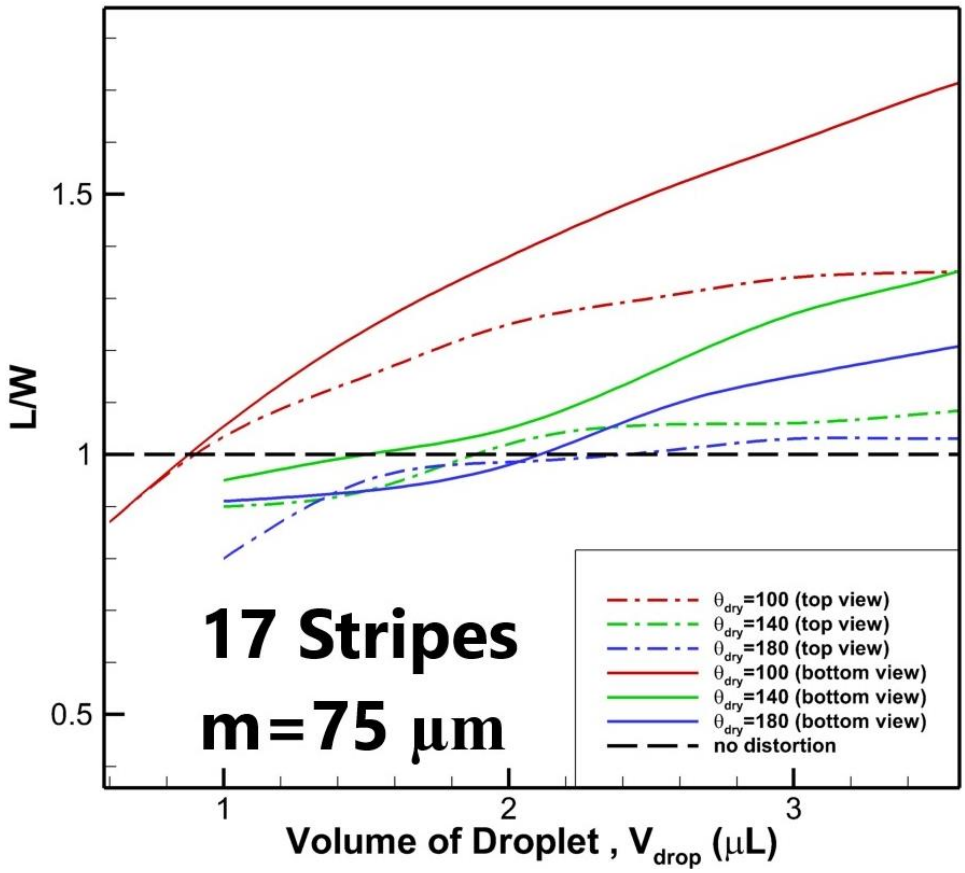

Fig 4.5 (b): distortion and elongation for 9,11,13,15,17 stripes having $\theta_{phobic}=80^0$, m=75μm; n=100 μm

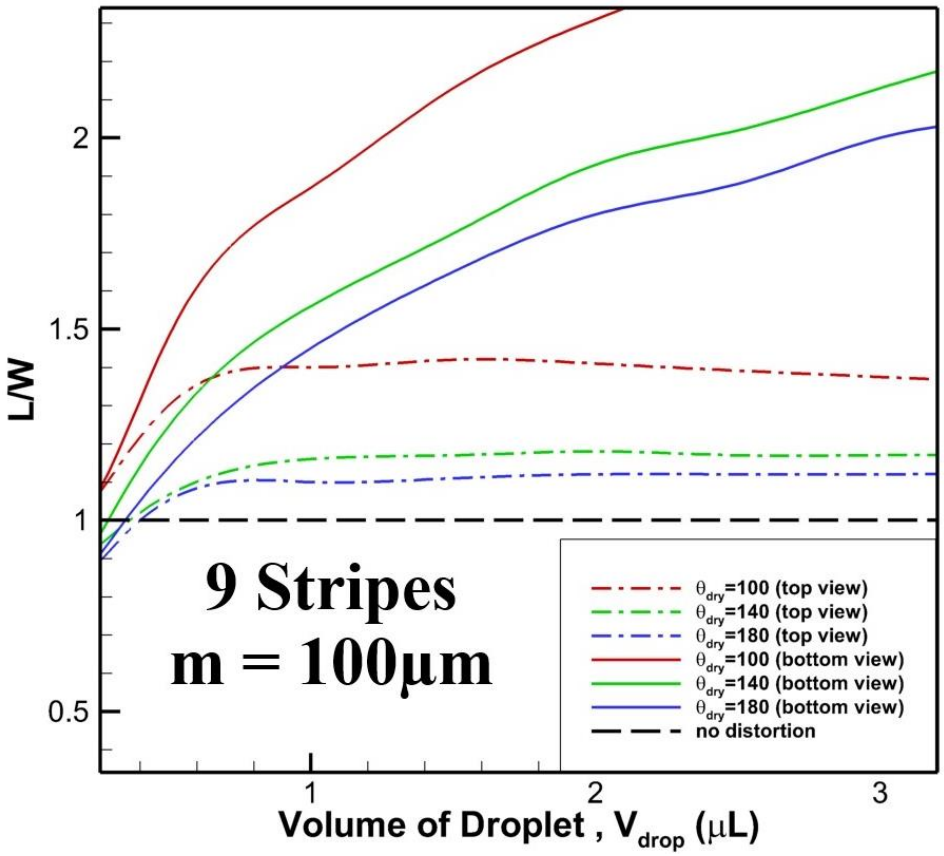
L/W
2
1.5
1
0.5
1
2
3
Volume of Droplet , V_{drop} (μL)
9 Stripes
m = 100μm
θ_{dry}=100 (top view)
θ_{dry}=140 (top view)
θ_{dry}=180 (top view)
θ_{dry}=100 (bottom view)
θ_{dry}=140 (bottom view)
θ_{dry}=180 (bottom view)
no distortion

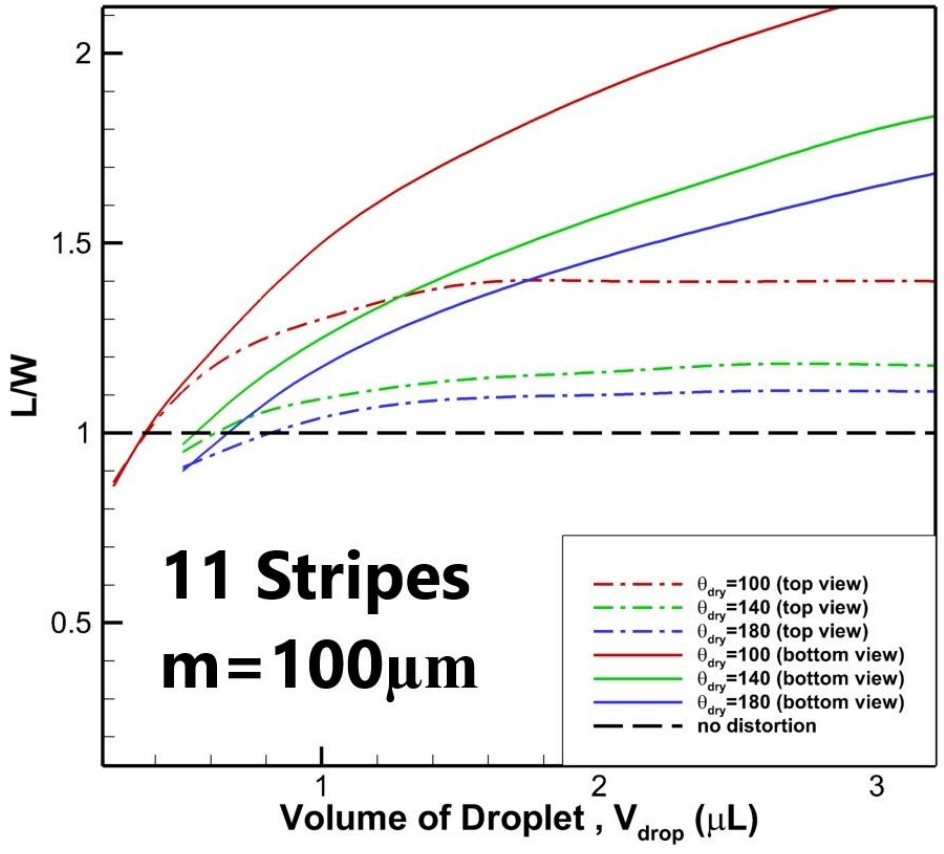
L/W
2
1.5
1
0.5
1
2
3
Volume of Droplet , V_{drop} (μL)
11 Stripes
m=100μm
θ_{dry}=100 (top view)
θ_{dry}=140 (top view)
θ_{dry}=180 (top view)
θ_{dry}=100 (bottom view)
θ_{dry}=140 (bottom view)
θ_{dry}=180 (bottom view)
no distortion

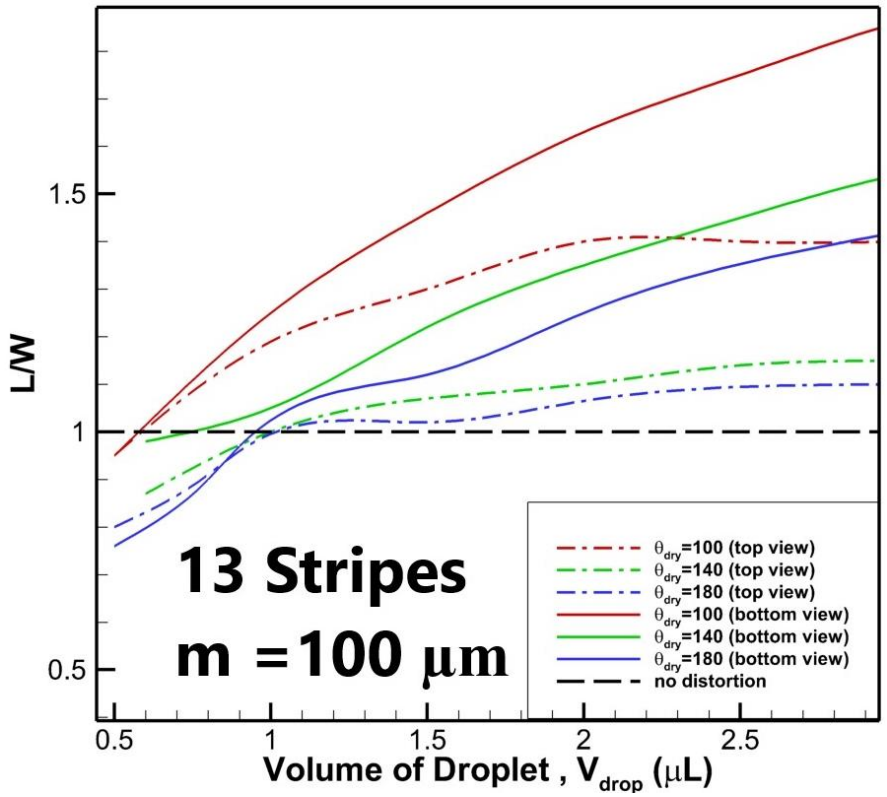
13 Stripes
m =100 μm
L/W
Volume of Droplet , V_drop (μL)
θ_dry=100 (top view)
θ_dry=140 (top view)
θ_dry=180 (top view)
θ_dry=100 (bottom view)
θ_dry=140 (bottom view)
θ_dry=180 (bottom view)
no distortion

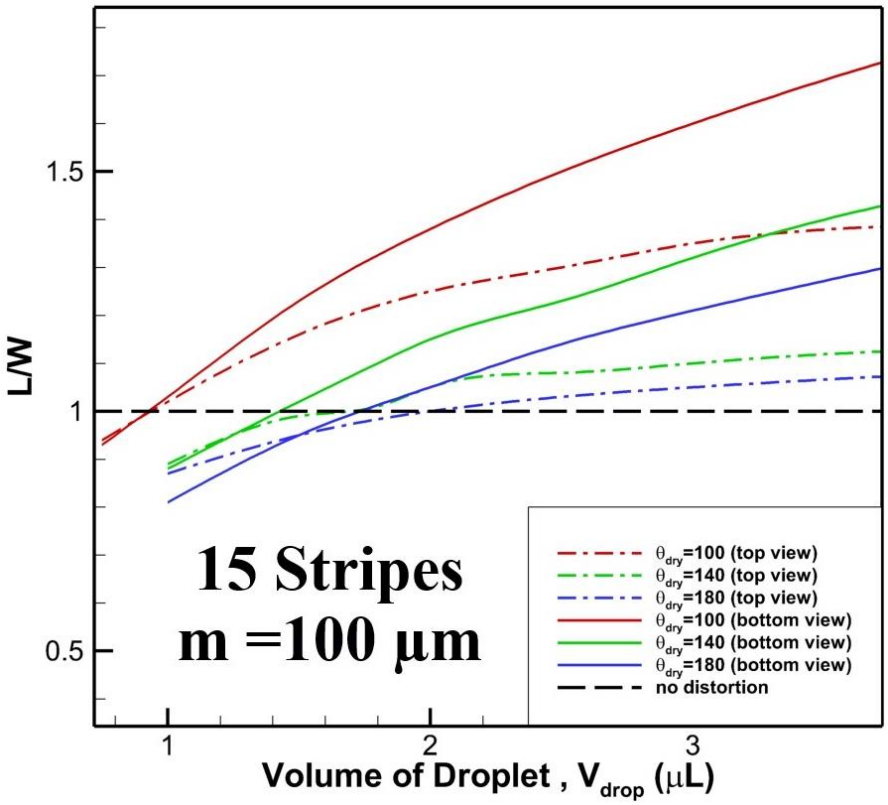
15 Stripes
m =100 μm
L/W
Volume of Droplet , V_drop (μL)
θ_dry=100 (top view)
θ_dry=140 (top view)
θ_dry=180 (top view)
θ_dry=100 (bottom view)
θ_dry=140 (bottom view)
θ_dry=180 (bottom view)
no distortion

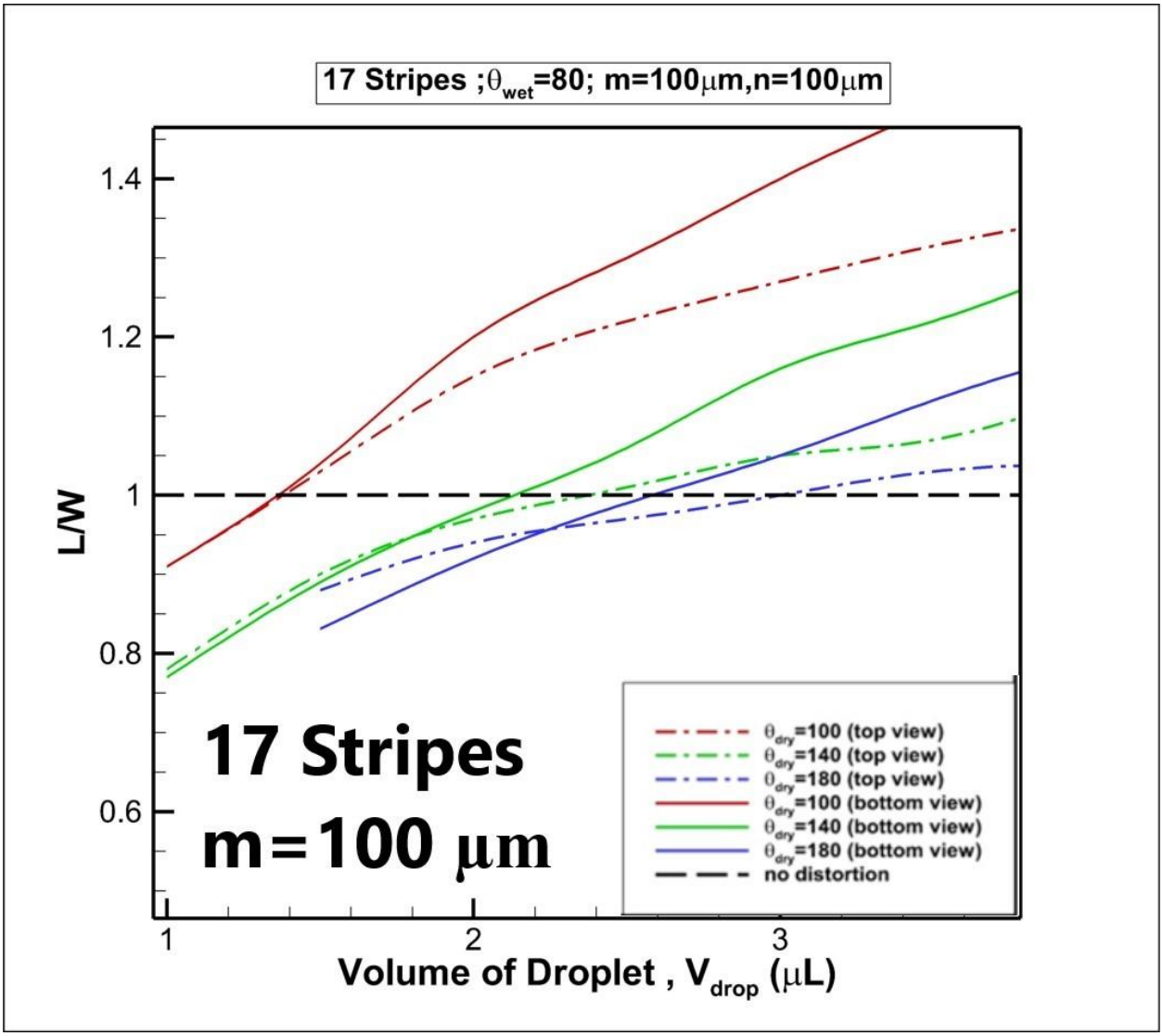

Fig 4.5 (c): distortion and elongation for 9,11,13,15,17 stripes having $\theta_{phobic} = 80^0$, m=100μm; n=100 μm

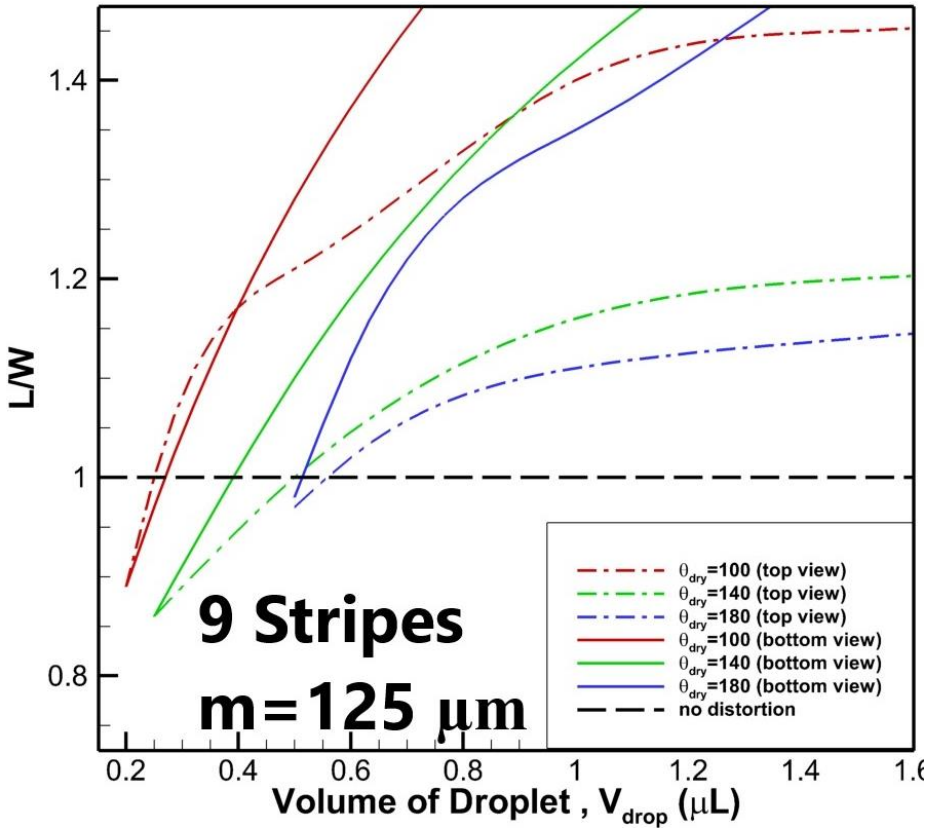
L/W
1.4
1.2
1
0.8
0.2
0.4
0.6
0.8
1
1.2
1.4
Volume of Droplet , V_{drop} (μL)
9 Stripes
m=125 μm
θ_{dry}=100 (top view)
θ_{dry}=140 (top view)
θ_{dry}=180 (top view)
θ_{dry}=100 (bottom view)
θ_{dry}=140 (bottom view)
θ_{dry}=180 (bottom view)
no distortion

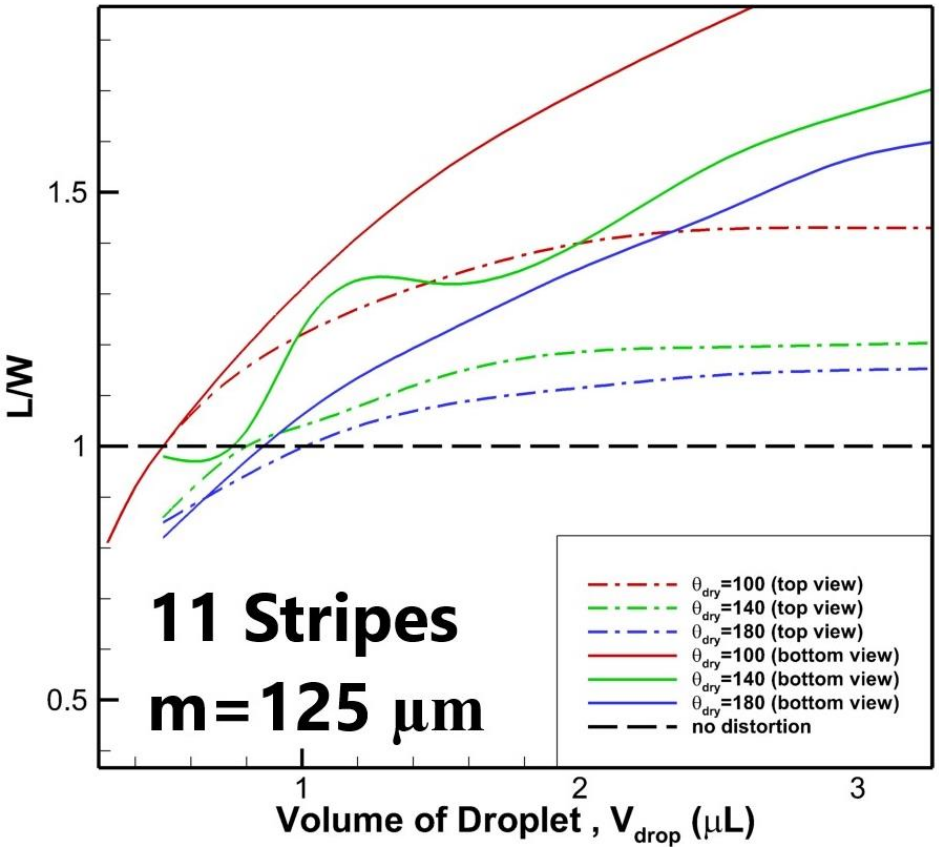
L/W
1.5
1
0.5
1
2
3
Volume of Droplet , V_{drop} (μL)
11 Stripes
m=125 μm
θ_{dry}=100 (top view)
θ_{dry}=140 (top view)
θ_{dry}=180 (top view)
θ_{dry}=100 (bottom view)
θ_{dry}=140 (bottom view)
θ_{dry}=180 (bottom view)
no distortion

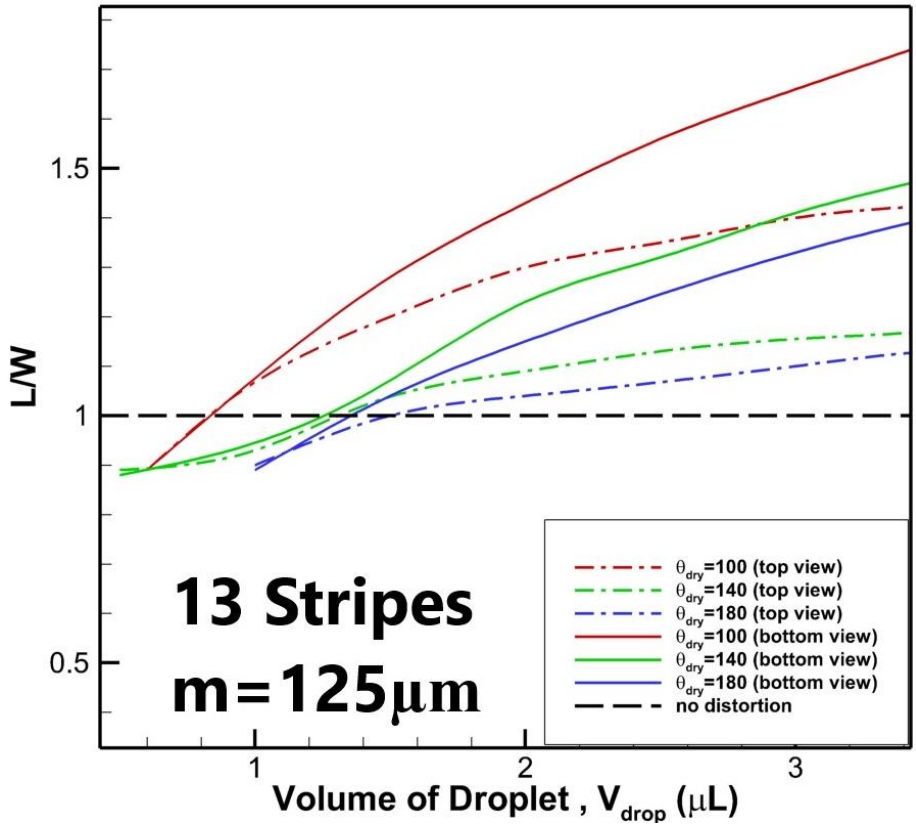
L/W
1.5
1
0.5
1
2
3
Volume of Droplet , V_{drop} (μL)
13 Stripes
m=125μm
θ_{dry}=100 (top view)
θ_{dry}=140 (top view)
θ_{dry}=180 (top view)
θ_{dry}=100 (bottom view)
θ_{dry}=140 (bottom view)
θ_{dry}=180 (bottom view)
no distortion

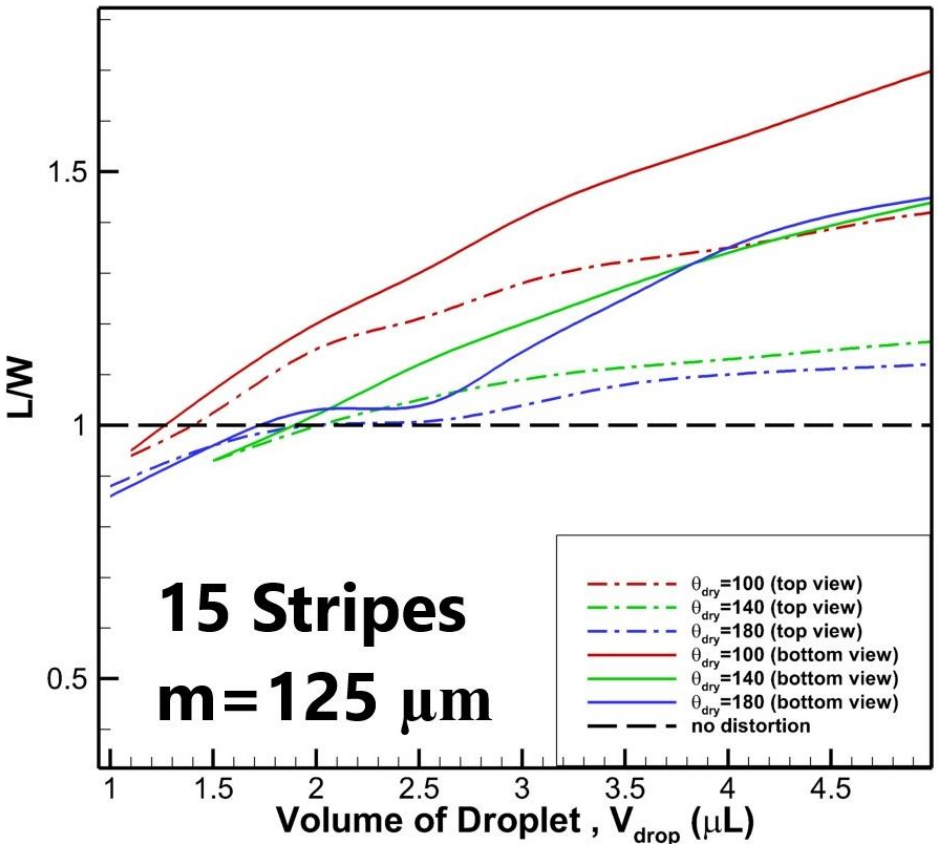
L/W
1.5
1
0.5
1
1.5
2
2.5
3
3.5
4
4.5
Volume of Droplet , V_{drop} (μL)
15 Stripes
m=125 μm
θ_{dry}=100 (top view)
θ_{dry}=140 (top view)
θ_{dry}=180 (top view)
θ_{dry}=100 (bottom view)
θ_{dry}=140 (bottom view)
θ_{dry}=180 (bottom view)
no distortion

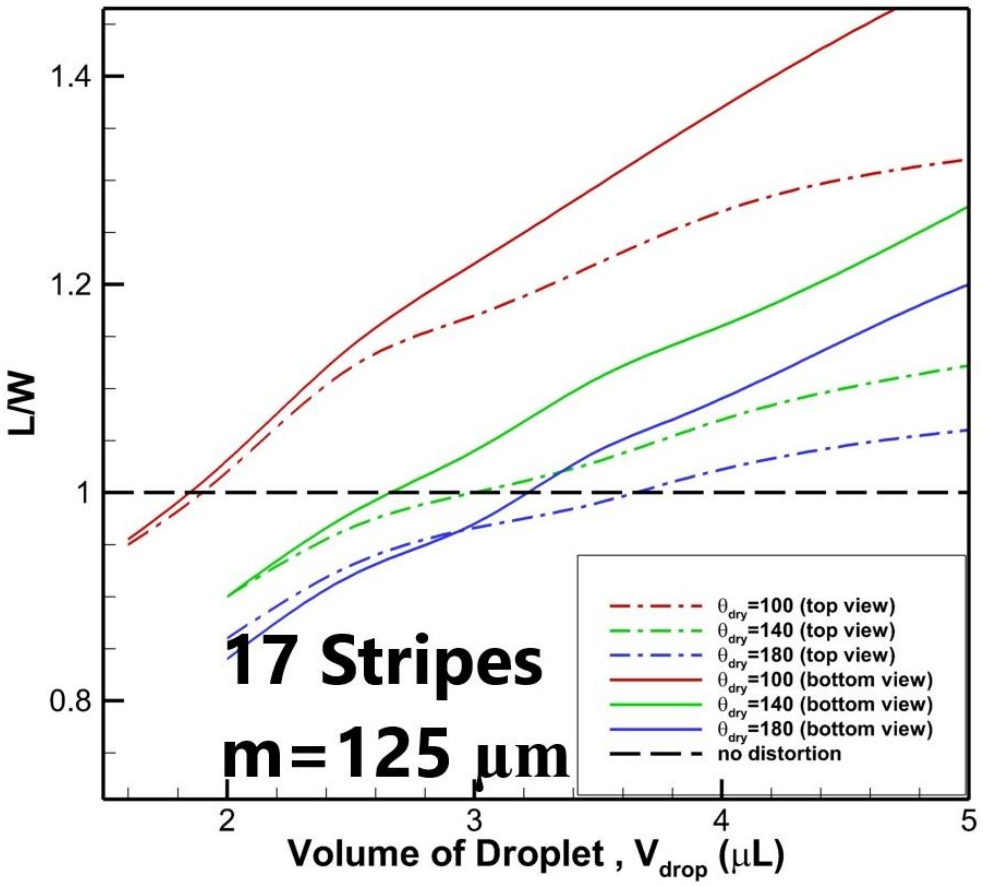

Fig 4.5 (d): distortion and elongation for 9,11,13,15,17 stripes having $\theta_{phobic} = 80^0$, m=125μm; n=100 μm

4.6 Shape Analysis

Droplet shape evolves with increasing volume from an oval shape to spherical shape to reach the stable state. After reaching this state, with increment of volume it starts elongating again and loses its spherical shape. At non-equilibrium or metastable states, droplet experiences additional forces (i.e., elastic force due to adhesion at the edges or energy surplus due to a sharp change of energy at boundary) on the three-phase contact line that it needs to overcome to reach at stable state. With increasing volume, total surface energy increases as well as it starts to store the necessary energy to encounter the forces as well as adjustment of volume happens. Just after reaching the equilibrium state, it is ready to jump to the next stripe. However, constrained boundary prevents it to elongate perpendicularly rather it starts to elongate parallelly. As a result, it loses its spherical shape again and oval/elliptical shape reappears that stores more energy on the substrate.

Fig. 4.6.1 illustrates an evolving droplet on 11 stripes. From top view we can understand that at this configuration at volume 0.9 µL, this droplet is most stable. The bottom view (Fig. 4.6.2) and isometric view (Fig. 4.6.3) of evolving droplets shows that at the most stable state, the width and length of spreading droplet becomes nearly equal that results in a spherical cap like shape if observed from an isometric perspective.

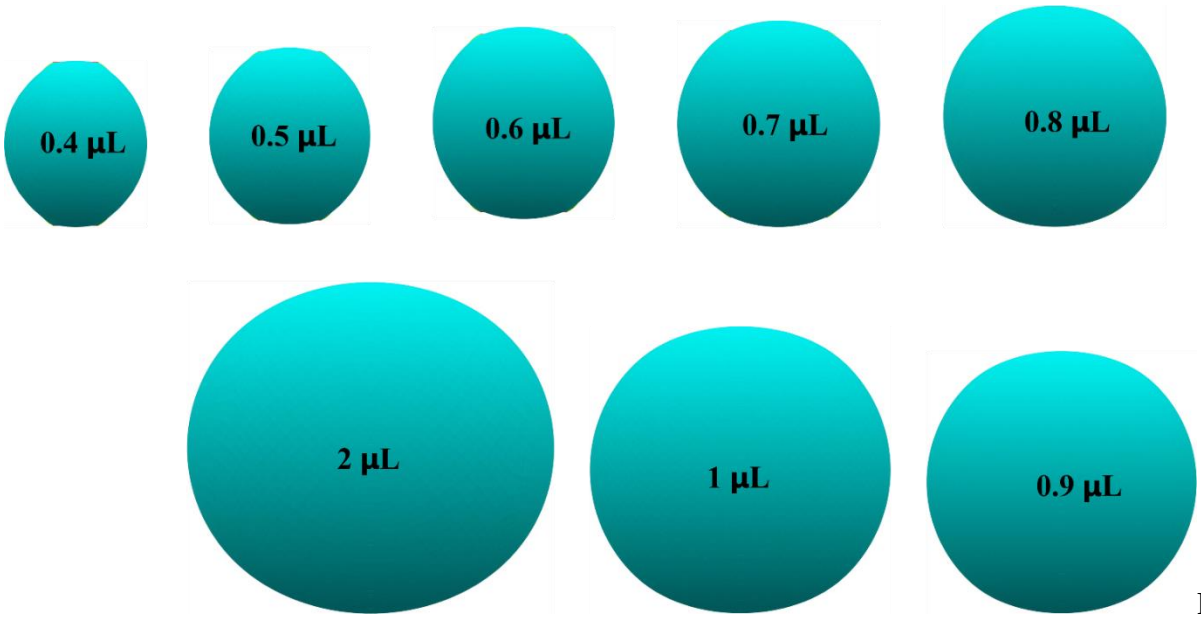

Fig 4.6.1: Top view of evolving droplet on 11 stripes. Most stable state is at 0.9 µL containing nearly spherical shape

While spreading, the contact line length of a droplet increases with volume. But just after it reaches the most stable state it shrinks a little [53]. Because, at this transition stage with volume increment it shows a tendency to jump to the next stripe that is referred as slip jump condition. Thus, at stable state droplet width is never equal to the line length rather slight less than length. He et al. [52] shows that, at 11 stripe configurations with angle 80 degree and 110 degrees, a droplet reaches its stable state at 0.65 µL volume. At that time, the length is 1.37 but the width is 1.3. from our distortion curve, we can roughly say that at stable state condition distortion is around unity, not exactly unity.

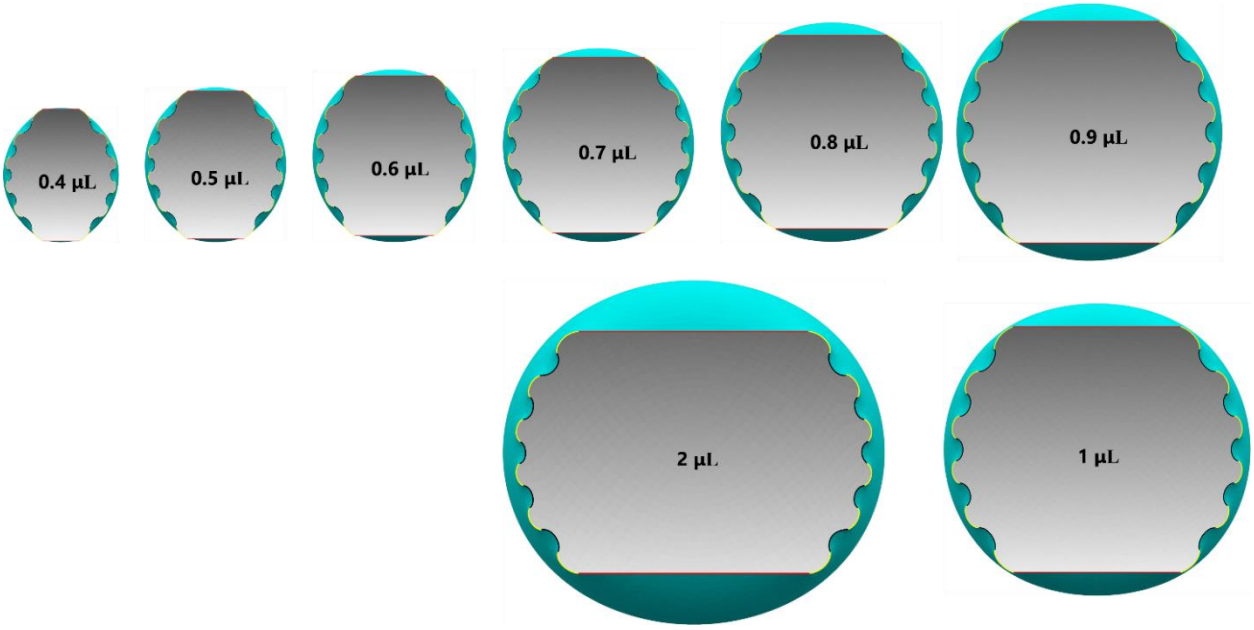

Fig 4.6.2: Bottom view of evolving droplet on 11 stripes. Most stable state is at 0.9 µL containing nearly spherical shape

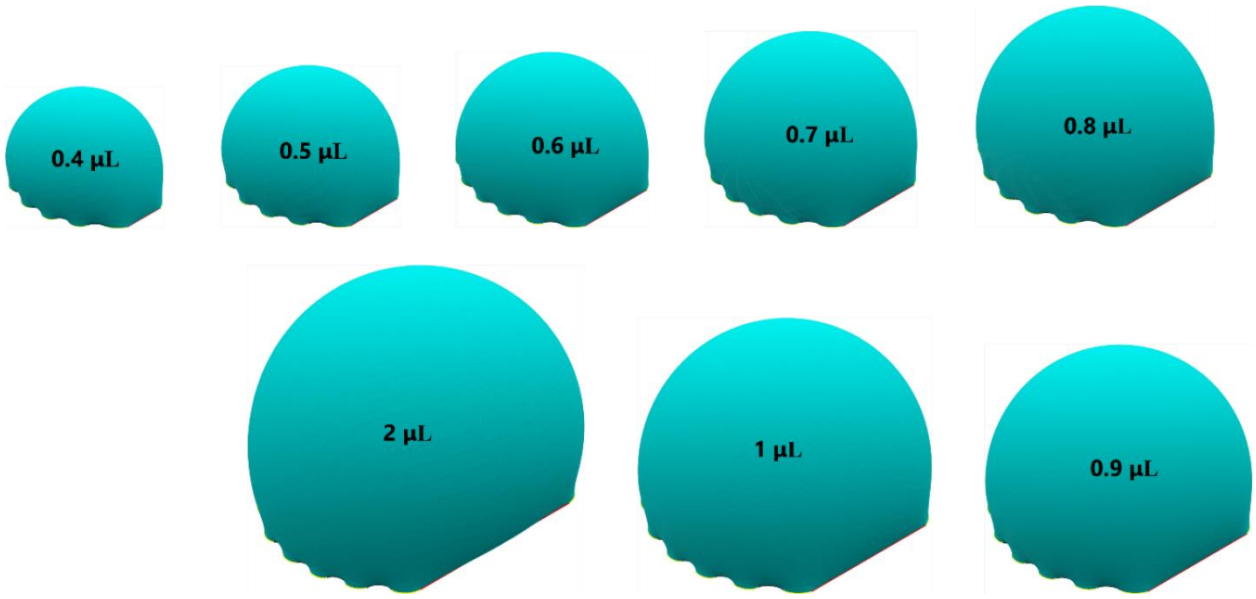

Fig 4.6.3 isometric view of evolving droplet on 11 stripes. Most stable state is at 0.9 µL containing nearly spherical shape

Chapter 05

Conclusions and Recommendations

5.1 Conclusions:

The primary focus of this study was to investigate the anisotropic wetting behavior of water droplet on chemical stripe-patterned surfaces with alternating stripes (hydrophilic/hydrophobic) by analyzing the shape, distortion and movement of three-phase contact line. Investigation of energetics and stability of droplet enable us to forecast about the wetting behavior of liquid on chemically inhomogeneous surfaces leading to a reliable guideline of designing tunable surfaces. The following points are the most important findings of this study:

(i) Lower hydrophobic stripe angle is always preferred for achieving a more stable state, along with larger hydrophilic stripe and few stripes. The system gets more stable when the wettability contrast between the varying stripes decreases.

(ii) With high wetting contrast between hydrophilic and hydrophobic stripe, parallel angle of the droplet always increases due to higher energy barrier and strong pinning effect that force the droplet to move inward thus increasing its height and resulting in achieving a large parallel angle eventually.

(iii) A higher degree of anisotropy is observed with a lower number of stripe configuration and for narrower hydrophilic stripe. For wider hydrophilic stripe, due to volume adjustment, stretching occurs and there is a sharp decline in degree of anisotropy.

(iv) With increment of volume, droplet shape starts evolving form an oval / elliptical to a circular sphere when it reaches an equilibrium state. More increase in volume initiates the elongation of shape and the oval shape reappears.

Findings in our thesis for varying patterned configuration as well as surface energy are in excellent agreement with those associated experimental and theoretical investigation. This model will be very helpful predicting the nature of wetting on surfaces that are chemically striped with a wide range of contrast in hydrophobic/hydrophilic portion. Not only for chemically stripe patterned surface, the developed model is also expected to be able to predict the anisotropic wetting phenomena of microgrooved surfaces, micro-V-shape grooved and wavy surfaces with high accuracy if appropriate geometric formulation as well as energies are introduced.

5.2 Scopes for Future Work

Previous studies of wetting on stripe patterned surface mostly comprised of 2D modeling. These models were unable to explain the evolution of three-phase contact line properly as well as low accuracy. In contrast, our development of 3D modeling for the present study is improved in terms of investigating the movement of three-phase line as well as measuring the contact angle more accurately. Thus, following recommendations are suggested for future research as there are many scopes for investigating new findings and developing the model.

(i) Though this model is developed for chemically pattern surface related phenomena it is totally analogous to parallel microgroove configuration when droplet is at Cassie-Baxter mode. With proper implementation of geometrical modeling and good understating in related acting energies, this model could be turned into a system to investigate other complex configurations with differently designed groove, spacing and height.

(ii) Measuring dynamic contact angle will be another scope of this model. Modification in the movement of vertex will allow this model to measure the advancing and receding contact angle while in movement. This will help revealing the hydrophobic or hydrophilic nature of a surface.

(iii) Studying with low wettability contrast difference will make this study more informative about the spreading of the liquid. This model is ready to handle such calculation if proper meshing is applied.

References

[1] Lv, C., Hao, P., Yao, Z. and Niu, F., “Departure of condensation droplets on superhydrophobic surfaces”, Langmuir, 31(8), pp. 2414-2420, (2015). (2015).

[2] Rahman, M.A., and Jacobi, A.M., “Study of the Effects of Microgrooved Geometry on Frost Structure”, International Refrigeration and Air Conditioning Conference at Purdue, (2012).

[3] Liang, Y., Ju, J., Deng, N., Zhou, X., Yan, J., Kang, W., & Cheng, B., “Super-hydrophobic self-cleaning beadlike SiO2@ PTFE nanofiber membranes for waterproof-breathable applications”, Applied Surface Science, 442, pp. 54-64, (2018).

[4] Boinovich, L. B., Emelyanenko, A.M., Ivanov, V. K., & Pashinin A. S., “Durable Icephobic Coating for Stainless Steel”, ACS Appl. Mater. Interfaces, 5, pp. 2549–2554, (2013)

[5] Choi, C. H., Lee, H. and Weitz, D. A., “Rapid patterning of PDMS microfluidic device wettability using syringe-vacuum-induced segmented flow in non-planar geometry”, ACS Applied Materials & Interfaces, 10(4), pp. 3170–3174, (2018).

[6] Tian, D., Song, Y., & Jiang, L., "Patterning of controllable surface wettability for printing techniques", Chemical Society Reviews, 42(12), p.p 5184-5209. (2013)

[7] Kim, S., Prasetio, A., Han, J. W., Kim, Y., Shin, M., Heo, J., Lim, D. C., “Enhanced flexible optoelectronic devices by controlling the wettability of an organic bifacial interlayer”. Communications Materials, 2(26), (2021).

[8] David, R., Neumann, A.W., “Anisotropic drop shapes on chemically striped surfaces”, Colloids and surfaces A: Physicochem. Eng. Aspects, 393, pp. 32-36, (2012).

[9] Morita, M., Koga, T., Otsuka, H., Takahara, A., “Macroscopic-Wetting Anisotropy on the Line-Patterned Surface of Fluoroalkylsilane Monolayers” Langmuir, 21(3), pp. 911–918, (2005).

[10] Brandon, S., Haimovich, N., Yeger, E., & Marmur, A., “Partial wetting of chemically patterned surfaces: The effect of drop size” Journal of Colloid and Interface Science, 263, pp. 237-243, (2003).

[11] Jansen, H. P., Bliznyuk, O., Kooij, E. S., Poelsema B., & Zandvliet, H.J. W., “Simulating Anisotropic Droplet Shapes on Chemically Striped Patterned Surfaces”, Langmuir, 28(1), pp. 499–505, (2012).

[12] Jansen, H. P., Sotthewes, K., Kooij, E. S., & Zandvliet, H.J. W., “Potential of lattice Boltzmann to model droplets on chemically stripe-patterned substrates”, Applied surface Science, 361, pp. 122-132, (2016).

[13] Léopoldès, J., Bucknall, D.G., “Droplet spreading on microstriped surfaces”, ACS J. Phys. Chem. B, 109(18), 8973-8977, (2005).

[14] Chatain, D., Lewis, D., Baland, J. P., & Carter, W. C., “Numerical analysis of the shapes and energies of droplets on micropatterned substrates”, Langmuir, 22(9), pp. 4237-4243, (2006).

[15] He, L., Liang, W., Wang, Z., Akbarzadeh, A., “A three-dimensional model for analyzing the anisotropic wetting” behavior of striped surfaces”, Colloids and surfaces A: Physicochem. Eng. Aspects, 552, pp. 67-74, (2018).

[16] Li, W., Amirfazli, A., “Hierarchical structures for natural superhydrophobic surfaces”, Soft Matter 4, pp.462-466, (2008).

[17] Liang, Y., Shu, L., Natsu, W., He, F., "Anisotropic wetting characteristics versus roughness on machined surfaces of hydrophilic and hydrophobic materials", Appl. Surf. Sci. 331 pp.41-49. (2015)

[18] Li, W., Fang, G.P., Lij, Y.F., Qiao, G.J., "Anisotropic wetting behavior arising from superhydrophobic surfaces: parallel grooved structure", J. Phys. Chem. B 112 ,pp.7234-7243, (2008).

[19] Zhenyu, S., Zhanqiang, L., Hao, S., Xianzhi, Z., "Prediction of contact angle for hydrophobic surface fabricated with micro-machining based on minimum Gibbs free energy", Appl. Surf. Sci. 364, pp. 597-603, (2016).

[20] Long, J., Hyder, M.N., Huang, R.Y.M., Chen, P., "Thermodynamic modeling of contact angles on rough, heterogeneous surfaces, Adv. Colloid Interface Sci 118 ,pp.173-190, (2005).

[21] Chung, J.Y., Youngblood, J.P., Stafford, C.M., "Anisotropic wetting on tunable micro-wrinkled surfaces", Soft Matter 3 (2007) 1163.

[22] Brakke, K. A., "The Surface Evolver", *Exp. Math.*, vol. 1(2), pp. 141–165, 1992.

[23] Young, T. (1805). "An Essay on the Cohesion of Fluids", Philosophical Transactions of the Royal Society of London", 95(0), pp.65–87.

[24] Wenzel, R. N., "Resistance of solid surfaces to wetting by water", Industrial and Engineering Chemistry, 1936, 28, pp. 988–994.

[25] Cassie, A. B. D., Baxter, S., "Wettability of Porous Surfaces", *Trans. Faraday Soc.*, vol. 40, pp. 546-551, 1944

[26] Wang, X. and Zhang, Q., "Insight into the Influence of Surface Roughness on the Wettability of Apatite and Dolomite", *Minerals*, vol. 10(2): 114, 2020.

[27] Gao, L. and McCarthy, T. J., "How Wenzel and Cassie Were Wrong", *Langmuir*, vol. 23(7), pp. 3762-3765, 2007.

[28] De Gennes, P. G., Brochard-Wyart, F., and Qu´er´e D., "Capillarity and wetting phenomena: drops, bubbles, pearls, waves", Springer Verlag, (2004).

[29] Bhushan, B., and Jung, Y. C., "Micro and nanoscale characterization of hydrophobic and hydrophilic leaf surface". Nanotechnology, 17, pp. 2758–2772, (2006).

[30] Bhushan, B., and Jung, Y. C., "Wetting, adhesion and friction of superhydrophobic and hydrophilic leaves and fabricated micro/nanopatterned surfaces", Journal of Physics: Condensed Matter, 20, 225010, (2008).

[31] Shirtcliffe, J. N., McHale, G. and Newton, M. I., "Learning from Superhydrophobic Plants: The Use of Hydrophilic Areas on Superhydrophobic Surfaces for Droplet Control Part of "Langmuir 25th Year: Wetting and Superhydrophobicity" Special Issue", *Langmuir*, vol. 115 25(24), pp. 14121 14128, (2009).

[32] Liu, K., and Jiang, L., 'Bio-inspired design of multiscale structures for function integration' Nano Today, 6, 155–175,(2011).

[33] H. Wu, R. Zhang, Y. Sun, D. Lin, Z. Sun, W. Pan and P. Downs, *Soft Matter*,2008, **4**, 2429-2433.

[34] Wagner, T., Neinhuis, C., and Barthlott, W, "Wettability and Contaminability of Insect Wings as a Function of Their Surface Sculptures", vol. 77(3), pp. 213-225, (1996).

[35] Parker, A. R., and Lawrence, C. R., “Water Capture by a Desert Beetle”, *Nature*, vol. 414, pp. 33-34, (2001).

[36] Bai, H., Wang, L., Ju, J., Sun, R., Zheng, Y. and Jiang, L., "Efficient Water Collection on Integrative Bioinspired Surfaces with Star-Shaped Wettability Patterns”, Adv. Mater., 26, pp. 5025-5030, (2014).

[37] Moller, G., Harke, M., Prescher, D., and Motschmann, H., “Controlling Microdroplet Formation by Light”, Langmuir, 14, 4955-4957, (1998).

[38] Jeyaprakash, J. D., Samuel, S., and Ruhe, J., “A Facile Photochemical Surface Modification Technique for the Generation of Microstructured Fluorinated Surfaces” Langmuir, 20, pp. 10080-10085, (2004).

[39] Dorrer, C., and Ruehe, J., “Mimicking the Stenocara Beetle—Dewetting of Drops from a Patterned Superhydrophobic Surface”, Langmuir, 24, pp. 6154-6158, (2008)

[40] Zhang, L., Wu, J., Hedhili, M. N., Yang, X., and Wang, P.J., “Inkjet printing for direct micropatterning of a superhydrophobic surface: toward biomimetic fog harvesting surfaces” Mater. Chem. A, 2015,

[41] Lai, Y., Pan, F., Xu, C., Fuchs H., and Chi, L., “Adv. In situ surface-modification-induced superhydrophobic patterns with reversible wettability and adhesion”, Mater., 2013, 25, 1682-1686.

[42] Geng, H., Bai, H., Fan, Y., Wang, S., Ba, T., Yu, C., Cao, M. and Jiang, L., “Unidirectional water delivery on a superhydrophilic surface with two-dimensional asymmetrical wettability barriers”, Mater. Horizons, 2018, 5, 303-308.

[43] Bikerman, J. J., “The Surface Roughness and Contact Angle”, *J. Phys. Chem.*, vol. 54(5), pp. 653-658, 1950.

[44] Hitchcock, S. J., Carroll, N. T., and Nicholas, M. G., “Some Effects of Substrate Roughness on Wettability”, *J. Mater. Sci.*, vol. 16, pp. 714-732, 1981.

[45] Sung, N. H., Lee, H. Y., Yuan, P., and Sung, C. S. P., “Surface Structure, Topology, and Liquid Wetting Behavior in Oriented Polymers”, *Polym. Eng. Sci.*, vol. 29(12), pp. 791-800, 1989.

[46] Chen, Y., He, B., Lee, J., and dorrer, N. A., “Anisotropy in the Wetting of Rough Surfaces”,*J. Colloid Interface Sci.*, vol. 281, pp. 458–464, 2005.

[47] Feng, L., Li, S., Lim, Y., Li, H., Zhong, L., Zhai, J., Song, Y., Liu, A., Jiang, L., and Zhu, D., “Supe-Hydrophobic Surfaces: From Natural to Artificial”, *Adv. Mater*., vol. 14 (24), pp.1857-1860, 2002.

[48] Rahman, M. A., and Jacobi, A. M., “Wetting Behavior and Drainage of Water Droplets on Microgrooved Brass Surfaces”, *Langmuir*, vol. 28, pp. 13441-13451, 2012.

[49] Rahman, M. A., and Jacobi, A. M., “Experimental Investigation of Wetting Anisotropy on Microgrooved Brass Surfaces”, in *2013 10th International Conference on Mechanical Enginnering (ICME 2013), Procedia Eng.*, vol. 90, July 2014, pp. 611 – 617.

[50] Rahman, M. A., and Jacobi, A. M., “Drainage of Frost Melt Water from Vertical Brass Surfaces with Parallel Microgrooves”, *Int. J. Heat Mass Transf.*, vol. 55, pp. 1596-1605, 2012.

[51] Farhat, N., Alen, S. K., and Rahman, M. A., “Numerical Study of the Wetting and Mobility of Liquid Droplets on Horizontal and Inclined Flat and Microgrooved Surfaces”, in *2014 Proceedings of the 6th International Conference on Thermal Engineering (ICTE), Procedia Eng.*, vol. 105, July 2015, pp. 576-585.

[52] He, L., Sun, Y., Sui, X., Wang, Z., & Liang, W. ,“Modeling and Measurement on the Sliding Behavior of Microgrooved Surfaces”. Langmuir. 35, 43, pp.14133–14140(2019,).

[53] He, L., Liang, W., Wang, Z., Akbarzadeh, A., “Numerical analysis of anisotropic wetting of chemically striped surfaces”, *RSC Adv.*, 2018,8, 31735-31744

[54] Patankar, N.A.,“On the Modeling of Hydrophobic Contact Angles on Rough Surfaces”, Langmuir,19,pp.1249-1253,(2003).

[55] Chen,Y., He,B., Lee,J., and Patankar, N.A., "Anisotropy in the wetting of rough surfaces", Journal of Collide and Interface Science, (281), pp. 458-464, (2005)

[56] He, B., Patankar, N. A., & Lee, J., “Multiple Equilibrium Droplet Shapes and Design Criterion for Rough Hydrophobic Surfaces”. Langmuir, 19(12), pp. 4999–5003, (2003).

[57] Khan, Md. I, and Rahman M.A.,“Wettability and droplet energetics on micro-scale wavy and V-grooved surfaces”, Results in Engineering, 16,100791,(2022).

[58] Dupuis, A., & Yeomans, J. M., “Droplet dynamics on patterned substrates”, Pramana, 64(6), pp.1019–1027, (2005).

[59] Azimi, A., He, P., Rohrs, C., & Yao, C.-W., “Developing a novel continuum model of static and dynamic contact angles in a case study of a water droplet on micro-patterned hybrid substrates”. MRS Communications, pp.1–10. (2018),

[60] Goswami, A., and Rahman, M. A., “Numerical study of energetics and wetting stability of liquid droplets on microtextured surfaces”, *Colloid Polym. Sci.*, vol. 295(10), pp. 1787–1796, 2017.

[61] Brakke, K. A., Surface Evolver Documentation, 2013.

APPENDIX

SURFACE EVOLVER (VERSION 2.70) CODES

Based on a bottom-up method to geometry development, SE geometry is specified using a text file in the necessary format (.fe). To build a body, one first lists the vertices (points in space), edges (directed connection between two vertices), and faces (ordered collection of three or more edges), then combines the faces to generate volume. Codes are also subjected to a number of geometric, energy, and volumetric limitations. Here is a list of the scripts we utilized in our work (comments are preceded by a double forward slash).

A.1 Code for Free Sessile Droplet on Flat Smooth Surface

```
parameter angle = 70
parameter vol = 4
parameter den = 1000*(10       (-9))
gravity_constant 0

#define T (-cos(angle*pi/180))

constraint 1
formula: z = 0
energy:
e1: -T*y
e2: 0
e3: 0

vertices
1 0 0 0 constraint 1
2 1 0 0 constraint 1
```

3 1 1 0 constraint 1

4 0 1 0 constraint 1

5 0 0 1

6 1 0 1

7 1 1 1

8 0 1 1

edges

1 1 2 constraint 1

2 2 3 constraint 1

3 3 4 constraint 1

4 4 1 constraint 1

5 5 6

6 6 7

7 7 8

8 8 5

9 1 5

10 2 6

11 3 7

12 4 8

faces

1 1 10 -5 -9 frontcolor cyan backcolor yellow

2 2 11 -6 -10 frontcolor cyan backcolor yellow

3 3 12 -7 -11 frontcolor cyan backcolor yellow

4 4 9 -8 -12 frontcolor cyan backcolor yellow

5 5 6 7 8 frontcolor cyan backcolor yellow

bodies

1 1 2 3 4 5 volume vol density den

```
read //computation
// ‘r’ = refinement of the mesh
// ‘g’ = iteration step
// ‘u’ = mesh equiangulation
// ‘V’ = vertex averaging
r
gogo := {{u; V; g50;}20};
```

A.2 Code for Droplet on Chemically Stripe-Patterned Surface

```
parameter yangle = 80 //for hydrophilic stripe
parameter cangle = 180 //for hydrophobic stripe
parameter vol = .5 //in microleter or cubic milimeter
parameter den = 1000*(10^(-9))
parameter ht = 1
parameter wp = 0.1
parameter wg = 0.1
parameter z1 = 0
parameter y1 = 0
parameter a1 = 1

parameter xleft = 0 //leftmost point

parameter g_1= xleft+0*wp+0*wg
parameter g_2= xleft+1*wp+0*wg

parameter g_3= xleft+1*wp+1*wg
parameter g_4= xleft+2*wp+1*wg

parameter g_5= xleft+2*wp+2*wg
parameter g_6= xleft+3*wp+2*wg
```

```
parameter g_7= xleft+3*wp+3*wg
parameter g_8= xleft+4*wp+3*wg

parameter g_9= xleft+4*wp+4*wg
parameter g_10= xleft+5*wp+4*wg

parameter g_11= xleft+5*wp+5*wg
parameter g_12= xleft+6*wp+5*wg

parameter g_13= xleft+6*wp+6*wg
parameter g_14= xleft+7*wp+6*wg
parameter xright =g_14 //rightmost point
gravity_constant 0

#define T1 (-cos(yangle*pi/180))
#define T2 (-cos(cangle*pi/180))

constraint 1
formula: z = 0

constraint 2
formula: x = g_1

constraint 3
formula: x = g_2

constraint 4
formula: x = g_3

constraint 5
```

formula: x = g_4

constraint 6
formula: x = g_5

constraint 7
formula: x = g_6

constraint 8
formula: x = g_7

constraint 9
formula: x = g_8

constraint 10
formula: x = g_9

constraint 11
formula: x = g_10

constraint 12
formula: x = g_11

constraint 13
formula: x = g_12

constraint 14
formula: x = g_13

constraint 15
formula: x = g_14

constraint 18

formula: z = 0

energy:

e1: (x>g_1 && x<g_2) ? -(T1*y):-(T2*y)

e2: 0

e3:0

constraint 19

formula: z = 0

energy:

e1: (x>g_2 && x<g_3) ? -(T2*y):-(T1*y)

e2: 0

e3:0

constraint 20

formula: z = 0

energy:

e1: (x>g_3 && x<g_4) ? -(T1*y):-(T2*y)

e2: 0

e3:0

constraint 21

formula: z = 0

energy:

e1: (x>g_4 && x<g_5) ? -(T2*y):-(T1*y)

e2: 0

e3:0

constraint 22

formula: z = 0

energy:

e1: (x>g_5 && x<g_6) ? -(T1*y):-(T2*y)

e2: 0

e3:0

constraint 23

formula: z = 0

energy:

e1: (x>g_6 && x<g_7) ? -(T2*y):-(T1*y)

e2: 0

e3:0

constraint 24

formula: z = 0

energy:

e1: (x>g_7 && x<g_8) ? -(T1*y):-(T2*y)

e2: 0

e3:0

constraint 25

formula: z = 0

energy:

e1: (x>g_8 && x<g_9) ? -(T2*y):-(T1*y)

e2: 0

e3:0

constraint 26

formula: z = 0

energy:

e1: (x>g_9 && x<g_10) ? -(T1*y):-(T2*y)

e2: 0

e3:0

constraint 27

formula: z = 0

energy:

e1: (x>g_10 && x<g_11) ? -(T2*y):-(T1*y)

e2: 0

e3:0

constraint 28

formula: z = 0

energy:

e1: (x>g_11 && x<g_12) ? -(T1*y):-(T2*y)

e2: 0

e3:0

constraint 29

formula: z = 0

energy:

e1: (x>g_12 && x<g_13) ? -(T2*y):-(T1*y)

e2: 0

e3:0

constraint 30

formula: z = 0

energy:

e1: (x>g_13 && x<g_14) ? -(T1*y):-(T2*y)

e2: 0

e3:0

constraint leftedge nonnegative
formula: x-xleft

constraint rightedge nonpositive
formula: x-xright

vertices
1 g_1 y1 z1 constraints 1, 2
2 g_2 y1 z1 constraints 1, 3
3 g_3 y1 z1 constraints 1, 4
4 g_4 y1 z1 constraints 1, 5
5 g_5 y1 z1 constraints 1, 6
6 g_6 y1 z1 constraints 1, 7
7 g_7 y1 z1 constraints 1, 8
8 g_8 y1 z1 constraints 1, 9
9 g_9 y1 z1 constraints 1, 10
10 g_10 y1 z1 constraints 1, 11
11 g_11 y1 z1 constraints 1, 12
12 g_12 y1 z1 constraints 1, 13
13 g_13 y1 z1 constraints 1, 14
14 g_14 y1 z1 constraints 1, 15
15 g_14 y1+a1 z1 constraints 1, 15
16 g_13 y1+a1 z1 constraints 1, 14
17 g_12 y1+a1 z1 constraints 1, 13
18 g_11 y1+a1 z1 constraints 1, 12
19 g_10 y1+a1 z1 constraints 1, 11
20 g_9 y1+a1 z1 constraints 1, 10
21 g_8 y1+a1 z1 constraints 1, 9
22 g_7 y1+a1 z1 constraints 1, 8

23 g_6 y1+a1 z1 constraints 1, 7

24 g_5 y1+a1 z1 constraints 1, 6

25 g_4 y1+a1 z1 constraints 1, 5

26 g_3 y1+a1 z1 constraints 1, 4

27 g_2 y1+a1 z1 constraints 1, 3

28 g_1 y1+a1 z1 constraints 1, 2

29 g_1 y1+a1 ht

30 g_1 y1 ht

31 g_14 y1 ht

32 g_14 y1+a1 ht

edges

1 1 2 constraint 18 color red

2 2 3 constraint 19 color red

3 3 4 constraint 20 color red

4 4 5 constraint 21 color red

5 5 6 constraint 22 color red

6 6 7 constraint 23 color red

7 7 8 constraint 24 color red

8 8 9 constraint 25 color red

9 9 10 constraint 26 color red

10 10 11 constraint 27 color red

11 11 12 constraint 28 color red

12 12 13 constraint 29 color red

13 13 14 constraint 30 color red

14 14 15 constraint 1, rightedge color red

15 15 16 constraint 30 color red

16 16 17 constraint 29 color red

17 17 18 constraint 28 color red

18 18 19 constraint 27 color red

19 19 20 constraint 26 color red

20 20 21 constraint 25 color red

21 21 22 constraint 24 color red

22 22 23 constraint 23color red

23 23 24 constraint 22 color red

24 24 25 constraint 21color red

25 25 26 constraint 20 color red

26 26 27 constraint 19color red

27 27 28 constraint 18 color red

28 28 1 constraints 1, leftedge color red

29 28 29

30 1 30

31 14 31

32 15 32

33 29 30

34 30 31

35 31 32

36 32 29

faces

1 28 30 -33 -29 frontcolor cyan backcolor yellow

2 1 2 3 4 5 6 7 8 9 10 11 12 13 31 -34 -30 frontcolor cyan backcolor yellow

3 14 32 -35 -31 frontcolor cyan backcolor yellow

4 15 16 17 18 19 20 21 22 23 24 25 26 27 29 -36 -32 frontcolor cyan backcolor yellow

5 33 34 35 36 frontcolor cyan backcolor yellow

bodies

1 1 2 3 4 5 volume vol density den

read

//r

//g5

//r

//g5

gogo1 := {{u; V; V; V; u; V; g50;}3}; //use it two three times

//r

//gogo1 use it two three times

//if still problem in triple line exists then run with fine mesh

//then check volume and go for further iteration